

GENETICAL INVESTIGATION OF BALYA-BALIKESİR LEAD-ZINC  
MINERALIZATIONS

A THESIS SUBMITTED TO  
THE GRADUATE SCHOOL OF NATURAL AND APPLIED SCIENCES  
OF  
THE MIDDLE EAST TECHNICAL UNIVERSITY

BY

GÜLSEVİM ÖZİŞİK

IN PARTIAL FULLFILMENT OF THE REQUIREMENTS  
FOR  
THE DEGREE OF MASTER OF SCIENCE  
IN  
THE DEPARTMENT OF GEOLOGICAL ENGINEERING

DECEMBER 2009

Approval of the thesis:

**GENETICAL INVESTIGATION OF BALYA-BALIKESİR LEAD-ZINC  
MINERALIZATIONS, TURKEY**

submitted by **GÜLSEVİM ÖZİŞİK** in partial fulfillment of the requirements for the degree of **Master of Science in Geological Engineering Department, Middle East Technical University** by,

Prof. Dr. Canan Özgen \_\_\_\_\_  
Dean, Graduate School of **Natural and Applied Sciences**

Prof. Dr. Zeki Çamur \_\_\_\_\_  
Head of Department, **Geological Engineering**

Prof. Dr. Nilgün Güleç \_\_\_\_\_  
Supervisor, **Geological Engineering Dept., METU**

Prof. Dr. İlkay Kuşçu \_\_\_\_\_  
Co-Supervisor, **Geological Engineering Dept., Muğla University**

**Examining Committee Members:**

Assoc. Prof. Dr. Sönmez Sayılı \_\_\_\_\_  
Geological Engineering Dept., Ankara University

Prof. Dr. Nilgün Güleç \_\_\_\_\_  
Geological Engineering Dept., METU

Pro. Dr. Asuman Günal Türkmenoğlu \_\_\_\_\_  
Geological Engineering Dept., METU

Prof. Dr. Yusuf Kağan Kadioğlu \_\_\_\_\_  
Geological Engineering Dept., Ankara University

Prof. Dr. İlkay Kuşçu \_\_\_\_\_  
Geological Engineering Dept., Muğla University

**Date:** 04.12.2009

**I hereby declare that all information in this document has been obtained and presented in accordance with academic rules and ethical conduct. I also declare that, as required by these rules and conduct, I have fully cited and referenced all material and results that are not original to this work.**

Name, Last name : Gülsevim Özışık

Signature :

## ABSTRACT

### GENETICAL INVESTIGATION OF BALYA-BALIKESİR LEAD-ZINC MINERALIZATIONS TURKEY

Özışık, Gülsevim

M.Sc., Department of Geological Engineering

Supervisor: Prof. Dr. Nilgün Güleç

Co-Supervisor: Prof. Dr. Ilkay Kuşçu

December 2009, 91 Pages

This thesis study is concerned with genetical investigation of Balıkesir Balya Pb-Zn mineralization through the mineralogic-petrographic and geochemical examination of the core samples obtained from a total of 9 holes drilled by Eczacıbaşı ESAN Madencilik.

The Pb-Zn mineralization in Balya is mainly of vein-type. Wall rocks hosting mineralizations are dacite, dacite porphyry and microdiorite. Major types of alteration are silicification, carbonatization and calc-silicate alteration, each of which is further subdivided into early and late stages and overprinted by argillic alteration of probable supergene origin. The ore minerals are mainly Zn- and Pb-sulphides and are hosted by the rocks with late calc-silicate alteration that underwent pervasive late silicification and late carbonatization. Sulfide mineralization is spatially and temporally associated with the late silicification and carbonatization stages. Lateral-vertical correlation of drill logs suggest that thickness of the ore zone tends to decrease towards north.

The volcanic rocks hosting the mineralization have calc-alkaline nature. Major, trace and rare earth element (REE) geochemistry suggests either crustal contamination or subduction signature in the mantle source of the volcanics. Multi element patterns and discrimination diagrams collectively point to a post-collisional setting for their generation. Alteration geochemistry reveals that  $\text{Fe}_2\text{O}_3$  and  $\text{CaO}$  are enriched during calc-silicate alteration in contrast to depletion of  $\text{SiO}_2$ .  $\text{Al}_2\text{O}_3$  and  $\text{TiO}_2$  are almost constant during late calc-silicate alteration. Enrichment of  $\text{Fe}_2\text{O}_3$  and  $\text{Na}_2\text{O}$ , and depletion of  $\text{K}_2\text{O}$  characterize the silicified zones. Carbonatization is accompanied by strong enrichment of  $\text{CaO}$  and depletion of  $\text{SiO}_2$ ,  $\text{Al}_2\text{O}_3$  and  $\text{K}_2\text{O}$ .

**Keywords:** Balya, Pb-Zn Mineralization, Calc-silicate alteration, Silicification, Carbonatization.

## ÖZ

### BALYA-BALIKESİR KURŞUN-ÇİNKO CEVHERLEŞMELERİNİN KÖKENSEL OLARAK İNCELEMELERİ TÜRKİYE

ÖZİŞİK, Gülsevim

Yüksek Lisans, Jeoloji Mühendisliği Bölümü

Tez Yöneticisi: Prof. Dr. Nilgün GÜLEÇ

Ortak Tez Yöneticisi: Prof. Dr. Ilkay Kuşçu

Aralık 2009, 91 Sayfa

Bu çalışma, Balya Pb-Zn cevherleşmesinin kökenisel olarak incelenmesini konu almaktadır. Çalışma, Eczacıbaşı ESAN Madencilik tarafından açılmış toplam 9 sondaj kuyusundan alınan karot örneklerinin mineralojik-petrografik ve jeokimyasal incelemeleri yoluyla gerçekleştirilmiştir.

Balya Pb-Zn cevherleşmesi başlıca damar tipi bir yataktır. Cevherleşmeleri içeren yan kayaçlar dasit, dasit porfiri ve mikrodiorit türü kayaçlardır. Başlıca alterasyon türleri silisleşme, karbonatlaşma ve kalk-silikat alterasyonudur. Bu alterasyonların her biri erken ve geç olmak üzere alt evrelere ayrılmakta ve olasılıkla süperjen orijinli bir arjilik alterasyon tarafından üzerlenmektedir. Cevher mineralleri, başlıca, Zn- ve Pb-sülfidlerden oluşmaktadır ve bu mineraller yaygın olarak geç silisleşme ve geç karbonatlaşmaya maruz kalan kalk-silikat kayaç içerisine yerleşmiştir. Sülfid cevherleşmesi, zaman-mekan ilişkisi göz önüne alındığında, geç silisleşme ve karbonatlaşma ile ilişkilendirilmektedir.

Sondaj loglarının yanal ve dūşey deneřtirilmesi, cevher zonunun kalınlıęının kuzey yōnünde azalmaya eęilimli olduęunu iřaret etmektedir. Cevherin yerleřmiř olduęu volkanik kayalar kalk-alkali niteliktedir. Ana, iz ve nadir toprak element jeokimyası, volkanikler iin, kabuksal kirlenme veya dalma-batma etkisi taşıyan bir manto kaynaęını dūřündürmektedir. oklu element profilleri ve ayırtman diyagramları volkaniklerin oluřumu iin “arpıřma sonrası” ortamı iřaret etmektedir. Alterasyon jeokimyası kalk-silikat alterasyon sırasında  $Fe_2O_3$  ve  $CaO$ 'in zenginleřtięini,  $SiO_2$ 'in ise tūketilmiř olduęunu ifade etmektedir.  $Al_2O_3$  ve  $TiO_2$  kalk-silikat alterasyon sūresince yaklařık sabit deęerlerde kalmıřtır. Silisifiye zonlar  $Fe_2O_3$  ve  $Na_2O$  zenginleřmesi ve  $K_2O$  tūketilmesi ile karakterize edilmektedir. Karbonatlařma ise kuvvetli  $CaO$  zenginleřmesi, ve  $SiO_2$ ,  $Al_2O_3$  ve  $K_2O$  tūketilmesi ile eřlenmektedir.

**Anahtar Kelimeler:** Balya, Pb-Zn Cevherleřmesi, Kalk-silikat alterasyonu, Silisleřme, Karbonatlařma.

## ACKNOWLEDGEMENTS

I would like to express my sincere gratitude to my supervisor, Prof. Dr. Nilgün Güleç, and my Co-Supervisor Assoc. Prof. Dr. İlkay Kuşcu for their support, suggestions and patience.

The major part of the research for this thesis was carried out with support by Eczacıbaşı ESAN Madencilik and Alican Akpınar, which I acknowledge with thanks.

I would also like to thank Prof. Dr. Yusuf Kaan Kadiođlu for his support about CRS (Confocal Raman Spectroscopy) analyses.

I extend my thanks to Mr. Erkan Yılmazer, Ms. Ezgi Ünal and Mr. Sercan Bozan for their support during various stages of this research.

Last but not the least, I thank my parents for their encouragement and support.

## TABLE OF CONTENTS

ABSTRACT .....	iv
ÖZ.....	vi
ACKNOWLEDGEMENTS.....	vii
TABLE OF CONTENTS .....	ix
LIST OF TABLES .....	xi
LIST OF FIGURES .....	xii
CHAPTERS	
1.INTRODUCTION.....	1
1.1. Purpose and Scope.....	1
1.2. Geographic Setting .....	1
1.3. Methods of Study .....	3
1.4. Previous works .....	5
1.5. Mining History .....	7
1.6. Layout of Thesis .....	9
2.TECTONIC SETTING AND REGIONAL GEOLOGY .....	10
3.LOCAL GEOLOGY .....	19
3.1. Rock Units.....	19
3.2. Rock units of the Karakaya Complex.....	19
3.2.1. Fine grained sedimentary rocks .....	19
3.2.2. Limestone.....	19
3.2.3. Conglomerates.....	21
3.3. Volcanic rocks .....	22
3.4. Structural Geology .....	23
4.MINERALIZATION AND ALTERATION.....	24

4.1. Mineralization .....	24
4.2. Wall Rocks .....	25
4.3. Wall Rock Alteration.....	27
4.3.1. Early silicification .....	42
4.3.2. Early carbonatization .....	44
4.3.3. Calc-silicate alteration: Skarn .....	46
4.3.3.1.Early calc-silicate alteration (Garnet±Pyroxene±actinolite).....	47
4.3.3.2.Late calc-silicate alteration (epidote±tremolite±calcite).....	50
4.3.4. Late silicification.....	52
4.3.5. Late Carbonatization .....	54
4.3.6. Argillization-clay alteration .....	57
4.4. Ore Mineralogy .....	58
4.5. Lateral-Vertical Correlation of Alterations .....	63
5.GEOCHEMISTRY .....	66
5.1. Geochemistry of volcanic rocks.....	66
5.2. Alteration Geochemistry .....	75
5.2.1. Element mobility during calc-silicate alteration.....	76
5.2.3. Element mobility during early-late carbonatization .....	78
5.3. Mass Balance Calculations - Mobility of Elements During Alteration.....	79
6.CONCLUSIONS .....	83
REFERENCES .....	86

## LIST OF TABLES

### TABLES

Tablo 1.1 UTM Coordinates of drilling wells which belongs to Eczacıbaşı-ESAN Mining (ES:ESAN sondaj).....	5
Table 4.1. Description of samples taken from drill hole ES-1.....	32
Table 4.2. Description of samples taken from drill hole ES-2.....	33
Table 4.3. Description of samples taken from drill hole ES-3.....	35
Table 4.4. Description of samples taken from drill hole ES-4.....	36
Table 4.5. Description of samples taken from drill hole ES-5.....	37
Table 4.6. Description of samples taken from drill hole ES-6.....	38
Table 4.7. Description of samples taken from drill hole ES-7.....	39
Table 4.8. Description of samples taken from drill hole ES-8.....	40
Table 4.9. Description of samples taken from drill hole ES-9.....	41
Table 4.10. Description of polished sections prepared from ES-3-6-9 drill core samples.....	59
Table 5.1. Major element contents of samples (Slc: Silicified, Crb: Carbonatized).....	68
Table 5.2. REE (Rare Earth Elements) element contents (ppm) of samples (Slc: Silicified, Crb: Carbonatized).....	69
Table 5.3. Trace element contents (ppm) of samples.....	70
Table 5.3.cont.....	71

## LIST OF FIGURES

### FIGURES

Figure 1.1 Geographic setting of the study area.....	2
Figure 1.2 Distribution of drilling holes in study area (Topographic map:1/10000)...	3
Figure 1.3. Old smelting plant for ore dressing established by the French Company.....	8
Figure 1.4. Mining base camp, and the smelting plant at the hill side, set up by Eczacıbaşı ESAN Madencilik.....	8
Figure 1.5. Ore dressing plant for ore production by Eczacıbaşı ESAN Madencilik.....	8
Figure 2.1. Tectonic map of the eastern Mediterranean region showing the major terranes and the bounding sutures. The filled triangles indicate the polarity of subduction (from Okay & Tüysüz,1999).....	11
Figure 2.2. The geological and tectonic map of the Biga Peninsula and the surrounding region (Okay and Altıner, 2004).....	12
Figure 2.3. Tectonic map of western Anatolia showing the distribution of the Karakaya Complex and related units (Okay and Göncüoğlu, 2004).....	13
Figure 2.4. Rift model for the evolution of the Karakaya Complex (Koçyiğit, 1987).....	15
Figure 2.5. Subduction-accretion model for the evolution of the Karakaya Complex (Pickett & Robertson 2004).....	16
Figure 2.6. Pre-Jurassic tectono-stratigraphic units in Sakarya Zone, Turkey (Okay 2001).....	17

Figure 3.1. Geological map of the Balya Mine district (A) showing the main rock types (Modified from Akyol, 1979) and locations of the drill holes used for sampling, (B) alterations.....	20
Figure 3.2. Recrystallized limestone with calcite veins and veinlets.....	21
Figure 3.3. Manganese veins in Permian Limestone.....	21
Figure 3.4 Contact between silicified dacite and limestone of Karakaya Complex in Kızıl Tepe (E-W).....	22
Figure 4.1. Typical volcanic quartz in dacite. (Sample taken from 19.2 m depth of ES-9, Q:Volcanic quartz).....	27
Figure 4.2. Microdiorite (Sample taken from 233,6 m depth of ES-9, plg: plagioclase, q:quartz).....	27
Figure 4.3 Drill logs of ES-1,2 and 3.....	29
Figure 4.4 Drill logs of ES-4, 5 and 6.....	30
Figure 4.5 Drill logs of ES-7, 8 and 9.....	31
Figure 4.6. Photomicrograph showing the silicified and brecciated rock (Qtz:Quartz).....	42
Figure 4.7. Photomicrograph showing the early silicification and hydrothermal brecciation rock (Qtz:Quartz).....	43
Figure 4.8 Coarse-grained, anhedral quartz crystals of silicified rock (Sample taken from 270.1 m depth of ES-9 (Qtz:Quartz)).....	43
Figure 4.9. Hydrothermally brecciated silicified rock (Sample taken from 270.1 m depth of ES-9 (Qtz:Quartz)).....	44
Figure 4.10. Composition of calcite from the early carbonatization (calcite by CRS).....	45
Figure 4.11. Early calcite vein cutting the quartz crystals of early silicification and hydrothermal breccia (Qtz:Quartz).....	45

Figure 4.12. Hydrothermal breccia and early silicification cut by calcite veinlets. (Sample taken from 270.1 m depth of ES-9. Brc. Slc.:Brecciated silicified rock).....	45
Figure 4.13. Calcite of early carbonatization within the argillitized rock ( Sample taken from 271 m depth of ES-9 Cly:clay).....	46
Figure 4.14. Zoned garnet (andradite) crystals with sector zoning within the early calc-silicate alteration.....	48
Figure 4.15. Composition of garnet from the early calc-silicate assemblage (andradite by CRS).....	48
Figure 4.16. Zoned andradite crystals in the early calc-silicate alteration, and calcite infill (Sample taken from 262.2 m depth of ES-9).....	49
Figure 4.17 Prismatic-euhedral actinolite crystals replacing the andradite.....	49
Figure 4.18. Epidote and calcite replacing andradite and pyroxene of early calc-silicate alteration (Sample taken from 390.9 m depth of ES-3). ....	50
Figure 4.19. Composition of epidote from the late calc-silicate assemblage (epidote by CRS).....	51
Figure 4.20. Epidote in late calc-silicate alteration (Sample taken from 432.9 m depth of ES-3) (2.5X).....	51
Figure 4.21. Epidote replacing pyroxene of early calc-silicate alteration (Sample taken from 432.9 m depth of ES-3) (10X).....	51
Figure 4.22. Tremolite (brown to red colored finer grained crystals) replacing early calc-silicate (Sample taken from 288.2 m depth of ES-9. Brc-slc-crb: Brecciated silicified carbonatized rock, Trml-Actl: Tremolite-Actinolite).....	52
Figure 4.23. Epidote, tremolite and calcite replacing early calc-silicate assemblage (Sample taken from 288.2 m depth of ES-9. Ept: Epidote, Trml: Tremolite, Actnl: Actinolite, Clc: Calcite, Brc-slc-crb: Brecciated silicified carbonatized rock.).....	52
Figure 4.24. Quartz crystals of late silicification (Sample taken from 288.2 m depth of ES-9).....	53

Figure 4.25. Composition of quartz from the late silicification (quartz by CRS)...	53
Figure 4.26. Late quartz filling fractures of silica in early silicification.....	54
Figure 4.27. Fine grained late quartz cutting early quartz and sphalerite (sph:sphalerite) .....	54
Figure 4.28. Calcite replacing, or filling the interstitial spaces of andradite crystals in early calc-silicate alteration (Sample taken from 271 m depth of ES-9).....	55
Figure 4.29. Silicification synchronous with late carbonate veinlet.....	55
Figure 4.30. Late calcite interstitial to garnet crystals .....	56
Figure 4.31. Relicts of andradite in late calcite and opaque mineral replacing andradite relicts.....	56
Figure 4.32. Calcite veining in brecciated, silicified, carbonatized rock (Sample taken from 438.9 m depth of ES-9. Slc+Crb+Brc: Silicification+Carbonatization+Brecciation, Ore min.:Ore minerals.).....	57
Figure 4.33. Photomicrograph showing textural relations among pyrite, galena, chalcopyrite, sphalerite (Sample taken from 403.1 m depth of ES-9. Sph+Chp: sphalerite including chalcopyrite exsolutions).....	60
Figure 4.34. Chalcopyrite (yellow) inclusions in sphalerite (light grey, centre) (Sample taken from at 262.2 m of ES-9).....	61
Figure 4.35. Euhedral pyrite (yellow, centre) replaced by galena (Sample taken from 406.5 m depth of ES-9. Gray color showing triangular pits) .....	61
Figure 4.36. Composition of iron sulfides the ore zone (pyrite by CRS).....	62
Figure 4.37. Sequential paragenetic diagram.....	62
Figure 4.38. NE-SW to E-W section using holes ES-9, ES-7, ES-6, ES-5, ES-2 and ES-4.....	63
Figure 4.39. N-S section using ES-3, ES-8, ES-1, ES-5 and ES-2.....	64
Figure 4.40. Drill logs of ES-8,1,5,2 (North to South).....	64
Figure 4.41. Drill logs of ES-1,5,6 (West to East).....	65

Figure 5.1. Major element characteristics of the volcanic rocks (discrimination lines are from (a) & (b): Irvine and Baragar (1971); (c): Gill (1981); (d) Peacock index (Peacock, 1931), (e) Maniar and Piccoli (1989)).....	67
Figure 5.2. Nomenclature of the volcanic rocks using discrimination diagrams (discrimination lines are from (a): Cox et al. (1979); (b), (c), (d): Winchester and Floyd (1977)).....	73
Figure 5.3. (a) multielement diagram (spidergram), and (b) REE pattern of the volcanic rocks (normalization values (primitive mantle and chondrite)are from Taylor and McLennan (1985)).....	74
Figure 5.4. Tectonic discrimination of the volcanic rocks in the Balya deposit (discrimination lines are from (a): Batchelor and Bowden (1985); (b) & (c): Pearce et al. (1984)).....	75
Figure 5.5. Major element distribution of ES-2 samples.....	77
Figure 5.6. Major element distribution of ES-3 samples (Slc: silicified).....	77
Figure 5.7. Major element distribution of ES-5 samples (Slc: silicification, crb: carbonatization).....	78
Figure 5.8. Isocon diagrams for samples no. B173 and 16923 (a: trace elements, b: major elements).....	80
Figure 5.9. Isocon diagrams for samples no. 16920 and 16923 (a: trace elements, b: major elements).....	81
Figure 5.10. Isocon diagrams for samples no. B173 and 16916 (a: trace elements, b: major elements).....	81
Figure 5.11. Isocon diagrams for samples no. B173 and 16920 (a: trace elements, b: major elements).....	82

## CHAPTER 1

### INTRODUCTION

This thesis study is concerned with genetical investigation of Balya- Balıkesir Pb-Zn mineralization. Although it is a well-known mineralization which has been mined since antique times, its genesis is a subject of current debate as to whether it is a skarn type mineralization or not. Within this framework, the present study focuses on the genesis of Balya Pb-Zn mineralization through petrographic and geochemical studies on cores obtained from the recent drillings by Eczacıbaşı Esan Madencilik.

#### 1.1. Purpose and Scope

This study is aimed to contribute to the understanding of the genesis of Balya-Balıkesir Pb-Zn deposit. For a better understanding of the genesis of Balya-Balıkesir Pb-Zn deposit, this study focuses on i) determination of the type and association of alterations hosting the mineralization, ii) determination of mineral paragenesis concerning mineralization and alterations, iii) establishing the geochemical characterization of volcanic host rocks, and alterations, and iv) revealing spatial distribution pattern of mineralization and alteration zones cut by different drillings. Within this study, drilling cores of 9 wells from different locations of study area were provided by Eczacıbaşı ESAN Madencilik. The core samples obtained from the drill holes were examined for their mineralogic-petrographic features and geochemical compositions.

#### 1.2. Geographic Setting

Study area is located about 50 km NW of the city of Balıkesir in the Biga Peninsula in NW Turkey (Figure 1.1) and is included in the Balıkesir-İ-19 quadrangle of the 1/100 000 scale topographic map of Turkey. Access to the vicinity is provided by an asphalt road separated from Balıkesir-Edremit main highway from a junction

towards north. The study area has moderate to high relief, and covered by moderate vegetation resulting in difficulties in exploration and field works. Maden Deresi is the main stream flowing along N-W direction in the area. Kırmızı tepe (397m) located to the eastern part of the area marks the highest peak at the mine site. Silicified dacite and limestones form the highland, whereas argillic zones generally form the low-lying to gentle topography. Mining operations and ore-dressing plant are located at the eastern, southeastern parts of the study area. Old smelting plant and remains of historical mining operation from a French company are situated at the NW of the mine site. Eczacıbaşı Esan Madencilik built a new facility for smelting and ore dressing to the SW of the ancient workings and shafts close to Kırmızıtepe. Local people do farming and agriculture for their living, and the recent mining operations by Eczacıbaşı Esan Madencilik appear to contribute to their annual incomes.

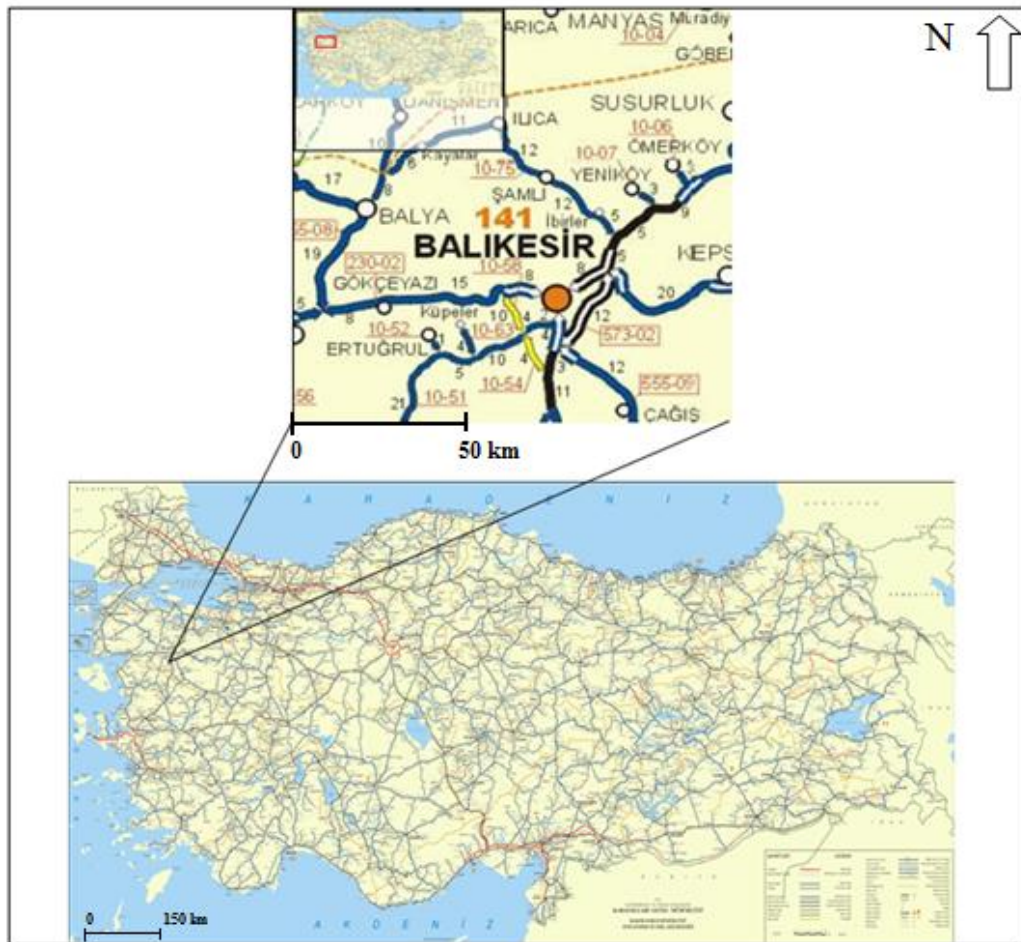


Figure 1.1 Geographic setting of the study area

### 1.3. Methods of Study

The objectives listed in the “Purpose and Scope” section are achieved by examining the core samples obtained from 9 recent drilling holes by Eczacıbaşı ESAN Madencilik in the Balya mine site close to the holes drilled by the General Directorate of the Turkish Mineral Research and Exploration (MTA) (Figure 1.2.)

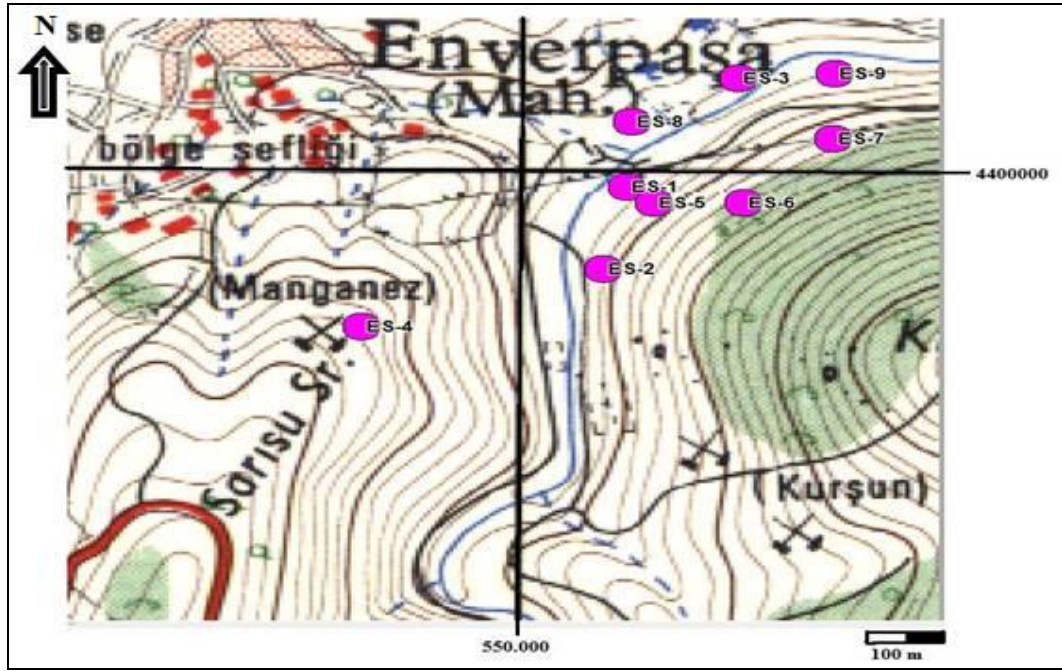


Figure 1.2 Distribution of drilling holes in study area (Topographic map:1/10000).

The sampling of the appropriate intervals through the drill cores are believed to fulfill the requirements for mineralogic and petrographic characteristics and geochemical data base. Although there is no certain sampling interval, a special attention was given to sample ore-bearing levels, and altered host rocks above and below the massive ore (sphalerite and galena)-bearing levels at the drill cores. Therefore, a total of 116 samples were collected from different rock types, alteration zones and ore body (Table 1.1).

The samples collected were prepared for geochemical and petrographical studies (transmitted and reflected light microscopy). The samples were grinded, crushed and powdered at Sample Preparation Laboratory of Eczacıbaşı ESAN Madencilik.

The thin and polished sections were prepared in the sample preparation laboratories of the Middle East Technical University (METU), Department of Geological Engineering (Ankara). Thin sections were examined using transmitted light microscope in Department of Geological Engineering, METU. The polished sections were examined using reflected light microscope in Ankara University, Department of Geological Engineering.

In addition to transmitted and reflected light microscopy, mineralogic-petrographic features of samples were further studied by Confocal Raman Spectroscopy (CRS) in Ankara University, Department of Geological Engineering. Confocal Raman Spectrometer is a well-known method for the analyses of minerals however; Raman confocal spectrometer has not yet been widely applied on ore bearing minerals identification and determination. Raman measurements were performed with a Horiba Jobin-Yvon equipped with a laser operating at a wavelength of 633 nm.

The major and trace element geochemistry was utilized in finding the geochemical tracers of the alteration, mass-balance calculations and element mobility during the alterations. The geochemical analyses necessary for this purpose were performed in the Activation Laboratories in Canada. Inductively Coupled Plasma Mass Spectroscopy (ICP/MS) and Inductively Coupled Plasma Optical Emission Spectroscopy (ICP-OES) were used for geochemical analysis. The entire sample is crushed to a nominal minus 10 mesh (1.7 mm) and then pulverized to at least 95% minus 150 mesh (106 microns) in Eczacıbaşı ESAN "Sample preparation laboratory". The major and trace element data was used to reveal the geochemical tracers, and element mobility (exchange reactions) along traverses in a few drill holes. For this purposes, the geochemical composition of the least altered samples for fresh volcanic rocks were compared with the geochemical composition of the alterations along traverses. This was done by preparing geochemical histograms for the major oxides and some trace elements. An isocon approach was also applied for the mass-balance calculations using isocon diagrams.

Tablo 1.1 UTM Coordinates of drilling wells which belongs to Eczacıbaşı-ESAN Mining (ES:ESAN sondaj).

<i>Well No</i>	<i>Easting</i>	<i>Northing</i>	<i>Sampling depths (in meter)</i>
ES-1	550120	4399975	33.6, 59.8, 157.3, 224, 386.9, 402.4, 433.9, 457.5, 476.3, 492.6, 496.1, 503
ES-2	550095	4399848	53.30, 126.2, 166.4, 178.3, 199.8, 203.7, 231.4, 252, 263.2, 272.9, 281.7, 305.7, 324.4, 350, 360.8, 386.10, 387.7, 396.4, 403.4, 413.9, 422, 426.8, 431.2, 437.9, 444.2, 456.4
ES-3	550243	4400142	161, 355, 391.8, 409.5, 427.2, 428.8, 429.8, 431.9, 432.9, 437, 455.6, 461.2, 483, 487.9, 499, 520
ES-4	549826	4399758	14.6, 32.6, 54.1, 88.6, 104.1, 127, 133.8, 145.6, 192.1, 214.2
ES-5	550150	4399950	12.3, 95, 103.8, 182.2, 215.8, 296.2, 309.5, 319.9, 330.7, 366.8, 382.6, 389.9, 413.8, 459.9
ES-6	550250	4399950	214, 250, 284.2, 310.4, 331.7, 377.4, 457.8
ES-7	550350	4400050	62.8, 137.1, 169, 215.2, 285.3, 306.8, 313, 366, 379.8
ES-8	550125	4400075	51.2, 145, 341, 367.8, 389.1, 416, 440.6, 465.4, 482.4, 491.6, 503, 512, 526.7
ES-9	550350	4400150	7.5, 19.4, 178.3, 233.6, 242.6, 246, 252, 256, 262.2, 270.1, 271, 272.2, 282, 298.8, 343.8, 353.7, 357.1, 365.8, 382.9, 403.1, 406.5, 438.9

The drill logs of previous drill holes by Esan were re-logged, re-classified on the basis of observed alteration mineralogy, and used for vertical and horizontal extend of alterations and ore-bearing levels. This contributed to a better understanding of spatial and temporal association of the alteration zones. Re-logging of the drill cores, and sampling was also accompanied by field geological mapping. The field works included revision of the geological map by Akyol (1979), and mapping of the prominent argillic alterations and silicification close to the present tunnel and smelting plant-site.

#### **1.4. Previous works**

The mineralization within the Balya area has been the continuous interest for ancient and modern miners leading to culmination of numerous studies for years. These resulted in publication of many articles and/or reports dealing with the observation

and findings about geology and mineral deposits of Balya. Some of these are summarized as follows;

Enderle (1900) did the first detailed investigation on limestones in the vicinity of Balya and found out that the limestones are Permo-Carboniferous in age.

Weiss (1901) and Berg (1901) claimed that mineral deposit is related with contact between augite-bearing andesite and Carboniferous limestones.

Phillipson (1915) established the first spatial-temporal relationships between the rocks of Paleozoic in age, and the volcanic rocks exposed in the region.

Kovenko (1940) identified 4 different types of mineral deposits as porphyric ore, mineralization in limestone, mineralization in between laminations of sedimentary rocks and contact veins.

Aygen (1956) claimed that contact type mineralization in Balya is of no economic importance.

Kaaden (1957) concluded that Balya mineral deposits are hosted along the contact zones of Tertiary volcanic rocks and other rock types exposed in the Balya area.

Mohr (1959) said that Tertiary formations consist of lavas, tuffs and dacitic-andesitic agglomerates and mineralization occurs between dacite and older sediments or contact zones close to dacite.

Gjelsvik (1962) stated that the rocks in the Balya consist of Permian limestone, Triassic shales, sandstones, and conglomerates, Tertiary volcanic rocks and said that “the complicated tectonics of the area is tentatively explained as a result of recumbent folding during the Alpine orogeny”.

Akyol (1979) explained that mineralization occurs both as skarn type along the contact between limestones and volcanic rocks, and as disseminations and veins in the volcanic rocks.

Ağdemir et al. (1994) reported that Balya thrust along which the Permian limestones are displaced over the Triassic series (resulting probably from recumbent folding) and the NE-SW and NW-SE trending normal faults are the major structural features of the Balya district.

The argillic /phyllic alteration stage is characterized by strong depletion in Na, Ca, Fe, Mg, Mn, P, Ba and Sr, and enrichment in Si, Sb and Rb relative to the unaltered host andesite. K shows sporadic enrichment. REEs, Sc, Ta, Th, Ti, Al, and Zr behave as relatively immobile elements. In order to determine the age of mineralization, Ađdemir et al. (1994) carried out whole rock K-Ar dating on samples from both the unaltered andesite and the (argillic/phyllic) alteration zones. The age data revealed a synchronous nature for the andesitic volcanism and the hydrothermal alteration, with a mean of  $25.3 \pm 1.2$  Ma, and suggested that the hydrothermal activity responsible for mineralization is genetically related to the Oligocene-Miocene aged calc-alkaline volcanism in NW Turkey.

Budakođlu and Pratt (2005) studied the sulfur isotope systematics, and reported that the values of  $\delta^{34}\text{S}$  for sulfides from Balya Mine ore, are mostly between -0.35 and 1.16‰ suggesting a deep magmatic origin.

## **1.5. Mining History**

The Balya Mine was the main producer of Pb and Zn in Turkey during the period 1880-1935. Its mining history goes back to antique times when the mine probably supplied the first known lead products to nearby Troy. It was mined on industrial scale from 1880 to 1939 by a French company (*Société des Mines de Balya-Karaaydın*). During that time smelting was done by an ore dressing plant (Figure 1.3) established by the French company. The Mining operations were done in 3 shafts and the total output of Balya was about 4 million metric tons (Mt) of ore, producing more than 400,000 tons of lead and 400,000 tons of zinc (Ađdemir et al.,1994). In between 1974 and 1979, 18 exploration boreholes were drilled in Balya over an area of around 26000 m<sup>2</sup>. On this basis, remaining ore reserve was calculated as 4.4 Mt with a grade of Pb+Zn+Cu around 7 %. Additional drillings until 1981 revealed an ore potential about 15 Mt (Ađdemir et al.,1994).

Recently, Eczacıbaşı by Eczacıbaşı ESAN Madencilik drilled 9 exploration wells in Balya between 2005-2006, and is currently having the exploration and exploitation licence in the area. Construction of new ore dressing plant and related infrastructure was recently completed, and the plant is fed by the ore since October 2009 (Figure 1.4 to1.5).



Figure 1.3. Old smelting plant for ore dressing established by the French Company



Figure 1.4. Mining base camp, and the smelting plant at the hill side, set up by Eczacıbaşı ESAN Madencilik



Figure 1.5. Ore dressing plant for ore production by Eczacıbaşı ESAN Madencilik.

## **1.6. Layout of Thesis**

This thesis contains 6 chapters. Following this introduction chapter, tectonic setting and regional geology of the study area are given in Chapter 2; local geology and an overview of the previous studies are presented in Chapter 3; mineralogic-petrographic features of wall rock alteration and mineralization are summarized in Chapter 4; geochemical data is presented in Chapter 5; conclusions reached in the study are given in Chapter 6.

## CHAPTER 2

### TECTONIC SETTING AND REGIONAL GEOLOGY

Turkey's present day geology and tectonic framework has been shaped by the separation, rotation, collision and deformation of many small continental fragments during the Alpine orogeny. These continental fragments are now bounded by suture zones representing the remnants of the closure of various branches of Neotethys (Şengör and Yılmaz, 1981; Bozkurt and Mittwede, 2001).

According to Okay and Tüysüz (1999), these continental fragments (Figure 2.1) are, from north to south;

- Pontides comprising Istranca and Rhodope Massifs and Sakarya Zone
- Anatolide-Tauride Platform comprising five major zones: i) Tavşanlı zone, ii) Afyon zone, iii) Bornova Flysch zone, iv) Menderes Massif, and v) Central Anatolian Crystalline Complex (CACC: Göncüoğlu et al., 1991) which is also known as Kırşehir Massif (Seymen, 1981).
- Arabian platform.

Within the framework of this classification, the studied area lies within the Biga peninsula (Figure 2.2) located in the Karakaya Complex (Okay and Göncüoğlu, 2004) which is situated as a belt in the Sakarya Zone. The Karakaya Complex is comprised of highly deformed and partly metamorphosed clastic and volcanic series of Permian and Triassic age (Figure 2.3) (Okay and Göncüoğlu, 2004).

In the regional context, the Karakaya Complex is overlain by younger sedimentary and volcanic rock associations of Tertiary age.

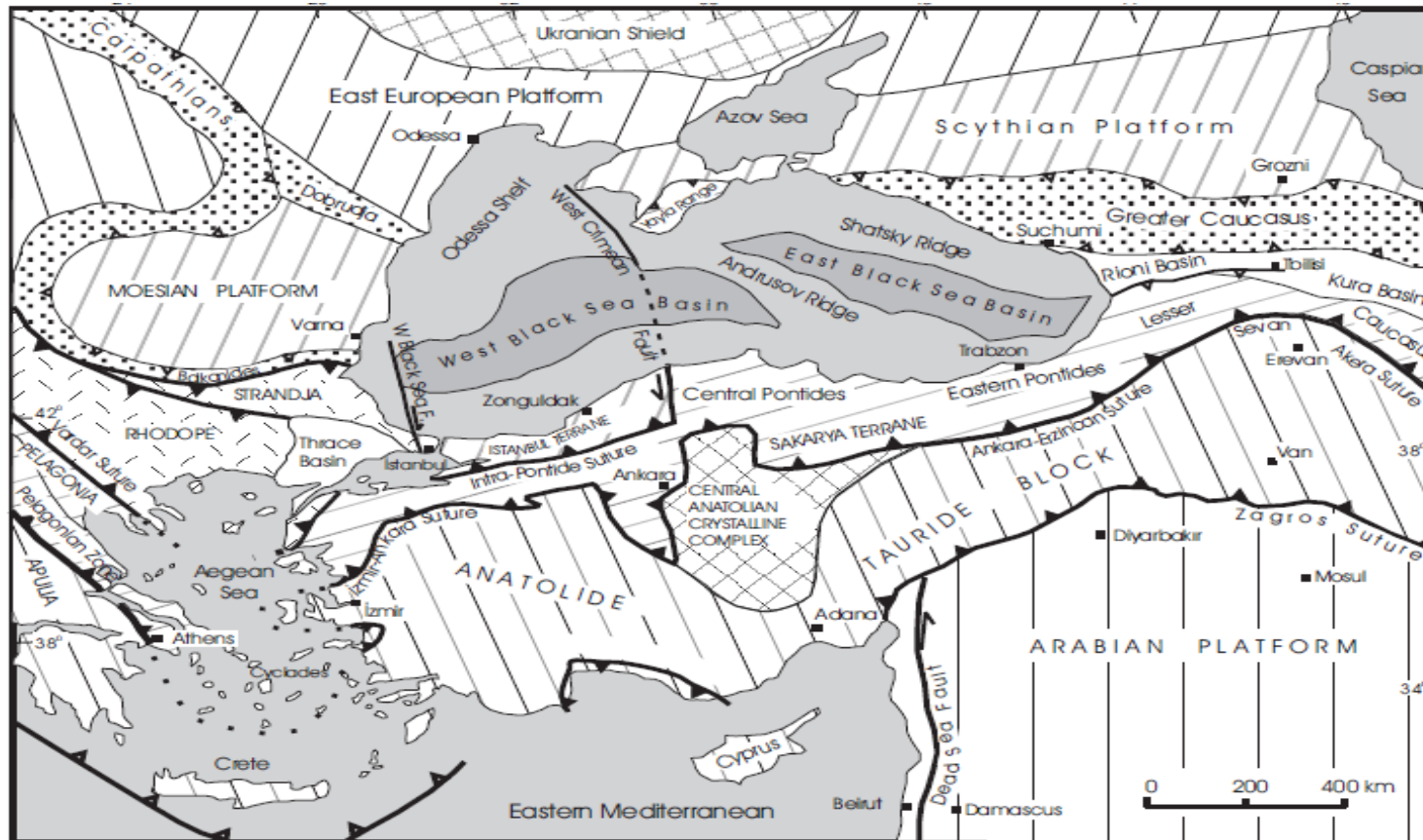


Figure 2.1. Tectonic map of the eastern Mediterranean region showing the major terranes and the bounding sutures. The filled triangles indicate the polarity of subduction (from Okay & Tüysüz, 1999)

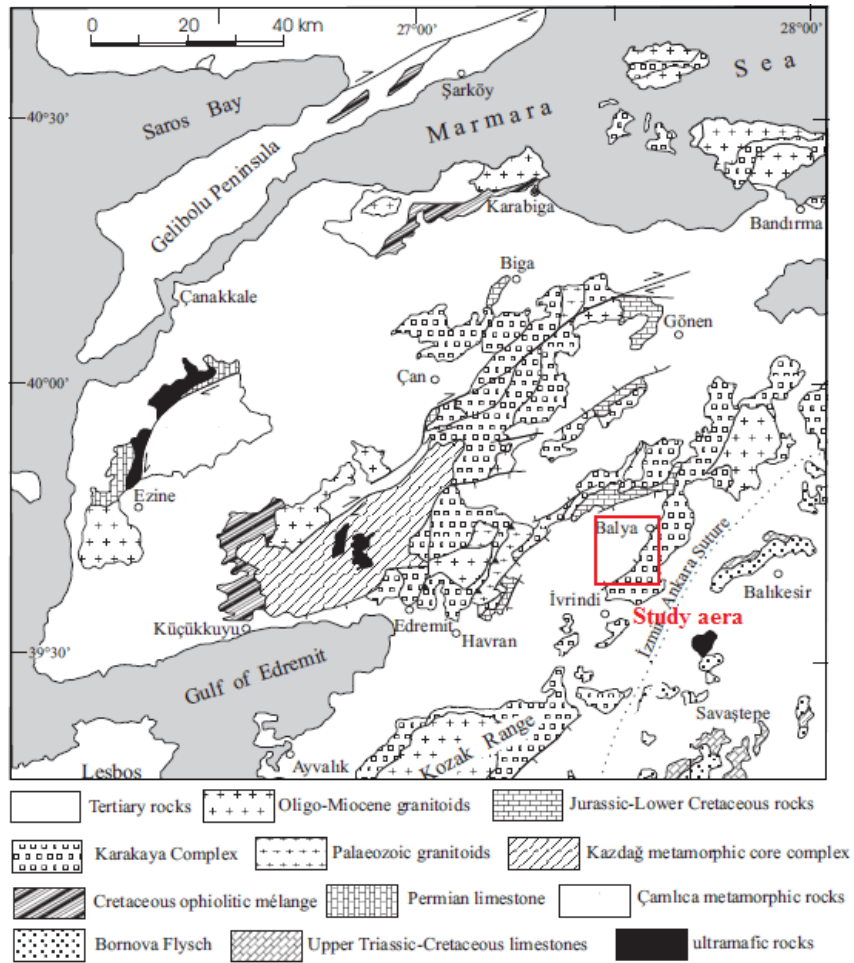


Figure 2.2. The geological and tectonic map of the Biga Peninsula and the surrounding region (Okay and Altıner, 2004)

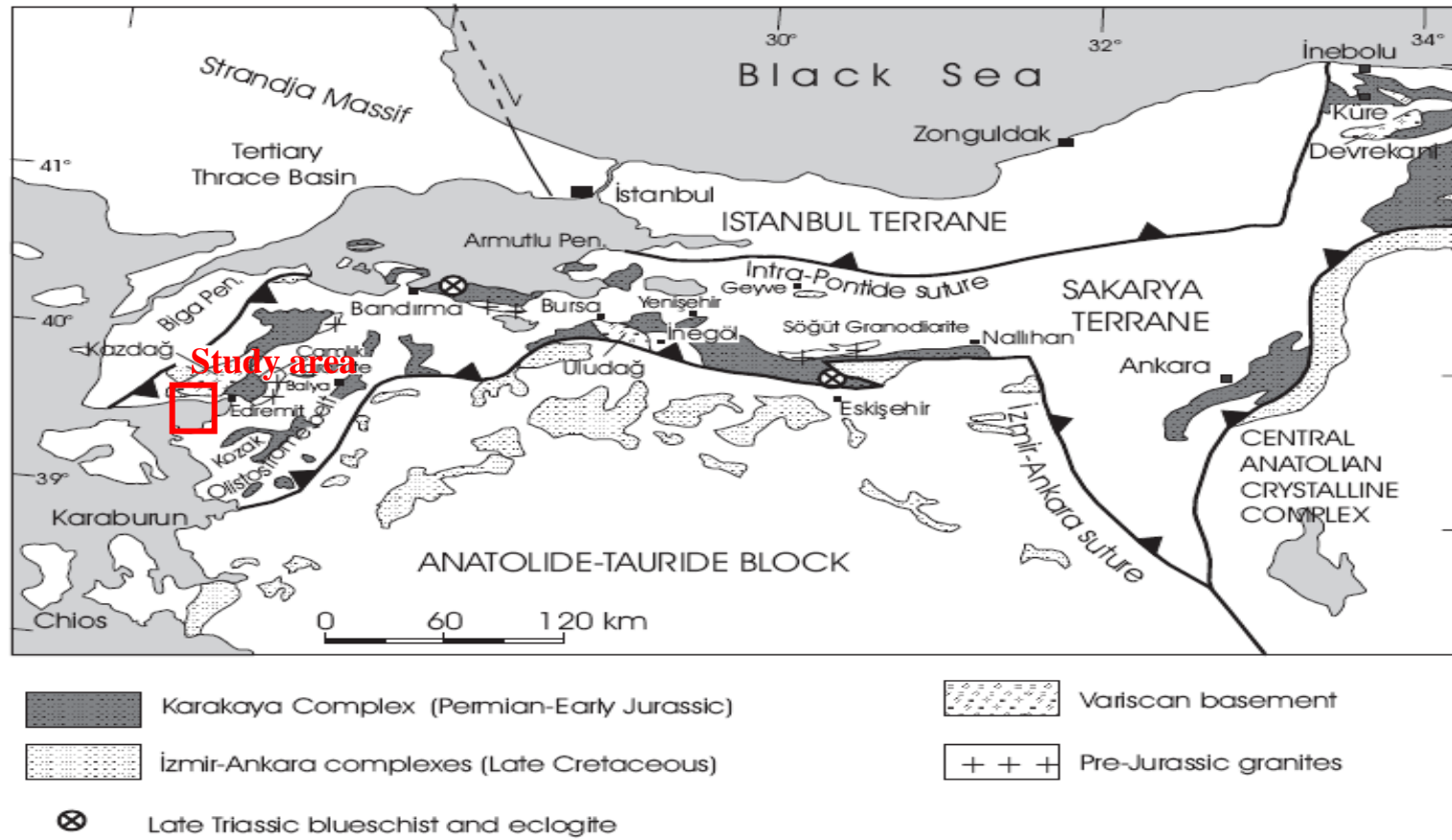


Figure 2.3. Tectonic map of western Anatolia showing the distribution of the Karakaya Complex and related units (Okay and Göncüoğlu, 2004).

As is summarized by Okay and Göncüoğlu (2004), there are two different models that explain depositional environment and tectonic evolution of the Karakaya Complex:

i) *Rift Model* (Bingöl et al., 1975; Şengör and Yılmaz, 1981; Şengör et al., 1984; Koçyiğit, 1987; Genç and Yılmaz, 1995; Göncüoğlu et al., 2000) assumes that the Karakaya Complex was deposited in a Late Permian rift, which developed into a small oceanic marginal basin, and closed in the Late Triassic, by southward subduction (Figure 2.4).

ii) *Subduction-Accretion Model* (Tekeli, 1981; Pickett and Robertson, 1996; Okay, 2000) assumes that the Karakaya Complex was formed by subduction - accretion of the oceanic crust during the Late Palaeozoic-Triassic (Figure 2.5).

The Karakaya complex is divided into two different tectono-stratigraphic units which are Nilüfer Unit and Hodul Unit. The Nilüfer Unit, comprising of strongly deformed, partially metamorphosed Permian-Triassic orogenic sequences (Tekeli 1981), is overlain by Hodul Unit that is strongly deformed but generally unmetamorphosed clastic sequences (Okay et al. 1991; Altıner et al. 2000).

Balya is situated in Hodul Formation of Karakaya Complex consisting of arkosic sandstone, siltstone, shale, carboniferous-permian limestone blocks, basalt blocks and olistostroms (Figure 2.6) (Akyol 1982; Okay et al. 1991). In the Hodul Unit, arkosic sandstones are intercalated with shales and siltstones, which pass upward into olistostromes and debris flows with blocks of basalt (Akyol 1982; Okay et al. 1991; Leven and Okay 1996). A several-hundred-meter thick and thickly bedded massive arkosic sandstones of the Hodul Unit are exposed at the northeast of Balya. These sandstones grade into greywackes with numerous Upper Permian neritic Limestone blocks up to one kilometer in size (Okay et al. 1991). Block of Carboniferous chert and pelagic limestone described from the arkosic sandstones are also exposed at the northeast of Balya (Okay and Monstler 1994)

THE KARAKAYA COMPLEX

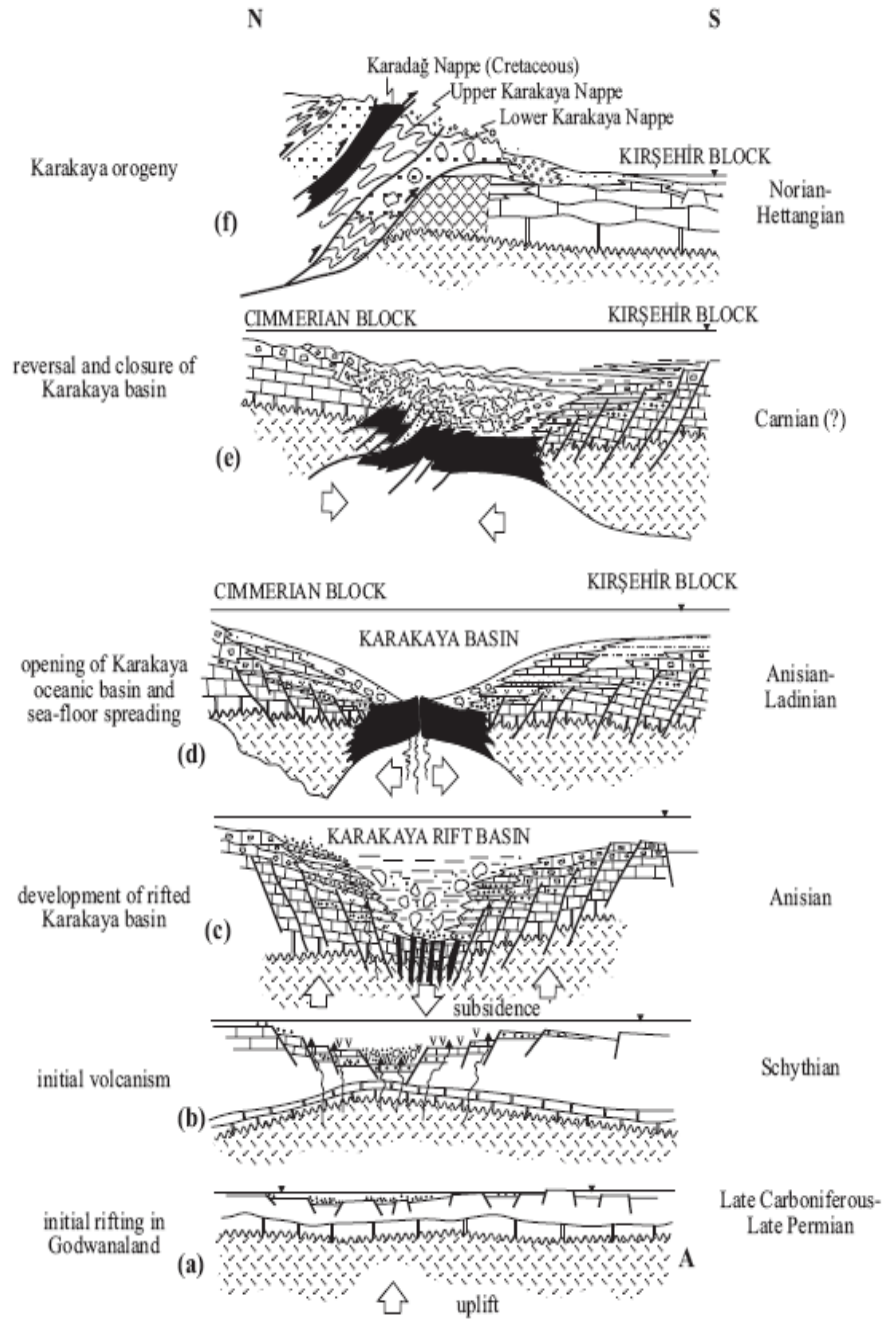


Figure 2.4. Rift model for the evolution of the Karakaya Complex (Koçyiğit, 1987).

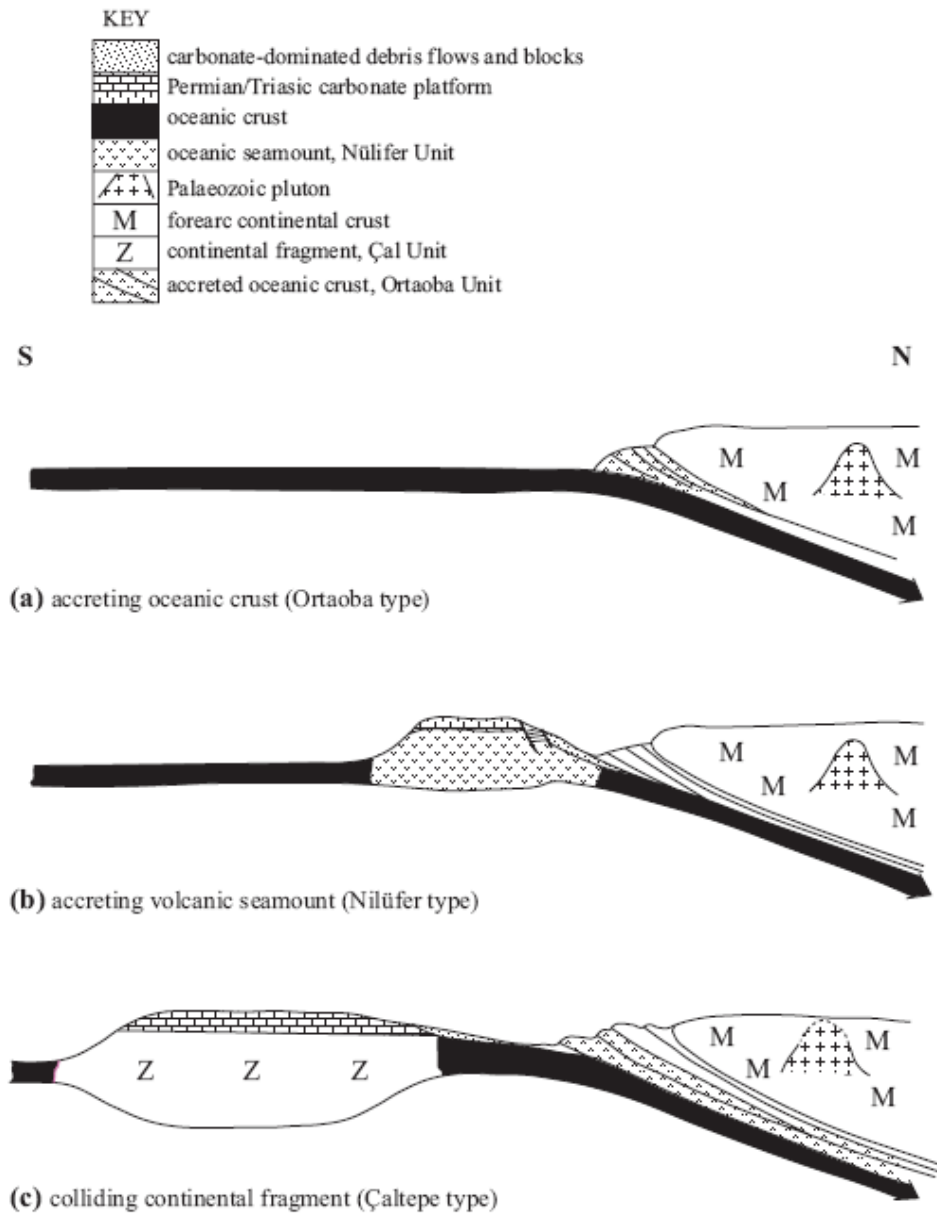


Figure 2.5. Subduction-accretion model for the evolution of the Karakaya Complex (Pickett & Robertson 2004).

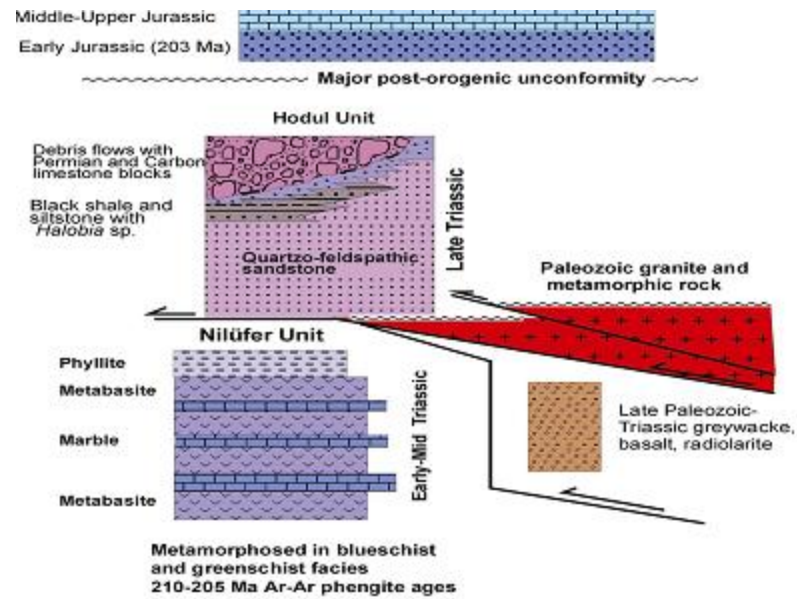


Figure 2.6. Pre-Jurassic tectono-stratigraphic units in Sakarya Zone, Turkey (Okay 2000)

The Karakaya Complex forms the basement for the Tertiary sedimentary and volcanic activities. These occur as younger unconformable rock units covering the older rock associations of the complex.

Tertiary sedimentary activities resulted in the formation of a very thick sedimentary series in Biga Peninsula. The most important lithological units formed during this period are turbiditic sediments consisting of sandstone, mudstone, limestone and marl of Eocene age (Ercan et al., 1998). Andesite, dacite and rhyodacite of Eocene age, produced by calc-alkaline volcanic activity, have irregular contact with Eocene sediments. Lower-Middle Miocene sediments are characterized by bituminous shale, claystone with coal interclations, siltstone and sandstone in the area. Conglomerates, sandstone, shale and limestone were deposited during Late Miocene-Pliocene and point out fluvial environment.

The Tertiary volcanism is intensive in Biga Peninsula and all around the western Turkey. Tertiary volcanic activities firstly started in Eocene time within the Biga Peninsula. Eocene volcanics which are locally intercalated with Middle Eocene aged sedimentary rocks are exposed in between Biga and Çanakkale. These volcanics consist of dacite-andesite, tuffs, agglomerates.

Eocene volcanism of the region is of calcalkaline arc volcanism originated from subduction zone. A new volcanic activity has started to be effective in the medial and eastern parts of the Biga Peninsula and locally in the vicinity of Gökçeada and Altınoluk from Late Oligocene onwards (Ercan et al., 1998). Oligocene volcanism is characterized by andesitic, dacitic, trachy-andesitic and rhyodacitic rocks which were altered over a large part of peninsula. This volcanism caused formation of most of the metallic mineral deposits of NW Anatolia. Miocene volcanism of the Biga peninsula has occurred in two episodes. An intensive volcanism, generating andesitic, dacitic, rhyodacitic, trachyandesitic and basaltic lavas, tuffs, agglomerates and ignimbrites, took place in the Biga peninsula in different stages during Early-Middle Miocene. During Late Miocene a new episode of volcanism occurred in the Biga Peninsula producing trachyandesitic rocks and alkali olivine basalts (Ercan, 1995). These volcanics are exposed as dykes cutting the previous Tertiary volcanics, or as lava flows in the vicinity of Ezine, Ayvacık, Çanakkale, Çan and Tavşan islands (Ercan et al., 1998). Upper Miocene volcanism is of alkaline character originated from the mantle.

The products of the Tertiary volcanism have widespread exposure in Balya and vicinity, and it is considered that this volcanism has relations with NE-SW trending faults in the area (Akyol, 1979). Dacite and andesite are the most common volcanic rock types in Balya. Mineralization in the area is genetically related with dacitic Tertiary volcanism.

## CHAPTER 3

### LOCAL GEOLOGY

#### 3.1. Rock Units

In the study area, mainly two different rock units are exposed; (1) rock units from the Karakaya Complex (marl-sandstone-shale alternation at the base, Permian limestone as blocks within the Karakaya complex, and conglomerates) and (2) Tertiary volcanics, mainly dacites and andesites (Akyol, 1979; Ağdemir et al., 1994) (Figure 3.1).

#### 3.2. Rock units of the Karakaya Complex

##### 3.2.1. Fine grained sedimentary rocks

Upper Triassic sedimentary rocks are exposed in the eastern, western and southern parts of the Balya district (Fig. 3.1). The rocks consist of shale-marl-siltstone-sandstone alternation, containing blocks of Permian limestones (Akyol, 1979; Ağdemir et al., 1994) which are reported to have displaced over the Triassic series along a thrust zone (Ağdemir et al., 1994). Akyol (1977) reports the presence of traces of macrofossils in the cemented, carbonate rich, sandy and silty series. Sandstone is comprised of coarse grained, rounded, monocrystalline quartz (45%), along with shale, chert, siltstone and orthoclase clasts, magmatic rock fragments, and cement (55%); in shale-siltstone levels, silt sized quartz crystals are disseminated in cement consisting of micritic calcereous shale (Akyol, 1977).

##### 3.2.2. Limestone

Permian limestone is found as blocks within the fine grained sedimentary rocks of the Triassic series, and as an allochthonous cover of the Triassic series.

Limestones are overlain by Tertiary calc-alkaline volcanics comprising part of the dacite-rhyolite sequence of regional extent (Akyol, 1979; Ağdemir et al., 1994). In the study area, limestone blocks are also observed in dacitic flows. Allochthonous limestone cover and massive recrystallized limestone blocks have gray to black color. Fossil rich allochthonous limestone contains calcite veins and veinlets (Figure 3.2); vein type mineralization is placed in irregular fractures of fossil-rich limestone (Figure 3.3).

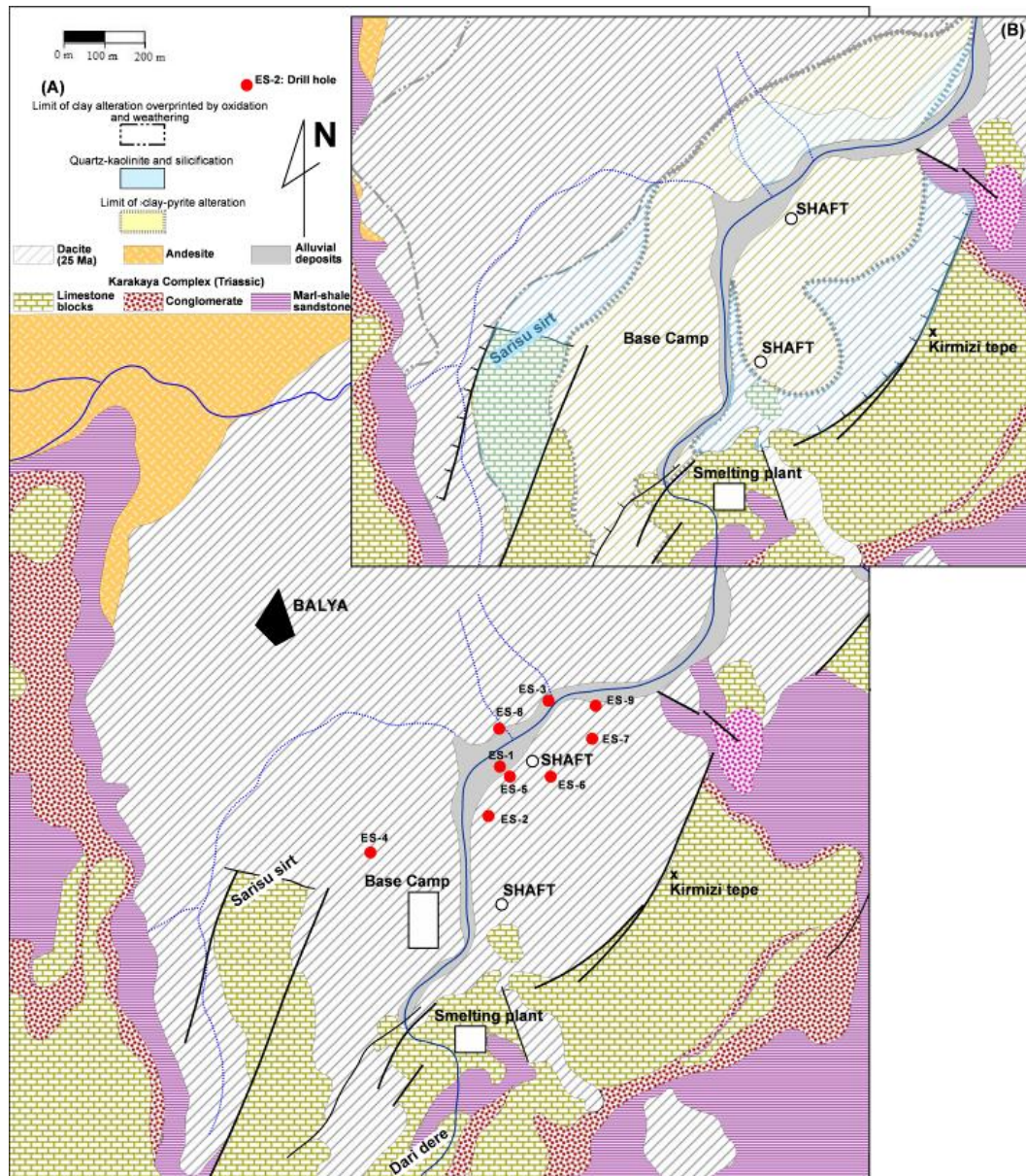


Figure 3.1. Geological map of the Balya Mine district (A) showing the main rock types (Modified from Akyol, 1979) and locations of the drill holes used for sampling, (B) alterations



Figure 3.2. Recrystallized limestone with calcite veins and veinlets



Figure 3.3. Manganese veins in Permian Limestone

### 3.2.3. Conglomerates

Conglomerates comprise the upper levels of the Triassic series and are located just below the Permian limestone (Aygen, 1956, Akyol 1977). Effects of tectonism are observed along the contact between the conglomerates and the Permian limestone. Conglomerates consist of yellow-brown and locally gray colored pebbles (0,8 mm to 1,5 cm) comprising clasts of microcline, orthoclase, albite and quartz, and fragments of hornfels, graphic granite, quartzite, micaschist, gneiss and Permian limestone (Aygen, 1956, Akyol 1977, 1979).

### 3.3. Volcanic rocks

Andesites and dacites are widely exposed in the Balya district. Permian and Triassic formations are cut by andesite and dacite, and andesites cut dacites around Kırmızı Tepe and south of Darıderesi (Aygen, 1956, Akyol 1977). Dacite has light gray to white color with the effect of hydrothermal alteration. In the study area, dacite is generally argillized and silicified particularly along the E-W trending fault contact between limestone of Karakaya Complex at the top of the Kızıltepe and Sarısu sırt (Figure 3.4). It has porphyritic texture and consists of quartz, K-feldspar, plagioclase and biotite phenocrysts and very fine-grained matrix comprising quartz crystals, altered feldspars and volcanic glass. Apatite occurs as accessory mineral. Quartz crystals are generally corroded, rounded and unhedral in shape. K-feldspars (sanidine) and plagioclases are subhedral. The altered dacite contains pyrite disseminations. Andesites have porphyritic texture and gray to dark gray color. They are comprised of hornblend, augite and zoned plagioclase phenocrysts and matrix including plagioclase, hornblend, biotite microlites and volcanic glass. Hydrothermal quartz and calcite are locally observed in andesites. Based on cross-cutting relation between andesite and dacite, andesites are younger than dacites (Aygen, 1956, Akyol 1977).

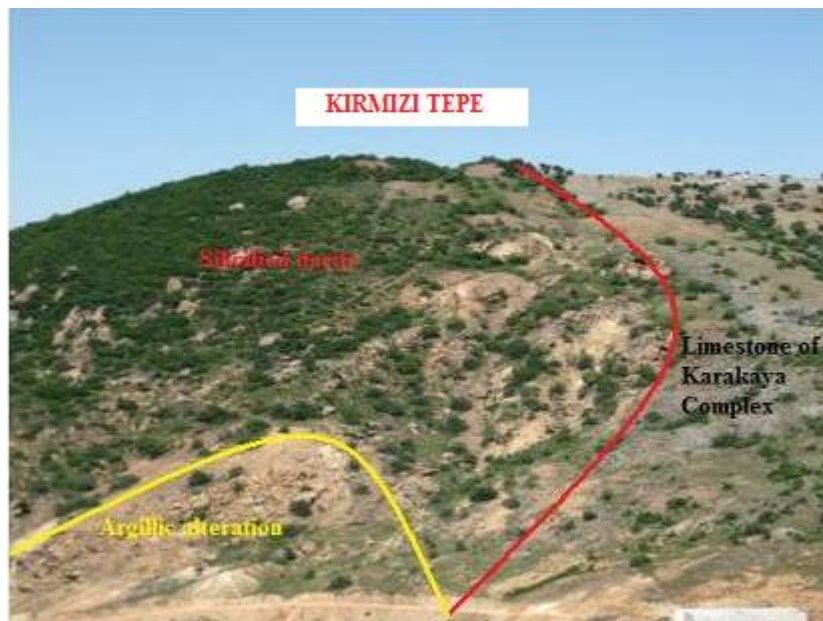


Figure 3.4 Contact between silicified dacite and limestone of Karakaya Complex in Kırmızı Tepe (E-W).

### **3.4. Structural Geology**

The major structural features of the Balya district are reported to be the Balya thrust along which the Permian limestone is displaced over the Triassic series (resulting probably from recumbent folding; Aygen, 1956) and the NE-SW and NW-SE trending normal faults (Ağdemir et al., 1994). The Balya thrust is not exposed in the study area. The Permian limestone that was subjected to recumbent folding whose axial plane dips to NW indicates that the whole sequence was compressed by an E to SE vergent pressure (Aygen,1956; Gjelsvik, 1962). In the Balya, there are at least two fold systems whose axes trend approximately in N-S and E-W directions (Gjelsvik,1962).

Major fracture zone in the study area is a normal fault called “Büyük Fay” passing through Kırmızı Tepe. This fault is located along the contact between Permian Limestone-Triassic series and Tertiary dacite. The previous works agree that this fault is an older structure, and provided a conduit for the dacitic volcanism en route to surface (Akyol 1977). The lacking of intense deformation and shearing on the dacites along the fault, are regarded as supportive evidence suggesting this fault was used as pathway for the volcanism (Akyol, 1977).

## CHAPTER 4

### MINERALIZATION AND ALTERATION

#### 4.1. Mineralization

The previous works argue that there are three main types of mineralization in the district, although all of these were not recognized in the present study. These types are skarn type, disseminations and veins hosted mainly by the volcanic and older rocks in the Balya district. Of these mineralization types, skarn has been regarded as the predominant one with more economic value compared to other types. Given below is a summary of the mineralization types as reported by the previous researchers.

Skarn type mineralization is irregular in shape, and is mainly confined to structural discontinuities within the volcanic rocks. This type also occurs along zones of weakness to the immediate contact between volcanics and older sediments, and in fractures of limestones situated near the contact. These zones are believed (Akyol, 1979) to have “*facilitated the transfer of ore forming fluids and gases responsible for mineralization which is thought to be related to an intrusion placed at the depth*”. Existence of the large pervasive alteration, continuity of mineralization towards the depth and disseminated type mineralization placed in the fractures of volcanics are regarded as the supportive evidence for a deeper intrusion (Akyol, 1979). “Skarn” type mineralization zones are not exposed at the surface, or they are deeply oxidized at the surface conditions so as to their original mineralogy and texture have been obscured. They could only be determined at the drill cores as being spatially associated with a dark colored subvolcanic intrusion of microdiorite or Hb-phyric andesite. The “skarns” are in the form of planar occurrences hosted by strongly silicified and carbonatized dacite and dacite porphyry.

Their thickness ranges from a few cm to several meters. Major ore minerals in the “skarns” are galena and sphalerite; chalcopyrite and pyrite are subordinate, chalcopyrite being enriched with depth. The “skarn” assemblage consists of epidote, quartz, calcite, garnet, chlorite, tremolite, clinozoisite and hedenbergite (Akyol, 1979).

Disseminated type mineralization is restricted to the weathered zones of volcanic rocks where silicification and sericitization predominate. Pyrite, galena and sphalerite are the predominant minerals of this type. This type has no spatial association with the skarn type, and occurs as isolated masses within the altered dacite and dacite porphyry in between the carbonatized and skarnified dacite. According to Gjelsvik (1957), the largest primary ore bodies are 100-300 m below the present surface. Galena is the predominant mineral in the upper parts of the primary mineralization zone, sphalerite increases downwards (Ağdemir et al., 1994). This type has been occasionally recognized during the field and petrographical works in the present study. The disseminations are usually confined to hanging wall of the ore zones with prominent carbonate minerals.

Vein type mineralization is placed in irregular fractures of limestone blocks and joints of volcanics. Limestone fractures contain galena, sphalerite, antimonite, pyrite, realgar and orpiment. The joint zones of volcanics contain pyrite, galena, sphalerite, realgar and orpiment (Akyol, 1979).

Although the presence of disseminated and vein type mineralization, along with skarn type, was reported in the literature as summarized above, in the present study, during the field work and petrographical analyses, only the calc-silicate (“skarn”) type was identified along with very limited vein and dissemination type mineralization.

#### **4.2. Wall Rocks**

The known mineralization in the Balya Pb-Zn deposit is strictly associated with 3 major rock types; limestone, dacite and a subvolcanic intrusion of microdiorite. The limestones appear to have acted as chemical and physical barriers preventing the discharge of the ore-bearing hydrothermal solutions.

The limestones are exposed at the SE parts of the area and juxtaposed with the silicified dacite along steeply dipping normal fault that traverses the Kırmızı tepe hill (Figure 3.1). The limestones occur either as silicified masses in contact with the dacite or as silicified blocks within the dacite flows particularly at the Sarisu hill. The blocks within the dacite flow are underlain by pyrite-quartz-sericite bearing alterations which were later oxidized to form acid-leaching of the limestone and intense manganese oxide-hydroxide and halloysite (personel communication with İ.Kuşçu) concentrations at and around the Sarisu hill. In such locations, the limestones are observed as intensively altered rocks with relicts of original calcite minerals.

The dacitic rocks, occurring as dacite and dacite porphyry, are the most common wall rock for the alterations and mineralization. These are exposed mostly as argillized, silicified and weathered rocks with a typical yellowish brown colored exposure all over the study area. The argillized and silicified dacite have spatial association at the southern parts of the area where the new smelting plant has been constructed, whereas argillized and weathered dacite crop out at the vicinities of the ruins of ancient smelting plant to the northern part of the study area, and at the Balya city center. The dacite and/or dacite porphyry is frequently intruded by dark colored, finer grained subvolcanic plugs or dikes, and there is a spatial and temporal association between this intrusion and “skarn” pockets within the dacite.

The least altered dacite consists of quartz, plagioclase and sanidine with oxidized mafic minerals, probably biotite and/or hornblende. The rock has a porphyritic texture. Matrix is made up of plagioclase microlites. Quartz occurs as typical corroded volcanic quartz phenocrysts (Figure 4.1). Plagioclase is observed either as microlites in the matrix or phenocrystal assemblage with typical albite twinning. Hornblende is largely altered to chlorite. The biotite is bleached and leached out to form biotite ghost and ironoxide-hydroxide stained pseudomorphs.

Subvolcanic mafic intrusion is observed in most of the drill holes as is revealed by the examination of the drill cores. It is spatially associated with silicified-carbonatized dacite and is found in contact with calc-silicate alteration (“skarn”). It has dark green color, porphyritic texture and consists of hornblend, plagioclase and

biotite phenocrysts and very fine grained matrix (Figure 4.2). Silicification, argillization and carbonatization appear to have commonly affected this subvolcanic rock and most of the hornblend and biotite phenocrysts and microlites of the rock seem to have altered to epidote and chlorite.

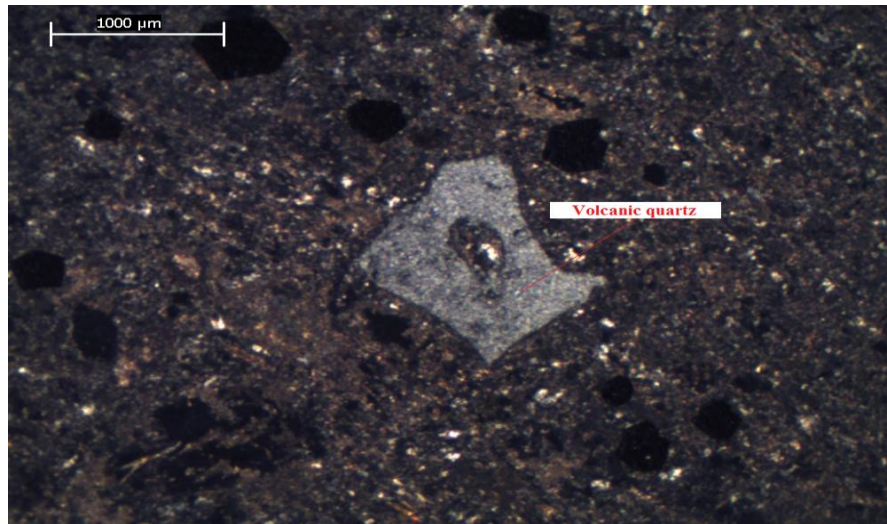


Figure 4.1. Typical volcanic quartz in dacite. (Sample taken from 19.2 m depth of ES-9)

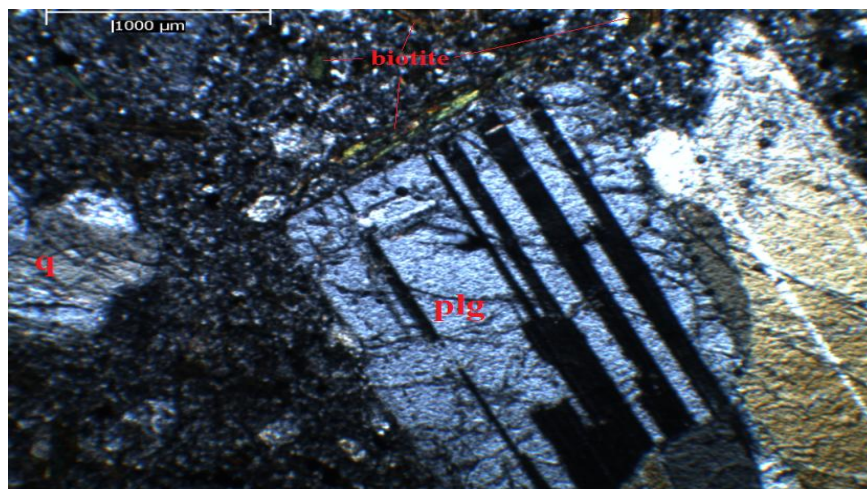


Figure 4.2. Microdiorite (Sample taken from 233,6 m depth of ES-9, plg: plagioclase, q:quartz)

### 4.3. Wall Rock Alteration

Alteration petrography in the Balya Mine was previously studied by Ağdemir, et al. (1994) who suggested three alteration styles i) Argillic/phyllitic alteration, ii)

Advanced argillic alteration, and iii) Propylitic alteration. These zones as defined by Ađdemir et al. (1994) are summarized as follows.

*I. Phyllic alteration:* This alteration is said to be at the central part of the hydrothermal system, and is overprinted mainly by argillic alteration. The characteristic hydrothermal mineral assemblage consist of fine grained sericite and quartz. Fine grained pyrite occurs in subordinate amounts. Accessory minerals are rutile, zircon, titanite, and green tourmaline.

*II. Advanced argillic alteration:* The characteristic hydrothermal mineral assemblage consist of alunite and jarosite together with quartz , kaolinite and sericite. Rutile, zircon, titanite and rare fined-grained pyrite also occur as subordinate mineral assemblage. Ađdemir et al. (1994) report that the samples of the advanced argillic alteration are not spatially distinguished from the samples of argillic/phyllic alteration because the advanced argillic alteration locally overprints the argillic/phyllic alteration in patchy zones.

*III. Propylitic alteration:* This is accepted as the outermost zone of the hydrothermal alteration by Ađdemir et al. (1994). The rock fabric is porphyritic with primary magmatic phenocrysts of rounded and corroded quartz, plagioclase (albitized, carbonatized and sericitized), relicts of biotite, hornblende (intensely chloritized and carbonatized, and locally replaced by rutile and fine grained pyrite) and very rare augite. Accessory minerals include epidote, apatite, zircon and titanite.

In the present study, the alteration zones described by Ađdemir et al. (1994) were not detected during the field work, since most of them are superimposed by argillic alteration and surface oxidation due to weathering effect of pyrite-bearing sericitic zones. In the regional scale, the only alterations that could be mapped from the surface exposures in the study area are argillic alteration and silicification (Figure 3.1). However, these two types are not homogeneous in terms of alteration mineralogy, and contain numerous, small-scaled alterations with characteristic mineral assemblages determined via the examination of the drill core samples collected from the 9 drill holes. The study of the mineralogic and petrographic characteristics of the drill core samples was performed using transmitted light microscopy, reflected light microscopy and Confocal Raman Spectroscopy (CRS).

Based on the alteration mineral assemblage and the textural features such as cross-cutting and replacement relationships, the alterations in the study area could be given, from the oldest to the youngest as (1) early silicification, (2) early carbonatization, (3) calc-silicate alteration (as early and late), (4) late silicification, (5) late carbonatization, and (6) argillic alteration that overprinted all of the alterations. The general characteristics and distribution of the alterations studied on the drill core samples from 9 drill holes, along with the least altered (fresh) rocks are given in Figure 4.3 to 4.5 and Table 4.1 to 4.9.

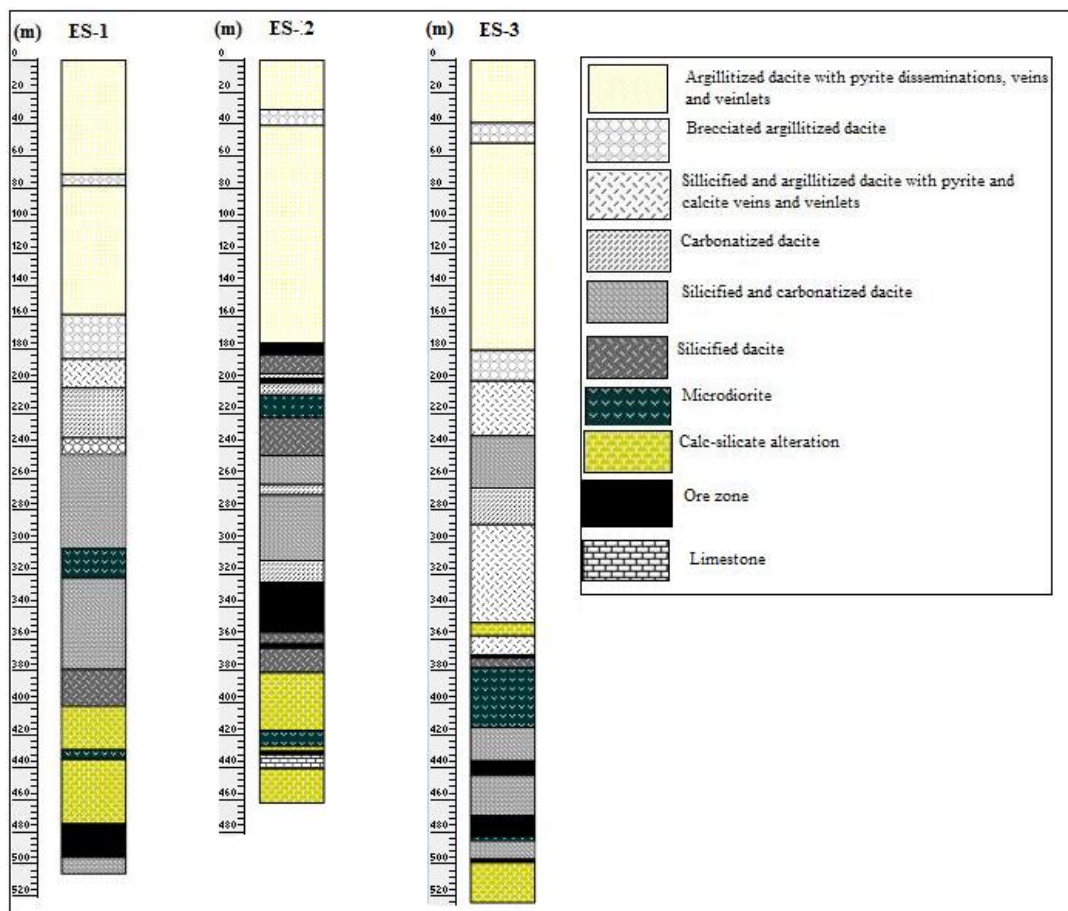


Figure 4.3 Drill logs of ES-1, ES-2 and ES-3

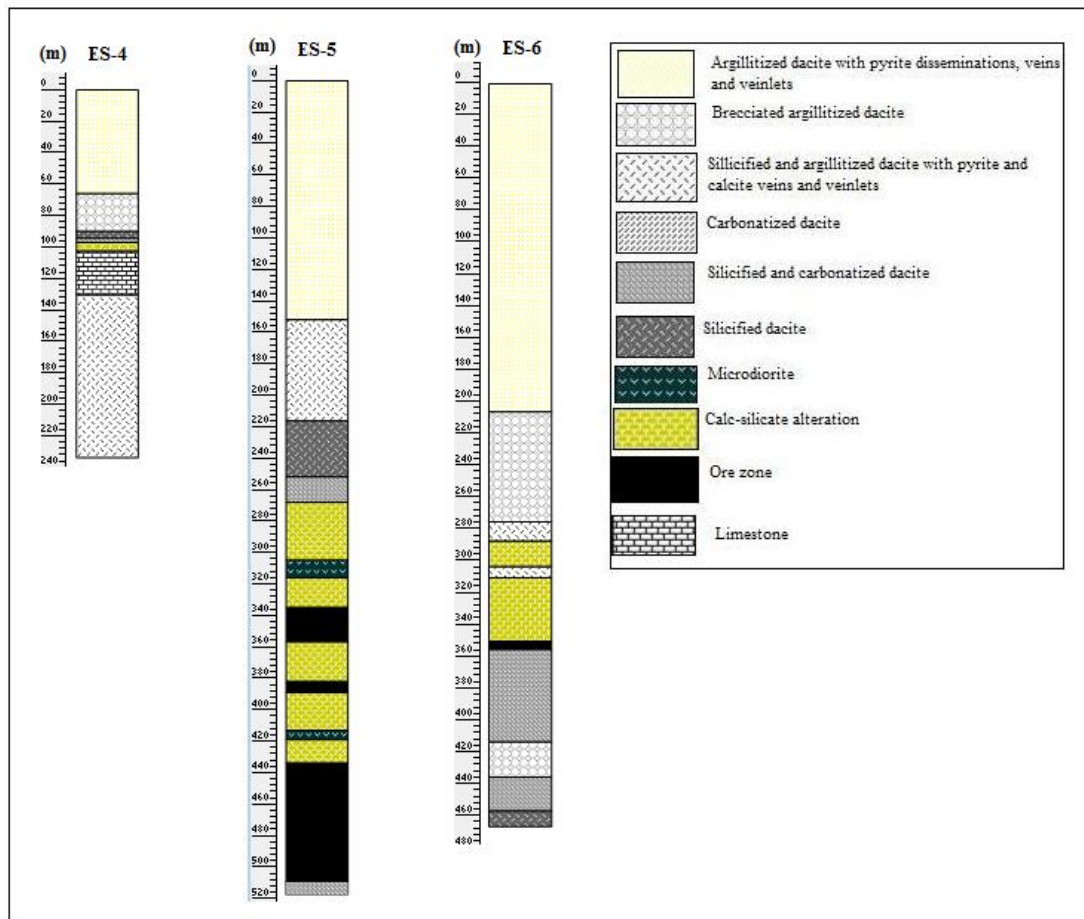


Figure 4.4 Drill logs of ES-4, ES-5 and ES-6

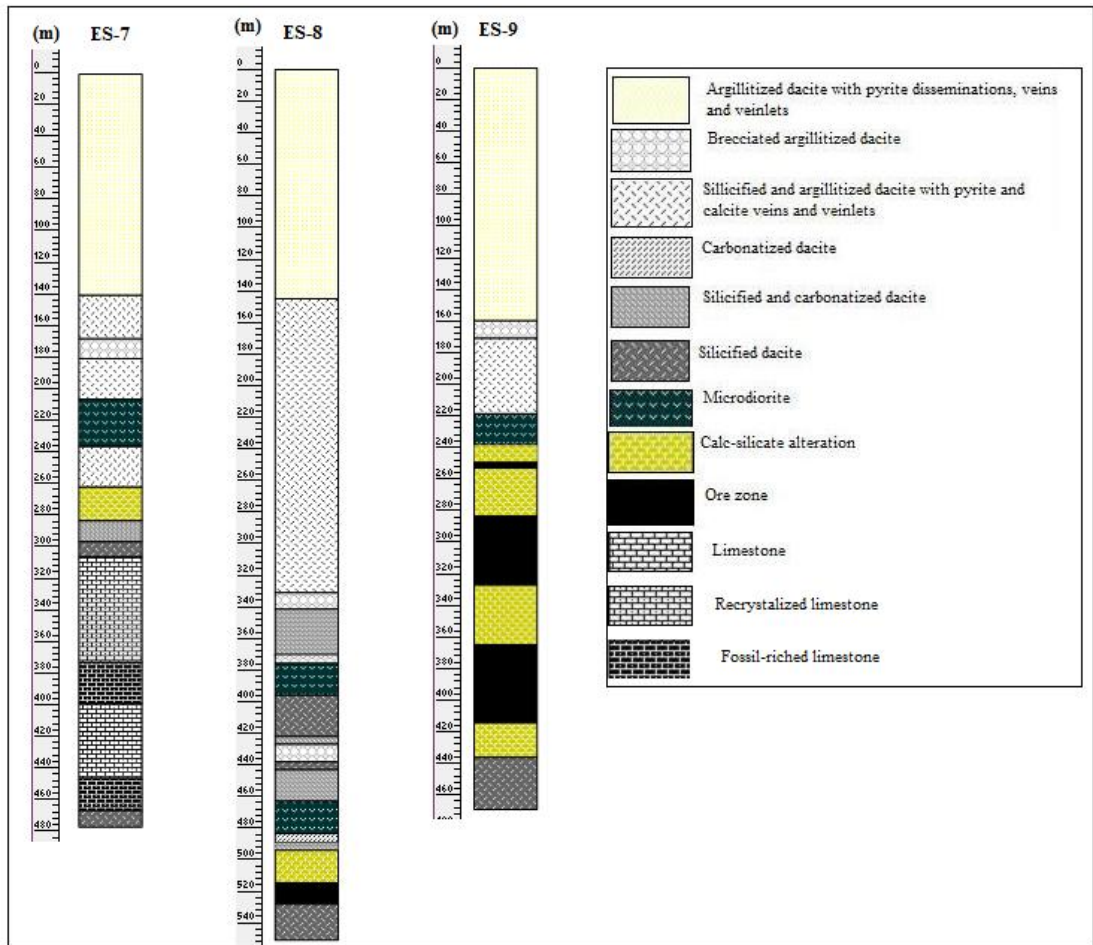


Figure 4.5 Drill logs of ES-7, ES-8 and ES-9

Table 4.1. Description of samples taken from drill hole ES-1

Depth	Sample No	Lithology/Alteration	Paragenesis	Texture
33.60 m	Es-1-1	Argillitized and brecciated dacite	Quartz, kaolinite, disseminated pyrite	Porphyritic, breccia
59.80 m	Es-1-2	Argillitized and brecciated dacite	Quartz, kaolinite, disseminated pyrite	Porphyritic
157.3 m	Es-1-3	Argillitized and brecciated dacite	Kaolinite, disseminated pyrite	Porphyritic
224 m	Es-1-4	Carbonatization, Argillitized and brecciated dacite	Quartz, calcite kaolinite, disseminated pyrite	Porphyritic, breccia
386.9 m	Es-1-15	Silicified and carbonatized dacite	Quartz, calcite, disseminated pyrite	Porphyritic
402.4 m	Es-1-17	Calc-silicate alteration	Andradite, epidote, calcite, quartz, pyrite, galena, sphalerite	Breccia
433.9 m	Es-1-18	Microdiorite	Plagioclase, hornblende, biotite	Porphyritic
457.5 m	Es-1-19	Calc-silicate alteration	Andradite, quartz, calcite, pyrite, galena, sphalerite	Replacement
476.3 m	Es-1-20	Ore zone	Pyrite, galena	Massive
492.6 m	Es-1-21	Ore zone	Pyrite, galena, sphalerite, calcite	Massive
496.1 m	Es-1-22	Ore zone	Pyrite, galena, sphalerite, quartz, calcite	Massive
503 m	Es-1-23	Silicified and carbonatized dacite	Quartz, calcite, disseminated galena and sphalerite	Breccia

Table 4.2. Description of samples taken from drill hole ES-2

Depth	Sample No	Lithology/Alteration	Paragenesis	Texture
<b>53.30 m</b>	Es-2-1	Argillitized dacite	Quartz, kaolinite, pyrite disseminations, veins and veinlets	Porphyritic
<b>126.2 m</b>	Es-2-2	Argillitized dacite	Quartz, kaolinite, pyrite disseminations, veins and veinlets	Porphyritic
<b>166.4 m</b>	Es-2-5	Argillitized dacite	Quartz eyes, kaolinite pyrite disseminations, veins and veinlets	Porphyritic
<b>178.3 m</b>	Es-2-6	Ore zone	Calcite, pyrite, galena, sphalerite	Breccia
<b>199.8 m</b>	Es-2-7	Ore zone	Quartz, calcite, pyrite, galena, sphalerite	Breccia
<b>203.7 m</b>	Es-2-9	Carbonatized dacite	Calcite, quartz	Porphyritic
<b>231.4 m</b>	Es-2-10	Silicified dacite	Quartz, calcite veins and veinlets	Porphyritic
<b>252 m</b>	Es-2-11	Silicified and carbonatized dacite	Quartz, calcite, disseminated pyrite	Porphyritic
<b>263.2 m</b>	Es-2-12	Silicified and carbonatized dacite	Quartz, calcite, disseminated pyrite	Breccia
<b>272.9 m</b>	Es-2-13	Silicified and carbonatized dacite	Quartz, calcite, disseminated pyrite	Breccia
<b>281.7 m</b>	Es-2-14	Silicified and carbonatized dacite	Quartz, calcite, disseminated pyrite	Breccia
<b>305.7m</b>	Es-2-16	Silicified and carbonatized dacite	Quartz, calcite, disseminated pyrite	Breccia
<b>324.4 m</b>	Es-2-18	Carbonatized dacite	Calcite, quartz	Porphyritic
<b>350 m</b>	Es-2-19	Ore zone	Massive quartz, pyrite, galena, sphalerite	Breccia
<b>360.8 m</b>	Es-2-20	Silicified dacite	Massive quartz, disseminated pyrite	Porphyritic
<b>386.10 m</b>	Es-2-21	Calc-silicate alteration	Andradite, calcite, silica, pyrite, galena, sphalerite	Breccia
<b>387.7m</b>	Es-2-22	Calc-silicate alteration	Andradite, calcite, silica, pyrite, galena, sphalerite	Breccia
<b>396.4 m</b>	Es-2-23	Calc-silicate alteration	Andradite, calcite, silica, pyrite, galena, sphalerite	Breccia

<b>403.4 m</b>	Es-2-24	Calc-silicate alteration	Epidote, calcite, silica, pyrite, galena	Breccia
<b>413.9 m</b>	Es-2-25	Calc-silicate alteration	Epidote, calcite, silica, pyrite, galena	Breccia
<b>422 m</b>	Es-2-26	Microdiorite	Plagioclase, hornblende, epidote, calcite veinlets	Porphyritic
<b>426.8 m</b>	Es-2-27	Calc-silicate alteration	Epidote, calcite, silica, pyrite, galena	Porphyritic
<b>431.2 m</b>	Es-2-28	Ore zone	Massive quartz, calcite, pyrite, galena, sphalerite	Breccia
<b>437.9 m</b>	Es-2-29	Limestone	Calcite	Fine-grained, breccia
<b>444.2 m</b>	Es-2-30	Calc-silicate alteration	Andradite, epidote, calcite, silica, pyrite, galena, sphalerite	Breccia
<b>456.4 m</b>	Es-2-31	Calc-silicate alteration	Andradite, calcite, silica, pyrite, galena, sphalerite	Breccia

Table 4.3. Description of samples taken from drill hole ES-3

Depth	Sample No	Lithology/Alteration	Paragenesis	Texture
161 m	Es-3-1	Argillitized dacite	Quartz, kaolinite, disseminated pyrite	Porphyritic
355 m	Es-3-2	Calc-silicate alteration	Andradite, calcite, pyrite, galena, sphalerite	Breccia
391.8 m	Es-3-3	Microdiorite	Plagioclase, hornblende, epidote, calcite veinlets	Porphyritic
409.5 m	Es-3-4	Microdiorite	Plagioclase, hornblende, epidote, calcite veinlets	Breccia
427.2 m	Es-3-5	Silicified and carbonatized dacite	Quartz, calcite, disseminated pyrite	Breccia
428.8 m	Es-3-6	Silicified and carbonatized dacite	Quartz, calcite, disseminated pyrite	Breccia
429.8 m	Es-3-7	Silicified and carbonatized dacite	Quartz, calcite, disseminated pyrite	Breccia
431.9m	Es-3-8	Silicified and carbonatized dacite	Quartz, calcite, disseminated pyrite	Breccia
432.9 m	Es-3-9	Silicified and carbonatized dacite	Quartz, calcite, disseminated pyrite	Breccia
437 m	Es-3-10	Ore zone	Pyrite, galena, sphalerite, quartz, calcite	Breccia
455.6 m	Es-3-11	Silicified and carbonatized dacite	Quartz, calcite, disseminated pyrite	Porphyritic
461.2 m	Es-3-12	Silicified and carbonatized dacite	Quartz, calcite, disseminated pyrite	Breccia
483 m	Es-3-13	Microdiorite	Plagioclase, hornblende, epidote, calcite veinlets	Porphyritic
487.9 m	Es-3-14	Silicified and carbonatized dacite	Quartz, calcite, disseminated pyrite, galena and sphalerite	Breccia
498.2 m	Es-3-15	Calc-silicate alteration	Andradite, epidote, quartz, calcite, pyrite, galena, sphalerite	Breccia
499m	Es-3-16	Calc-silicate alteration	Andradite, epidote, quartz, calcite, pyrite, galena, spha	Breccia

Table 4.4. Description of samples taken from drill hole ES-4

Depth	Sample No	Lithology/Alteration	Paragenesis	Texture
14.6 m	Es-4-1	Argillitized dacite	Quartz eyes, kaolinite, disseminated pyrite	
32.6 m	Es-4-2	Argillitized dacite	Quartz, kaolinite, disseminated pyrite	Porphyritic
54.1 m	Es-4-4	Argillitized dacite	Quartz, kaolinite, disseminated pyrite	Porphyritic
88.6 m	Es-4-5	Argillitized and brecciated dacite	Massive silica, calcite, quartz,	Breccia
104.1 m	Es-4-6	Limestone	Calcite, garnet, massive silica, disseminated pyrite	Fine grained
127 m	Es-4-7	Limestone	Calcite	Breccia, fine-grained
133.8 m	Es-4-8	Argillitized and silicified dacite	Kaolinite, quartz eyes	Porphyritic
145.6 m	Es-4-10	Argillitized, silicified dacite	Kaolinite, massive silica, quartz eyes	Porphyritic
192.1 m	Es-4-11	Argillitized, silicified dacite	Kaolinite, massive silica, quartz eyes, disseminated pyrite	Porphyritic
214.2 m	Es-4-13	Argillitized, silicified, carbonatized dacite	Kaolinite, massive silica, calcite veinlets, quartz eyes, disseminated pyrite	Porphyritic

Table 4.5. Description of samples taken from drill hole ES-5

Depth	Sample No	Lithology/Alteration	Paragenesis	Texture
12.3 m	Es-5-1	Argillitized dacite	Quartz eyes, kaolinite, disseminated pyrite	Porphyritic
95 m	Es-5-2	Argillitized dacite	Quartz eyes, kaolinite, disseminated pyrite	Porphyritic
103.8 m	Es-5-3	Argillitized dacite	Quartz eyes, kaolinite, disseminated pyrite	Porphyritic
182.2 m	Es-5-7	Argillitized and silicified dacite	Kaolinite, massive silica, quartz eyes, calcite veinlets, disseminated pyrite	Porphyritic
215.8 m	Es-5-10	Argillitized and silicified dacite	Kaolinite, massive silica, quartz eyes, calcite veinlets, disseminated pyrite, galena	Porphyritic
296.2 m	Es-5-12	Calc-silicate alteration	Massive quartz, calcite, andradite, epidote, disseminated pyrite, galena, sphalerite	Breccia
309.5 m	Es-5-14	Microdiorite	Hornblende, plagioclases were leached and filled by calcite	Porphyritic
319.9 m	Es-5-16	Calc-silicate alteration	Andradite, calcite, massive silica	Breccia
330.7 m	Es-5-17	Calc-silicate alteration	Epidote, chlorite, actinolite, calcite, pyrite veinlets	Breccia
366.8 m	Es-5-18	Calc-silicate alteration	Epidote, chlorite, actinolite, calcite veinlets, pyrite veinlets and sphalerite disseminations	Breccia
382.6 m	Es-5-21	Ore zone	Sphalerite	Massive
389.9 m	Es-5-22	Calc-silicate alteration	Garnet, epidote, massive pyrite, galena, sphalerite	Breccia
413.8 m	Es-5-24	Microdiorite	Hornblende, plagioclases were leached and filled by calcite	Porphyritic
459.9 m	Es-5-25	Ore zone	Calcite, pyrite and sphalerite	Massive

Table 4.6. Description of samples taken from drill hole ES-6

Depth	Sample No	Lithology/Alteration	Paragenesis	Texture
214 m	Es-6-1	Argillitized silicified brecciated dacite	Massive silica, kaolinite, calcite veinlets, disseminated pyrite	Breccia, porphyritic
250 m	Es-6-2	Argillitized silicified brecciated dacite	Massive silica, calcite veinlets, disseminated pyrite	Breccia, porphyritic
284.2 m	Es-6-4	Argillitized and silicified dacite	Kaolinite, massive silica, quartz eyes, calcite veinlets, disseminated pyrite	Porphyritic
310.4 m	Es-6-5	Calc-silicate alteration	Andradite, calcite veinlets, massive silica, pyrite veinlets, galena and sphalerite	Breccia
331.7 m	Es-6-7	Calc-silicate alteration	Epidote, calcite veinlets, massive silica, pyrite veinlets, galena and sphalerite, hematite	Breccia
377.4 m	Es-6-9	Silicified and carbonatized dacite	Quartz, calcite, disseminated pyrite	Porphyritic
457.8 m	Es-6-11	Silicified dacite	Massive quartz, disseminated pyrite	Breccia, porphyritic

Table 4.7. Description of samples taken from drill hole ES-7

Depth	Sample No	Lithology	Paragenesis	Texture
<b>62.8 m</b>	Es-7-1	Argillitized dacite	Quartz eyes, kaolinite, pyrite disseminations	Porphyritic
<b>137.1 m</b>	Es-7-3	Argillitized dacite	Quartz eyes , kaolinite, calcite and pyrite veinlets, pyrite disseminations	Porphyritic
<b>169 m</b>	Es-7-4	Argillitized and silicified dacite	Quartz eyes , kaolinite, calcite and pyrite veinlets, pyrite disseminations	Breccia, porphyritic
<b>215.2 m</b>	Es-7-5	Microdiorite	Massive silica, calcite replacing plagioclase, hornblende, biotite	Porphyritic
<b>285.3 m</b>	Es-7-7	Silicified and carbonatized dacite	Mainly pyrite, massive silica, calcite	Breccia
<b>306.8 m</b>	Es-7-8	Recrystallized limestone	Calcite	Fine-grained
<b>313 m</b>	Es-7-9	Brecciated recrystallized limeston	Carbonate matrix, and limestone clasts	Breccia
<b>366 m</b>	Es-7-10	Recrystallized limestone	Calcite, disseminated pyrite, galena, sphalerite	Fine-grained
<b>379.8 m</b>	Es-7-11	Limestone with macro fossils	Calcite, fossil shells	Fine-grained

Table 4.8. Description of samples taken from drill hole ES-8

Depth	Sample No	Lithology	Paragenesis	Texture
51.2 m	Es-8-1	Argillitized dacite	Kkaolinite, quatz eyes, disseminated pyrite	Porphyritic
145 m	Es-8-2	Argillitized dacite	Kaolinite, quartz eyes, disseminated pyrite	Porphyritic
341 m	Es-8-3	Brecciated, silicified dacite	Massive silica, quartz eyes, calcite veinlets, pyrite disseminations and veinlets	Porphyritic, breccia
367.8 m	Es-8-4	Silicified and carbonatized dacite	Massive quartz, calcite veins, pyrite disseminations and veinlets	Breccia
389.1 m	Es-8-5	Microdiorite	Plagioclase, hornblende, biotite, calcite veinlets	Porphyritic
416 m	Es-8-6	Silicified dacite	Massive silica, calcite veinlets, disseminated pyrite	Fine-grained
440.6 m	Es-8-7	Silicified dacite	Massive silica, calcite veinlets, disseminated pyrite	Breccia
465.4 m	Es-8-8	Microdiorite	Hornblende, biotite, plagioclase, calcite veinlets	Porphyritic
482.4 m	Es-8-10	Microdiorite	Hornblende, biotite, plagioclase, calcite veinlets	Breccia
491.6 m	Es-8-11	Silicified and carbonatized dacite	Massive quartz, calcite veins, pyrite disseminations and veinlets	Porphyritic
503 m	Es-8-12	Calc-silicate alteration	Massive silica, andradite, epidote, pyrite, galena and sphalerite	Breccia
512 m	Es-8-15	Calc-silicate alteration	Massive silica, andradite, epidote, pyrite, galena and sphalerite	Breccia
526.7 m	Es-8-16	Ore zone	Calcite, pyrite and sphalerite	Massive

Table 4.9. Description of samples taken from drill hole ES-9

Depth	Sample No	Lithology	Paragenesis	Texture
7.5 m	Es-9-1	Argillitized dacite	Quartz, kaolinite, pyrite disseminations, veins and veinlets	Porphyritic
19.4 m	Es-9-2	Argillitized dacite	Quartz, kaolinite, pyrite disseminations, veins and veinlets	Porphyritic and brecciated
178.3 m	Es-9-4	Argillitized, silicified dacite	Quartz, kaolinite, pyrite	Porphyritic
233.6 m	Es-9-5	Microdiorite	Plagioclase, hornblende, biotite, pyrite, chlorite	Porphyritic
242.6 m	Es-9-7	Calc-silicate alteration	Andradite, calcite, epidote, quartz	Breccia
246 m	Es-9-6	Calc-silicate alteration	Epidote, pyroxene, calcite, quartz	Breccia
252 m	Es-9-8	Ore zone	Pyrite, galena, sphalerite, calcite	Massive
256 m	Es-9-9	Calc-silicate alteration	Andradite, calcite, epidote, quartz	Breccia
262.2 m	Es-9-11	Calc-silicate alteration	Andradite, calcite, quartz, pyrite, galena, sphalerite	Massive
270.1 m	Es-9-12	Calc-silicate alteration	Andradite, calcite, quartz, pyrite, galena, sphalerite	Breccia
271 m	Es-9-13	Calc-silicate alteration	Andradite, quartz, calcite, pyrite, galena, sphalerite	Breccia
272.2 m	Es-9-14	Calc-silicate alteration	Pyroxene, actinolite, quartz, calcite	Breccia
282 m	Es-9-15	Calc-silicate alteration	Actinolite, epidote, quartz, calcite	Breccia
298.8 m	Es-9-18	Ore zone	Pyrite, galena, sphalerite, quartz	Massive
343.8 m	Es-9-20	Calc-silicate alteration	Andradite, quartz, calcite, pyrite, galena, sphalerite	Breccia
353.7 m	Es-9-21	Calc-silicate alteration	Andradite, quartz, calcite, pyrite, galena, sphalerite	Breccia
357.1	Es-9-20	Calc-silicate alteration	Andradite, calcite, pyrite, galena, sphalerite	Breccia
365.8 m	Es-9-22	Ore zone	Pyrite, galena, sphalerite, calcite	Massive
382.9 m	Es-9-23	Ore zone	Calcite, sphalerite, pyrite	Breccia
403.1 m	Es-9-24	Ore zone	Pyrite, galena, sphalerite, calcite	Massive

406.5 m	Es-9-25	Ore zone	Pyrite, galena, sphalerite, calcite, quartz	Massive quartz
438.9 m	Es-9-26	Silicified dacite	Quartz, calcite, pyrite, galena	Breccia

### 4.3.1. Early silicification

Strong to pervasive hydrothermal quartz enrichment and replacement within the dacitic rocks are termed as the silicification. It is the most common alteration type in study area and is observed both as pervasive-massive silicification and vein quartz within the dacite. As a result of this alteration, the characteristic textural and mineralogical contents of dacite were destroyed. However, it is also possible to see the original textural characteristics whereby the dacite has not undergone pervasive silicification. The most common form of early silicification replacing the whole rock is coarse-grained quartz.

Early silicification can be easily distinguished from other alterations as it serves as a groundmass for other alterations to develop, and is cross-cut by carbonate minerals, “skarn” assemblages, and late silicification. Quartz formed during early silicification infills the fractures, and matrix of the brecciated dacite resulting in silicified breccia as well. The quartz and other mineral assemblages formed during later hydrothermal alteration events infill the fractures and open spaces of silicified rock right after the early silicification (Figure 4.6 and 4.7).

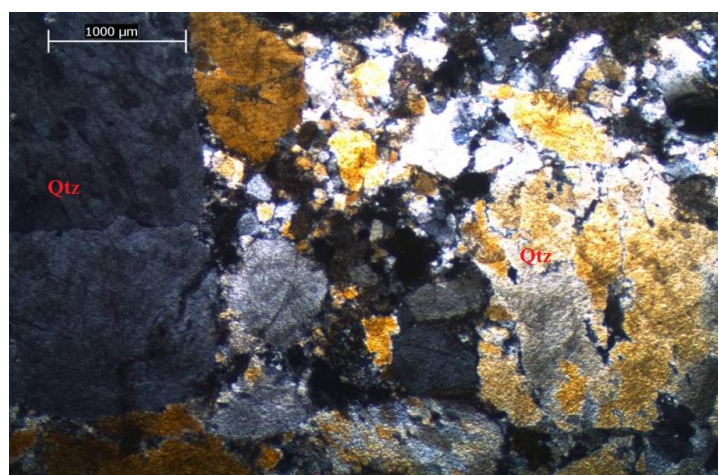


Figure 4.6. Photomicrograph showing the silicified and brecciated rock (Qtz:Quartz).

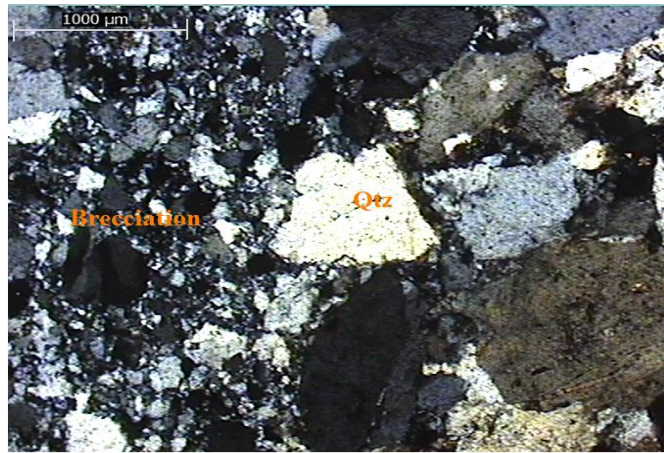


Figure 4.7. Photomicrograph showing the early silicification and hydrothermal brecciation rock (Qtz:Quartz).

Early silicification basically appears to form big, anhedral quartz crystals (Figure 4.8) which probably precipitated from hydrothermal solutions. These crystals show undulose extinction typical for hydrothermal quartz. Early silicification is believed to be accompanied by the brecciation of the dacite that also contributed to the initiation of the hydrothermal cells throughout the host rock. The brecciation is highly likely to be hydrothermal breccia based on textural arrangement of angular pieces and jig-saw puzzle nature of the breccia. The hydrothermal brecciation usually takes place along fractures and veins that consist of sub-angular, monomictic silicified dacite clasts and fine grained matrix. Clasts are crushed-smashed-quartz crystals which have different crystal sizes. Hydrothermal breccia (Figure 4.9) also appears to be cemented by hematite during later phases following the early silicification.



Figure 4.8 Coarse-grained, anhedral quartz crystals of silicified rock (Sample taken from 270.1 m depth of ES-9 (Qtz:Quartz)).

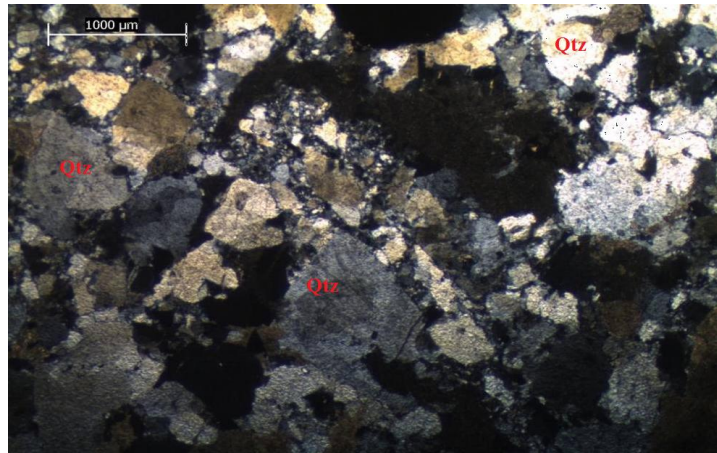


Figure 4.9. Hydrothermally brecciated silicified rock (Sample taken from 270.1 m depth of ES-9 (Qtz:Quartz)).

#### 4.3.2. Early carbonatization

Early carbonatization (Figures 4.10 to 4.13) is the second alteration formed during the hydrothermal evolution of the entire system. Therefore, it is considered that calcite of early stage is younger than early silicification, hydrothermal brecciation. This is evidenced by observations summarized below;

- 1) Calcite veinlets cuts through the silicified and hydrothermally brecciated dacite.
- 2) Fractures and open spaces within the silicified rock are filled by calcite crystals.
- 3) Calcite commonly replaces minerals of silicified and hydrothermally brecciated dacite.

The mineralogical composition of the carbonates were identified by Confocal Raman Spectroscopy (CRS) analyses. These analyses have shown that the early carbonatization is characterized by single or isolated calcite crystals (Figure 4.7) along the vein and veinlets of silicified-brecciated dacite and commonly replaces minerals of early silicification and hydrothermally brecciated rock. The calcite crystals formed at this alteration occurs as single crystals filling the interstices of early quartz crystals and cavities of hydrothermal breccia (Figure 4.8 and 4.9). Calcite also replaces sanidine and plagioclase minerals of dacite (Figure 4.10).

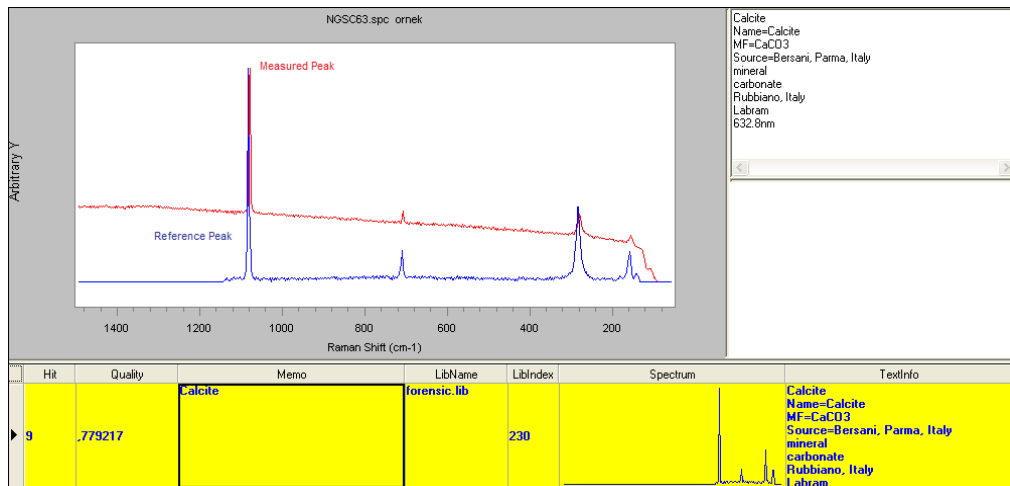


Figure 4.10. Composition of calcite from the early carbonatization (calcite by CRS).

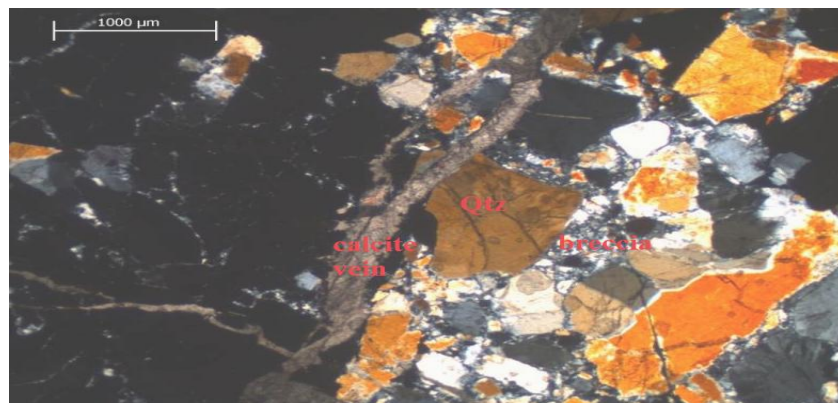


Figure 4.11. Early calcite vein cutting the quartz crystals of early silicification and hydrothermal breccia (Qtz:Quartz)



Figure 4.12. Hydrothermal breccia and early silicification cut by calcite veinlets. (Sample taken from 270.1 m depth of ES-9. Bre. Slc.:Brecciated silicified rock)

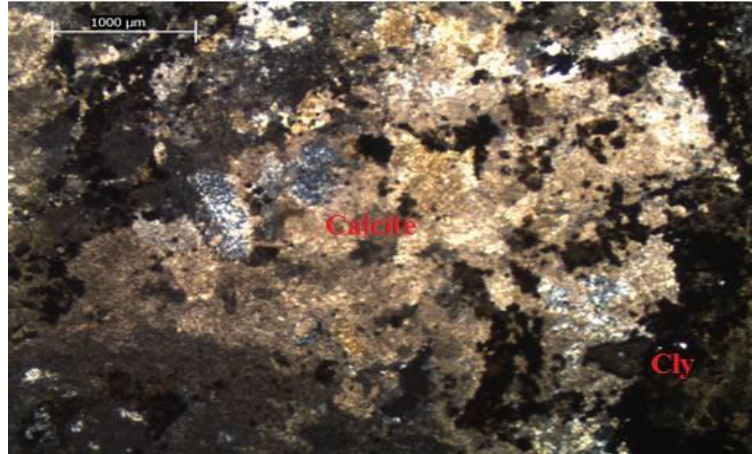


Figure 4.13. Calcite of early carbonatization within the argillitized rock ( Sample taken from 271 m depth of ES-9 Cly:clay)

The early carbonatization seems to be an alteration process whereby the “ground preparation” took place for the next alteration that produced the calc-silicate assemblage close to or within the brecciated and carbonatized levels throughout the drill logs.

#### **4.3.3. Calc-silicate alteration: Skarn**

Garnet, pyroxene, epidote and amphibole bearing alterations mostly occurring as veins along the silicified-carbonatized dacite are called as the calc-silicate alterations. These collectively could be termed as “skarn” since these minerals are also the index minerals forming the assemblage in the skarns. However, since the contacts between dacitic rocks and limestones are free of skarn assemblage, or the limestone blocks within the dacitic rocks are altered to form quartz only, the use of term “skarn” is not appropriate. This terminology used in this study is free of genetic meaning and stands for an assemblage of calc-silicate minerals formed during hydrothermal alteration. This type of alteration do not obey the general morphological characteristics of the “skarn around intrusive” scheme or “distal skarns” scheme formed through the major fault zones cut by a deeper hot magmatic intrusion. In study area, these characteristic mineral assemblages are observed pervasively at the levels whereby the host rock breaks into pieces in drill cores, and are the major host rock for the mineralization.

The calc-silicate alteration is localized either i) at intervals close to the brecciated and carbonatized dacitic rocks, suggesting that silicified, brecciated and carbonatized dacite and dacite porphyry are the primary host for calc-silicate alteration, or ii) as a zone overlying and/or underlying the dark colored dike-like intrusions of microdiorite, pointing to a genetical relation with that intrusion.

The garnet, pyroxene and amphibole (actinolite) group minerals usually occur as groundmass pervasively replaced by epidote and tremolite. In that sense, the garnet-pyroxene-actinolite assemblage appears to be the early product (prograde) of this alteration, whereas epidote, tremolite and to some extent calcite are related to later phases of calc-silicate alteration due to retrograde effect of low-T fluids. Therefore, they could be regarded as calc-silicate alteration formed during retrograde stage.

#### **4.3.3.1. Early calc-silicate alteration (Garnet±Pyroxene±actinolite)**

In macro scale, this skarn is pale-brown to greenish brown in color and consists mainly of garnet group minerals (Figure 4.14), pyroxene and rosettes of actinolite minerals. Garnet and pyroxene occurs in all of the drill holes except ES-7 and ES-8. Based on the relative temperature of formation of garnet and pyroxene, this alteration could be regarded as the prograde stage of the calc-silicate alteration. Depth interval (thickness) of prograde assemblage observed in drill cores is 1-50 m. The early calc-silicate assemblage is strictly associated with and hosted within the dacitic rocks that undergone carbonatization. This further supports the argument that the early carbonatization is the likely process leading to ground preparation for calc-silicate alteration. The early calc-silicate alteration has a close association with the ore bearing levels in a way that ore bodies are generally found just under the early calc-silicate assemblage in the drill holes.

The garnets are the predominant minerals of the early calc-silicate assemblage, and occur as medium to coarse-grained euhedral and zoned anisotropic crystals replacing the silicified and carbonatized dacite. These commonly exhibit sector zoning (Figure 4.14). In macro scale, garnet is commonly dark red brown in color close to microdiorite dikes, but becomes lighter brown to greenish away from the dike intrusion where is available.

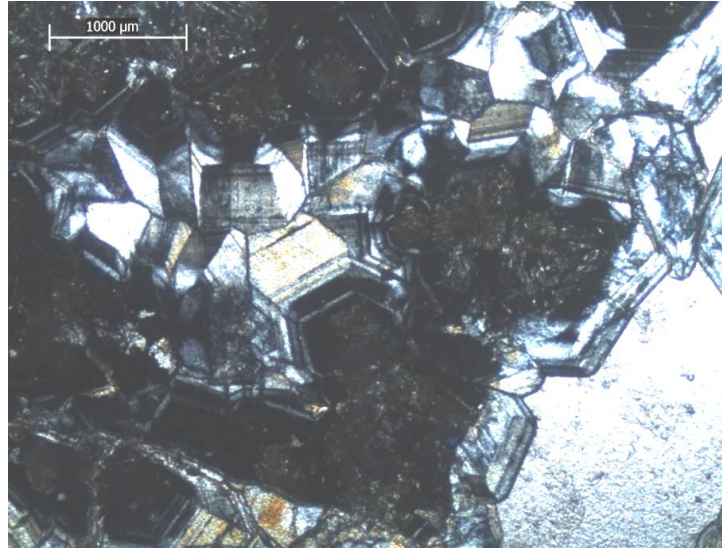


Figure 4.14. Zoned garnet (andradite) crystals with sector zoning within the early calc-silicate alteration

CRS studies revealed that the garnets are andradite ( $\text{Ca}_3\text{Fe}_2(\text{SiO}_4)_3$ ) in composition close to the microdiorite dikes (Figure 4.15). There is no information about the composition of light colored garnets that tend to increase away from the dike contacts.

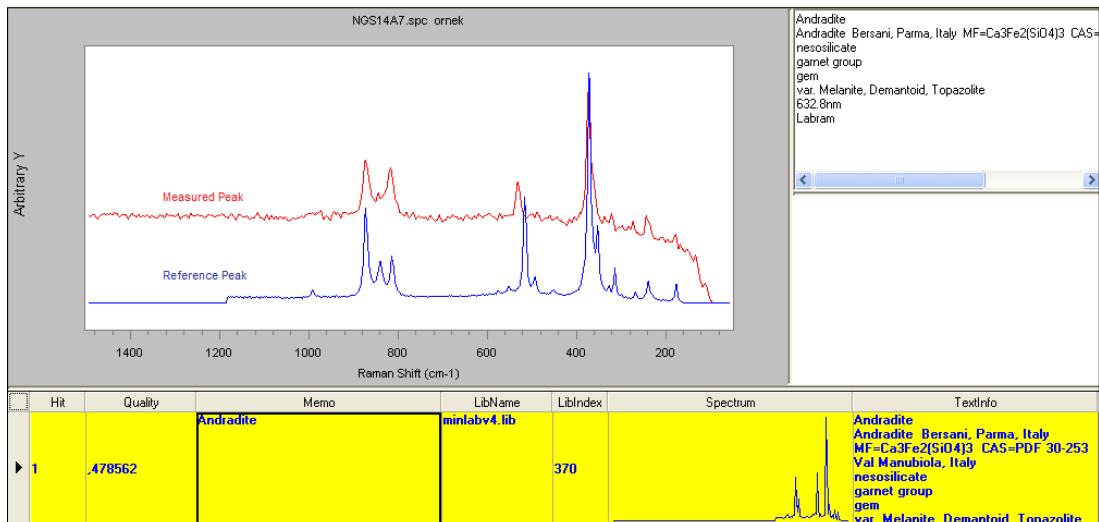


Figure 4.15. Composition of garnet from the early calc-silicate assemblage (andradite by CRS).

In thin section, these andradites are generally euhedral in shape and show zonal anisotropy at the rims (Figure 4.16.); however, they are occasionally observed as isotropic. The interstitial spaces of the garnets are filled by calcite probably formed during late carbonatization (Figure 4.16). Pyroxene typically occurs as prismatic crystals with euhedral shape and strong birefringence colors. It is always accompanied by garnets, and is generally replaced by needle-like prismatic crystals of actinolite (Fig. 4.17). Unlike the garnets, pyroxenes are finer grained.



Figure 4.16. Zoned andradite crystals in the early calc-silicate alteration, and calcite infill (Sample taken from 262.2 m depth of ES-9).



Figure 4.17 Prismatic-euhedral actinolite crystals replacing the andradite

#### 4.3.3.2. Late calc-silicate alteration (epidote±tremolite±calcite)

The late calc-silicate alteration refers to an assemblage consisting of epidote, tremolite, and calcite typically overprinting or superimposing garnet, pyroxene and actinolite (Figure 4.18, 4.19). This alteration is the most widely exposed calc-silicate alteration both at macro and micro-scale, and represents the main host rock for sulfide mineralization in all drill holes. Thickness of this alteration reaches up to about 20 m at the drill holes. In some samples, this alteration almost completely obliterates garnets and pyroxenes of early calc-silicate assemblage.

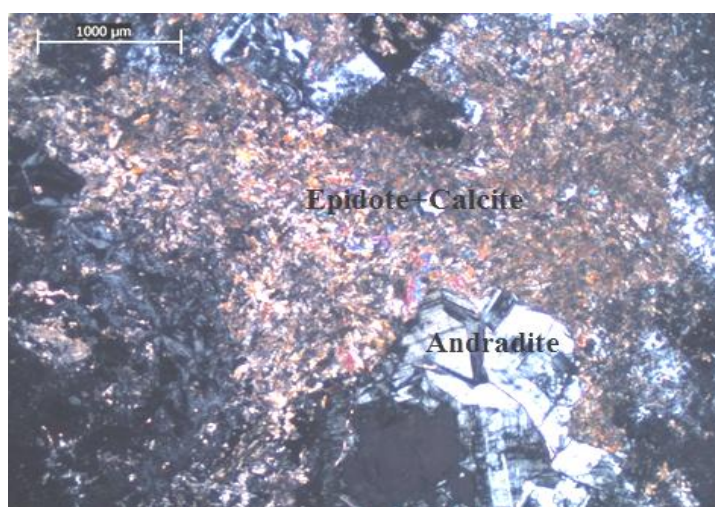


Figure 4.18. Epidote and calcite replacing andradite and pyroxene of early calc-silicate alteration (Sample taken from 390.9 m depth of ES-3).

Epidote is prismatic and generally observed as subhedral needle shaped crystals (Figures 4.20 and 4.21). The CRS analyses have shown that the epidote group minerals are mainly epidote in composition. The lacking of pistacite or clinozoisite (the other end-members of epidote group) indicates that the hydrothermal solutions are not oxidized or weakly oxidized during the late calc-silicate alteration. Calcite occurs as veins and massive replacement bodies in this alteration. Tremolite is found as euhedral needle-shaped radial crystals (Figures 4.22 and 4.23).

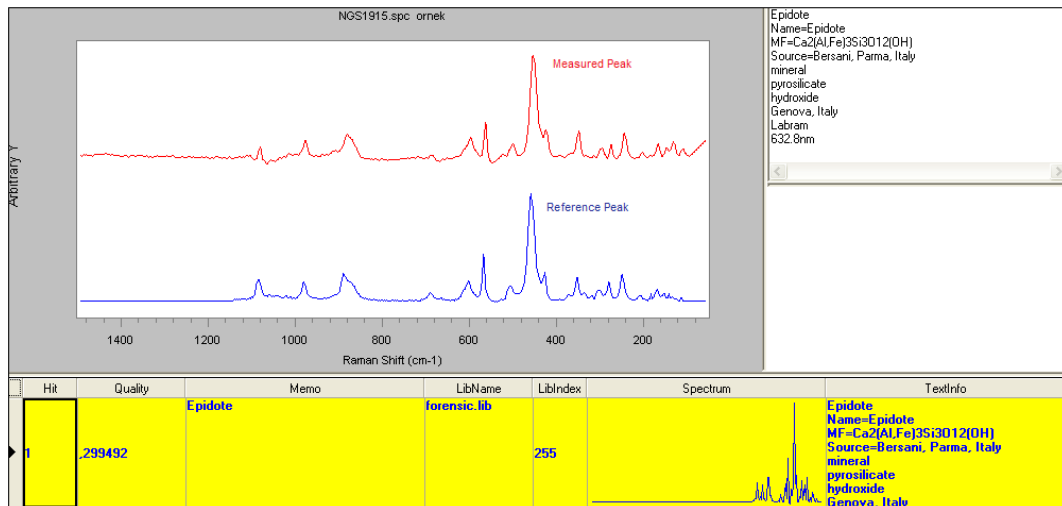


Figure 4.19. Composition of epidote from the late calc-silicate assemblage (epidote by CRS).

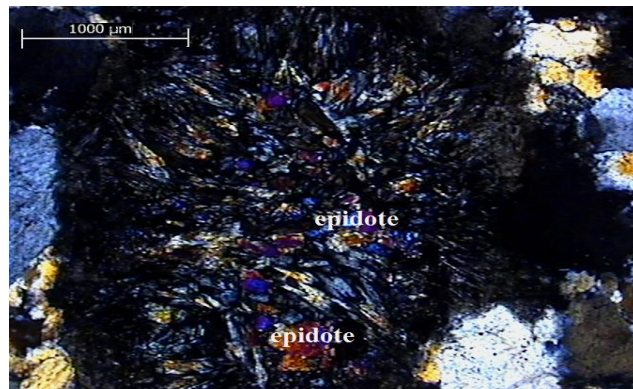


Figure 4.20. Epidote in late calc-silicate alteration (Sample taken from 432.9 m depth of ES-3) (2.5X)

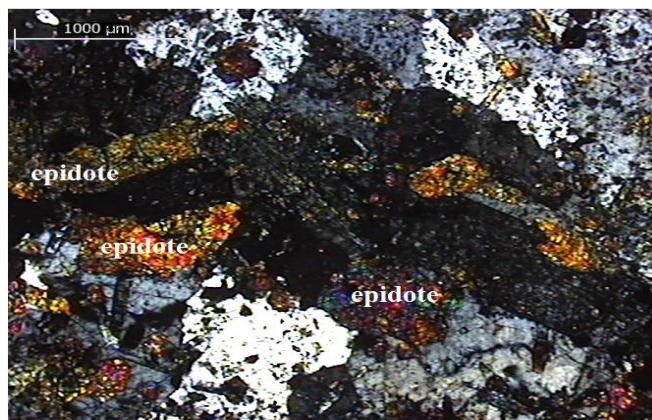


Figure 4.21. Epidote replacing pyroxene of early calc-silicate alteration (Sample taken from 432.9 m depth of ES-3) (10X).

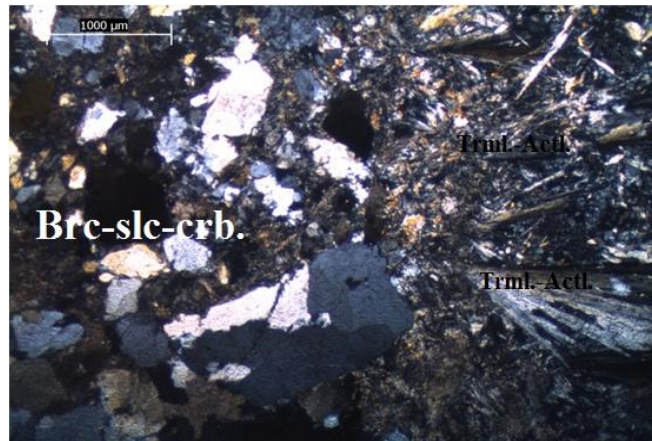


Figure 4.22. Tremolite (brown to red colored finer grained crystals) replacing early calc-silicate (Sample taken from 288.2 m depth of ES-9. Brc-slc-crb: Brecciated silicified carbonatized rock, Trml-Actl: Tremolite-Actinolite).

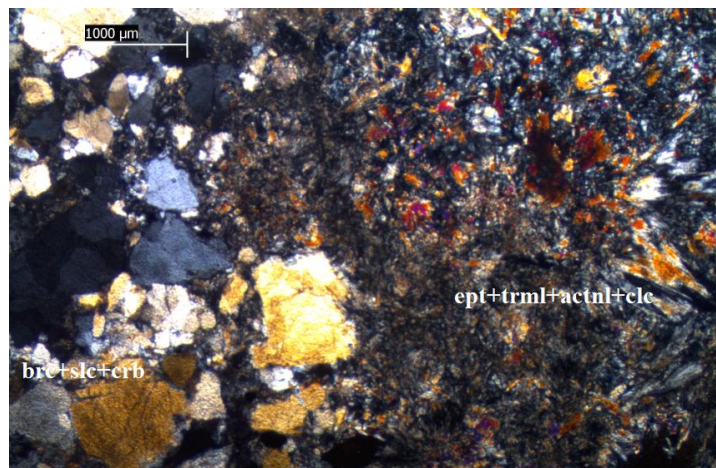


Figure 4.23. Epidote, tremolite and calcite replacing early calc-silicate assemblage (Sample taken from 288.2 m depth of ES-9. Ept: Epidote, Trml: Tremolite, Actnl: Actinolite, Clc: Calcite, Brc-slc-crb: Brecciated silicified carbonatized rock.)

The relative temperature estimates based on the presence of garnet and pyroxene suggest high temperature (>400 °C) for the early calc-silicate alteration. However, predominancy of epidote and tremolite are indicative of relatively medium temperature (<400 °C) for late calc-silicate alteration.

#### 4.3.4. Late silicification

Late silicification refers to pervasive silicification of limestone and dacite that already underwent early silicification, and calc-silicate alteration. It occurs as

infilling of the interstitial spaces, cavities and microfractures by fine-grained quartz crystals (Figure 4.24, 4.25).

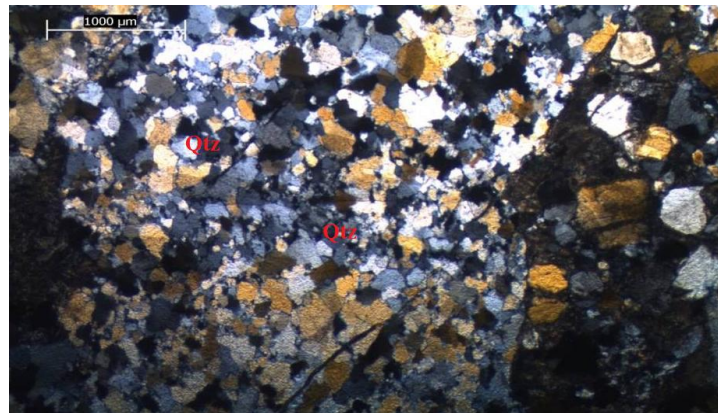


Figure 4.24. Quartz crystals of late silicification (Sample taken from 288.2 m depth of ES-9 (Qtz:Quartz))

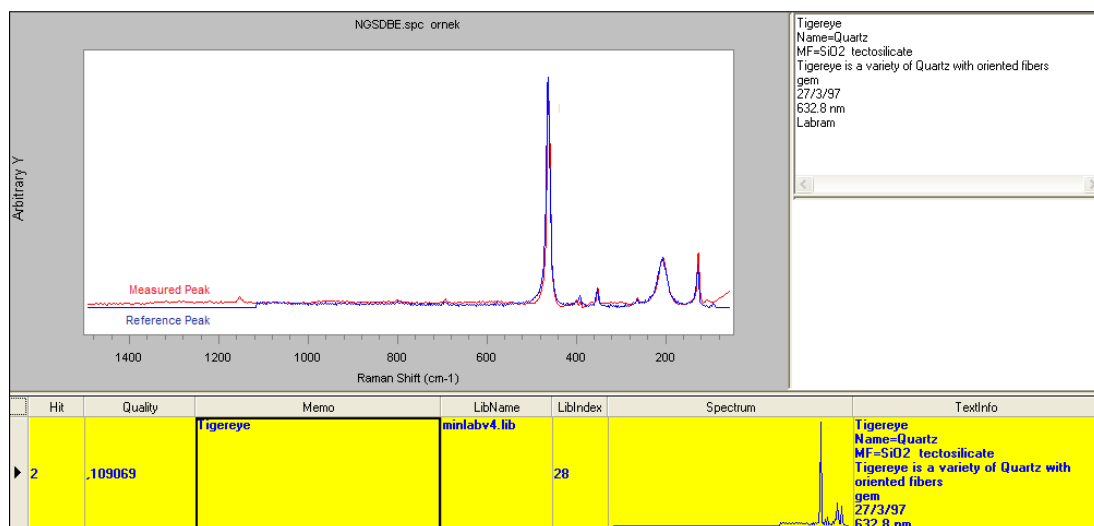


Figure 4.25. Composition of quartz from the late silicification (quartz by CRS)

Fine grained quartz crystals characterizing this alteration are precipitated along the fractures in quartz of early silicification and early silicified rock (Figure 4.26-4.27). The most typical example of this type is related with the intensely silicified limestones along the E-W trending normal faults, and limestone blocks within the dacitic rocks.

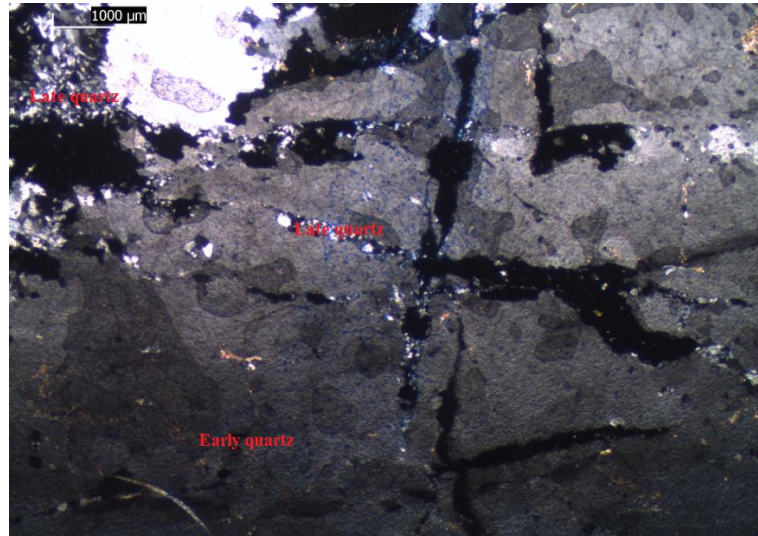


Figure 4.26. Late quartz filling fractures of silica in early silicification

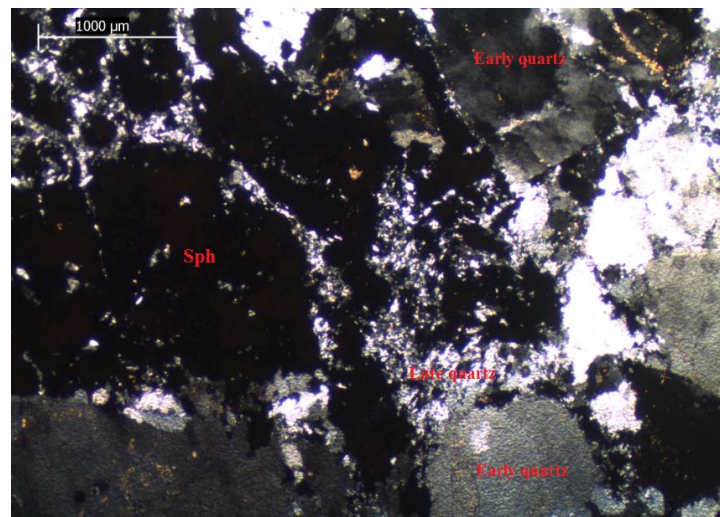


Figure 4.27. Fine grained late quartz cutting early quartz and sphalerite (sph:sphalerite)

#### 4.3.5. Late Carbonatization

Late carbonatization is observed as calcite crystals replacing the garnet and pyroxene as calcite veins and veinlets (Figure 4.28). Calcite in this alteration is locally accompanied by quartz, and these two occur as quartz-calcite veins cutting through the early calc-silicate alteration (Figure 4.29). Ore body is generally hosted by rocks with late calc-silicate alteration that underwent pervasive late carbonatization, and hence sulfide mineralization is contemporaneous with late carbonatization.

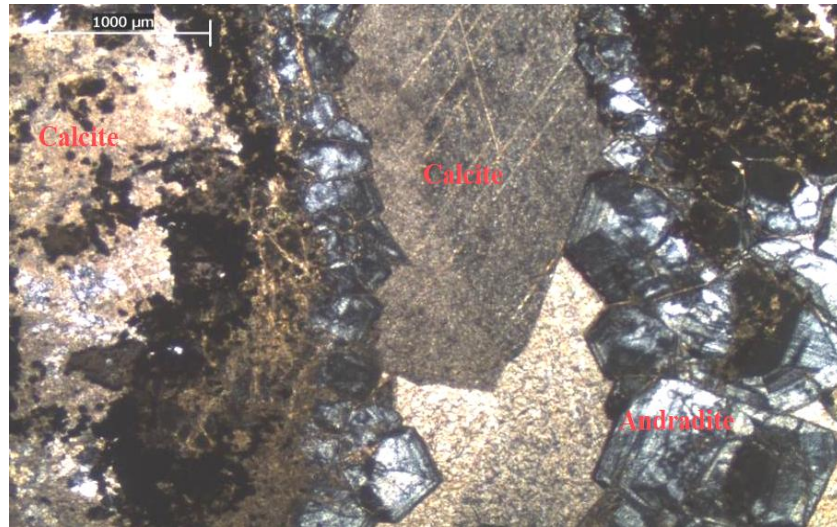


Figure 4.28. Calcite replacing, or filling the interstitial spaces of andradite crystals in early calc-silicate alteration (Sample taken from 271 m depth of ES-9).

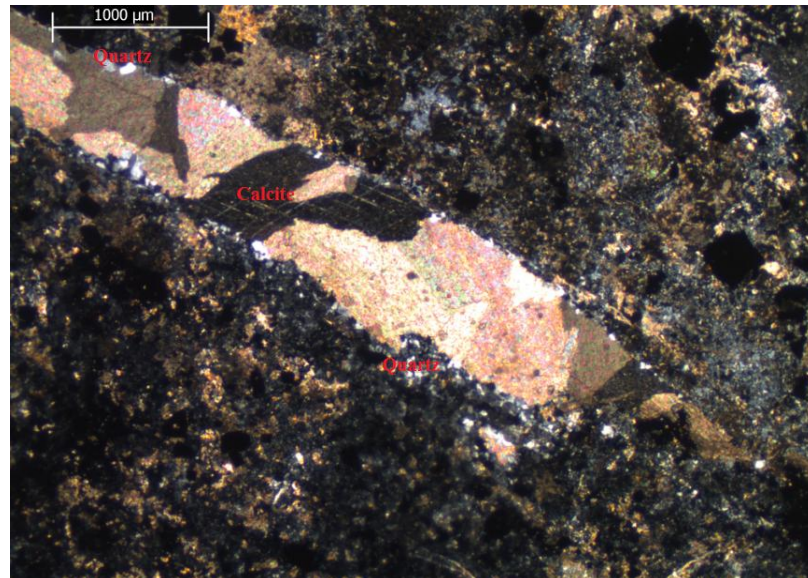


Figure 4.29. Silicification synchronous with late carbonate veinlet

Calcite formed in this alteration is called late calcite and is observed also as interstitial to euhedral garnet crystals (Figure 4.30). Occasionally, the andradite in the calc-silicate alteration is almost completely replaced by late calcite, and only crystal shape of andradite is preserved as relicts (Figure 4.31).

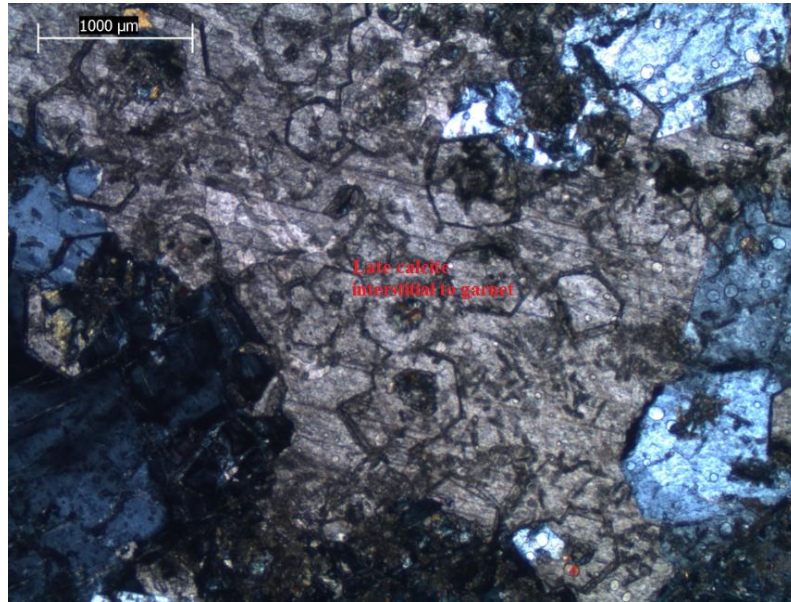


Figure 4.30. Late calcite interstitial to garnet crystals

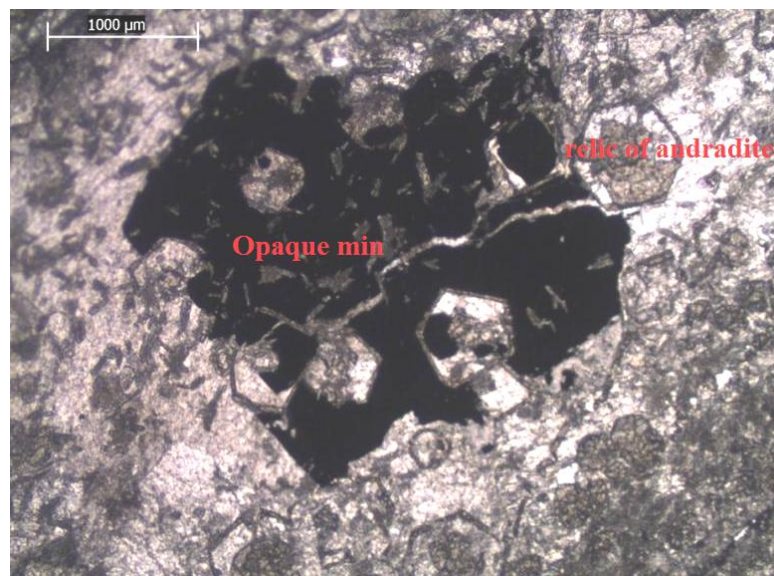


Figure 4.31. Relicts of andradite in late calcite and opaque mineral replacing andradite relicts

This alteration is the last alteration in the hydrothermal evolution of the entire system. The sulfide mineralization is spatially and temporarily associated with the late carbonatization and silicification, and is generally observed within the late calcite veinslets (Figure 4.32).

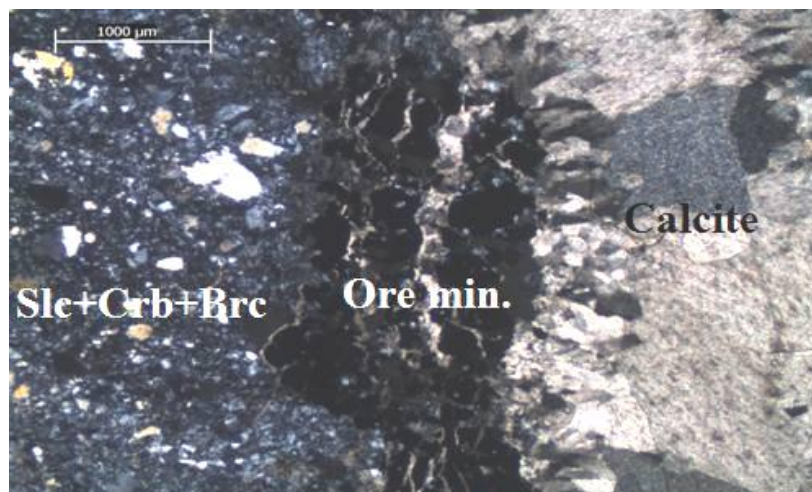


Figure 4.32. Calcite veining in brecciated, silicified, carbonatized rock (Sample taken from 438.9 m depth of ES-9. Slc+Crb+Brc: Silicification+Carbonatization+Brecciation, Ore min.:Ore minerals.)

#### 4.3.6. Argillization-clay alteration

White to beige-yellow colored patches or exposures all over the dacitic rocks within the study area are comprised predominantly of clay minerals (Figure 3.1) whose composition has not been detected by petrographical and geochemical means. Therefore, this thesis is unable to provide evidence if these clay minerals are of hypogene- or supergene-type. Since these minerals are usually associated with manganese oxide-hydroxide-bearing, clay-altered dacitic rocks with abundant oxidized pyrite, or occur as blanket-like exposures just above the pyrite-quartz altered dacitic rocks, it is highly likely that the clay alteration has resulted from the leaching of the pyrite-rich dacitic rocks by circulating meteoric water throughout the fractures within the pyrite-rich dacitic rocks. Besides, the presence of halloysite pockets and veins along with manganese oxide-hydroxide precipitation at the Sarisu hill, provide clues about the source and genesis of the clay alteration. Considering the fact that the halloysite is known as a mineral within argillic assemblage formed by supergene processes at epithermal systems, a supergene origin is more likely for the clay alteration in the study area. The common association of iron-hydroxide staining throughout the fractures within the clay alteration and halloysite-bearing levels also favors surficial or supergene origin for the formation of clay alteration.

#### **4.4. Ore Mineralogy**

The sulfides are the main constituents of the ore mineral assemblage and consist of galena, sphalerite and pyrite with occasional chalcopyrite. Galena and sphalerite with occasional chalcopyrite are predominant ore minerals forming the economic potential of the deposit, pyrite is of secondary economic importance. The sulfide minerals were identified and examined by ore microscopy. Among the sulfides, pyrite is the earliest mineral precipitated from the solution, and is followed by galena. Replacement of pyrite by galena is very common throughout the samples collected from the ore-bearing levels. The galena is followed by sphalerite with well developed chalcopyrite exsolutions from the ore-bearing solution. As also indicated in the alteration mineralogy, the ore mineral assemblage is hosted by late carbonatization following the late calc-silicate assemblage. The quartz-calcite and calcite veins and coarse calcite crystal-bearing levels replacing the late calc-silicate alteration are favorable settings for the ore minerals to precipitate. Cross-cutting and replacement relations of ore minerals reveal that the precipitation of ore minerals is closely related with late silicification and carbonatization. Ore microscopy studies on polished sections prepared from core samples of well no. 3 , 6 and 9 are given in Table 4.10. Anhedral galena and sphalerite with occasional chalcopyrite, are the primary ore minerals in the Balya deposit. Galena occurs as massive ore bodies in the late calc-silicate assemblage and as disseminations away from the calc-silicate alteration. It is replaced by sphalerite and overprints pyrite. Under the microscope, triangular pits or blebs are, characteristic textural features of galena, observed mainly within massive galena crystals.

Table 4.10. Description of polished sections prepared from ES-3-6-9 drill core samples.

Sample No	Hole No	Depth	Paragenesis	Texture
ES-3-10	3	434.7 m	Pyrite, sphalerite.	Replacement texture (euhedral pyrite is replaced by sphalerite)
ES-6-3	6	274.4 m	Pyrite, galena, chalcopyrite, sphalerite	Exsolution texture (chalcopyrite exsolution in sphalerite), replacement texture (sphalerite and galena replace euhedral pyrite)
ES-6-4	6	284.2 m	Pyrite and galena	Replacement texture (galena replace euhedral pyrite), cataclastic texture
ES-6-9	6	404.25 m	Pyrite and minor galena.	Cataclastic texture
ES-9-8	9	252 m	Pyrite, sphalerite, chalcopyrite	Replacement texture (pyrite is replaced by sphalerite and chalcopyrite; sphalerite is replaced by chalcopyrite)
ES-9-11	9	262.2 m	Pyrite, galena, chalcopyrite, sphalerite	Replacement texture (Pyrite is replaced by sphalerite and chalcopyrite), exsolution texture (chalcopyrite exsolution in sphalerite)
ES-9-18	9	298.8 m	Pyrite, galena, chalcopyrite, sphalerite.	Replacement texture (sphalerite and galena replace pyrite), cataclastic texture, intergrowth (between galena and sphalerite)
ES-9-22	9	360.8 m	Pyrite, galena, chalcopyrite, sphalerite	Replacement texture (Pyrite is replaced by sphalerite, galena is replaced by sphalerite), exsolution texture (chalcopyrite exsolution in sphalerite)
ES-9-24	9	403.1 m	Pyrite, galena, chalcopyrite, sphalerite	Cataclastic texture, replacement texture (anhedral deformed pyrites is replaced by sphalerite and galena, and galena is replaced by sphalerite), exsolution texture (chalcopyrite exsolution in sphalerite)
ES-9-25	9	406.5 m	Pyrite, galena, chalcopyrite, sphalerite.	Replacement texture (pyrite is replaced by galena and sphalerite, and galena is replaced by sphalerite), cataclastic texture (especially in galena), intergrowth (between galena and sphalerite) exsolution texture (chalcopyrite exsolution in sphalerite).

As can be seen in the Table 4.10, most common textures of ore minerals are replacement, cross-cutting and exsolution textures (Figure 4.33, 4.34).

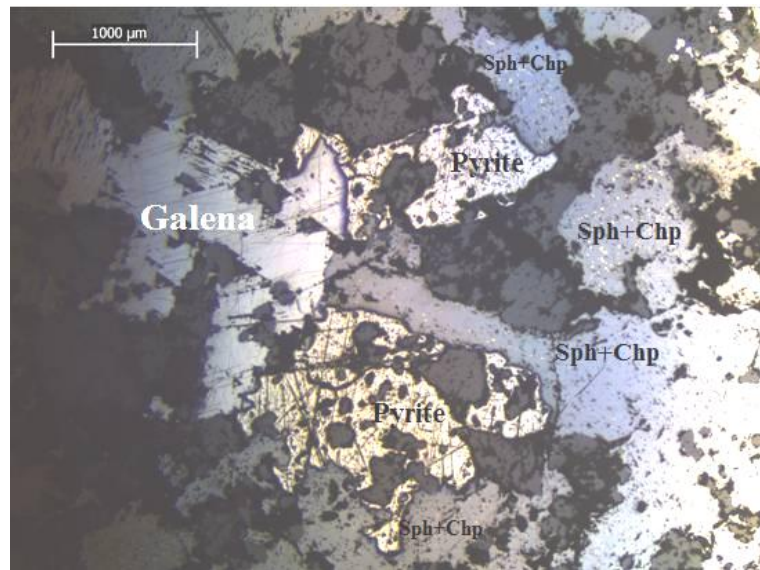


Figure 4.33. Photomicrograph showing textural relations among pyrite, galena, chalcopyrite, sphalerite (Sample taken from 403.1 m depth of ES-9. Sph+Chp: sphalerite including chalcopyrite exsolutions).

Chalcopyrite is one of the primary ore mineral in terms of its relative time of formation and importance, and occurs generally as exsolved mineral phase in sphalerite (Figure 4.34) or rare veins close to sphalerite contacts. It also occurs as massive crystals rimming the sphalerite along with galena. The previous works agree that the amount and intensity of chalcopyrite tend to increase with depth. However, such relationship has not been verified in this study. This might be because of erratic sampling interval or inadequate drill holes to sample.

Sphalerite occurs either as massive or disseminated types. The crystal size is highly variable, and ranges from fine to coarse. Sphalerite is not only confined to or hosted by calc-silicate alteration assemblage, but it is also associated with carbonatized dacite away from the calc-silicate alteration zones. Under the microscope, sphalerite is anhedral and carries chalcopyrite exsolutions (chalcopyrite disease). It is anisotropic and has red, strong internal reflections.

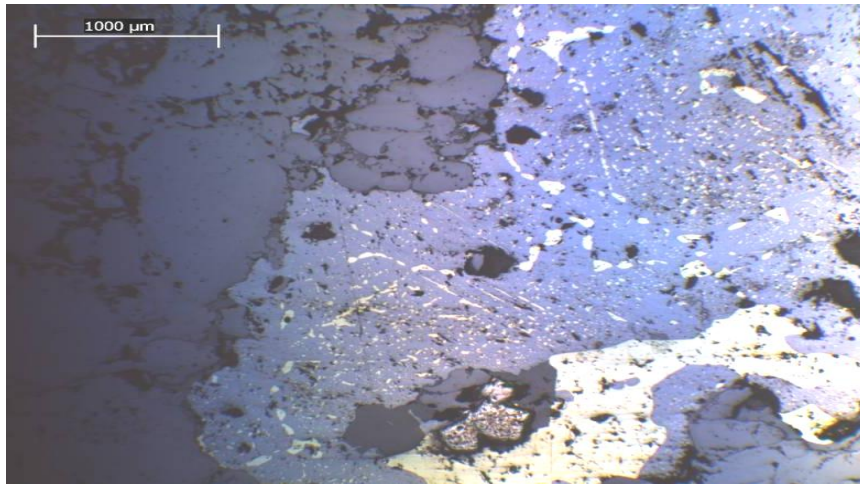


Figure 4.34. Chalcopyrite (yellow) inclusions in sphalerite (light grey, centre)  
(Sample taken from at 262.2 m of ES-9).

Anhedral and/or euhedral cubic pyrite crystals are commonly observed as minerals along rims of galena and sphalerite. Clay-altered and silicified dacite commonly include pyrite as disseminations, veins and veinlets. Pyrite crystals in the veins are cubic and euhedral in shape. These crystals are also precipitated along the walls of calcite veinlets formed at the late carbonatization. All pyrite crystals are replaced by galena and sphalerite commonly along the fracture zones, or as marginal replacement (Figure 4.35, 4.36).

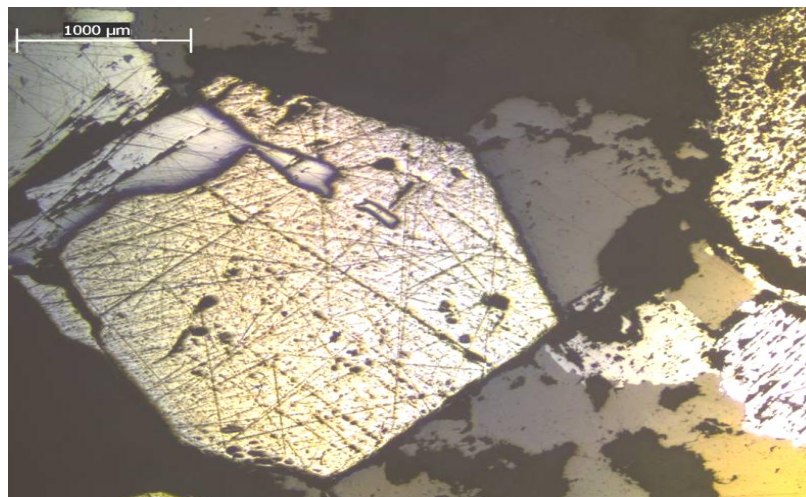


Figure 4.35. Euhedral pyrite (yellow, centre) replaced by galena (Sample taken from 406.5 m depth of ES-9. Gray color showing triangular pits)

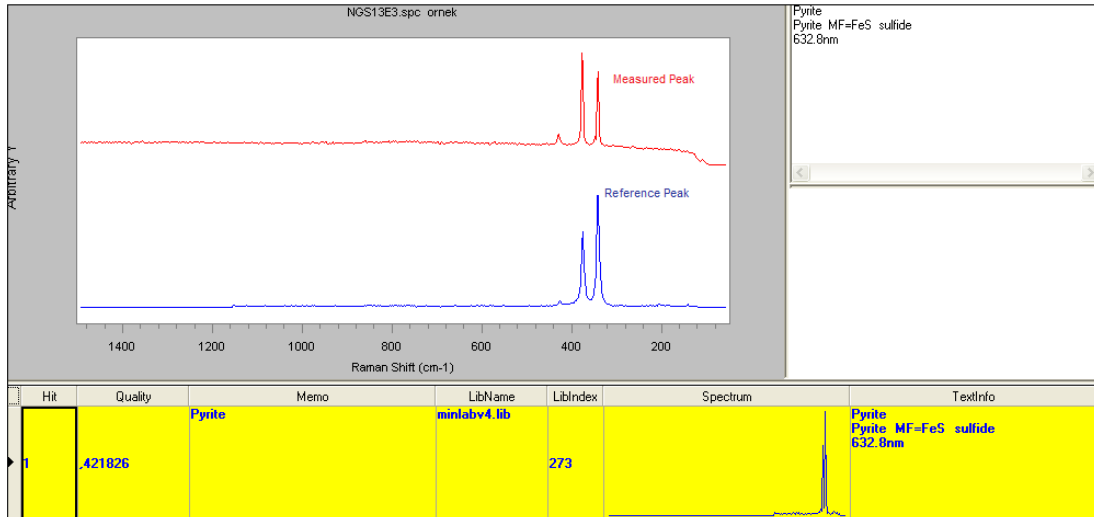


Figure 4.36. Composition of iron sulfides the ore zone (pyrite by CRS).

Based on the identified minerals and their textural relations, the relative time of formation of sulfide minerals can be summarized as a sequential paragenetic diagram (Figure 4.37)

TIME Ore Mineral	t <sub>1</sub>	t <sub>2</sub>	t <sub>3</sub>	t <sub>4</sub>
	Pyrite	_____		
Galena 1		_____		
Sphalerite 1		_____		
Sphalerite 2			_____	
Chalcopyrite 1			_____	
Chalcopyrite 2				_____

Figure 4.37. Sequential paragenetic diagram

#### 4.5. Lateral-Vertical Correlation of Alterations

Lateral-vertical correlation of alteration and ore zones was obtained by alteration zones defined in this thesis at each drill hole. For a comprehensive picture of the spatial association of the alteration holes and related ore zones, two traverses have been used; a NE-SW to E-W section using holes ES-9, ES-7, ES-6, ES-5, ES-2 and ES-4 (Figure 4.38), and a N-S section using ES-3, ES-8, ES-1, ES-5 and ES-2 (Figure 4.39). The faults have been inferred from the field observations and brecciated-sheared core samples defined during re-logging of the drill holes (Figures 4.40 and 4.41). In general, it appears that the major normal fault traversing the Kırmızı tepe is not a single fault plane, instead it consists of several sub-parallel branches that dip towards north with nearly same dip amount. The vertical distribution and depth of supergene argillic alteration is more likely controlled by the frequency and depth of the faulted volcanic rocks containing abundant pyrite. For example, the thickest section of the argillic alteration corresponds to drill hole cut by a buried-blind normal fault.

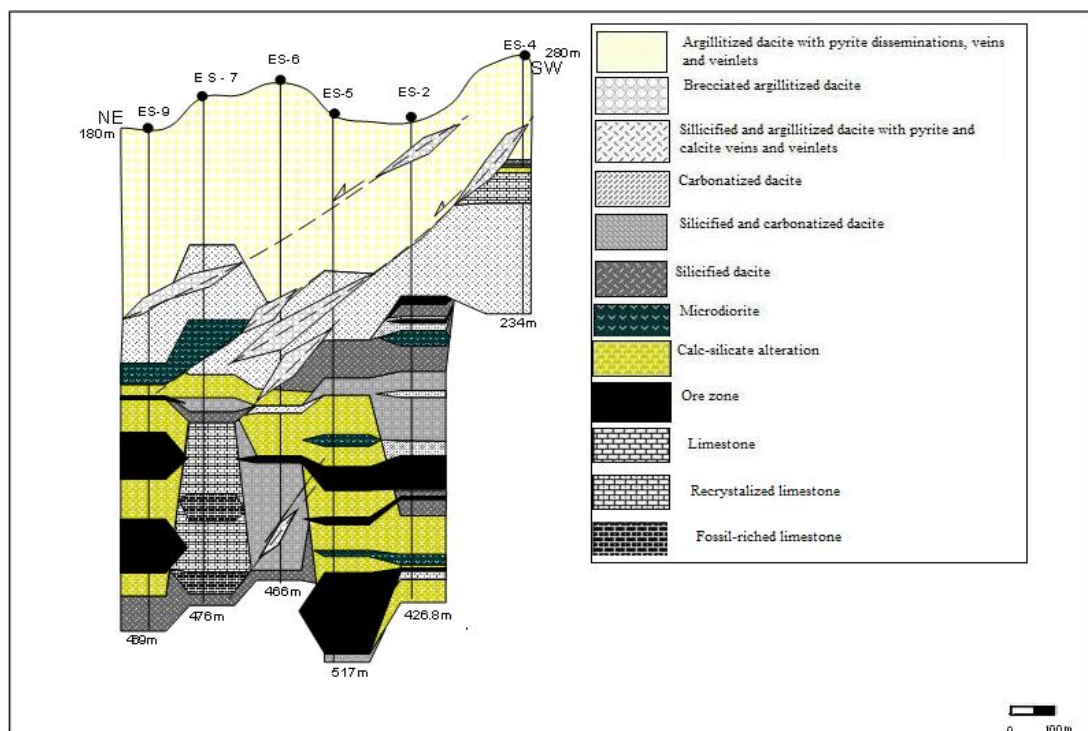


Figure 4.38. NE-SW to E-W section using holes ES-9, ES-7, ES-6, ES-5, ES-2 and ES-4

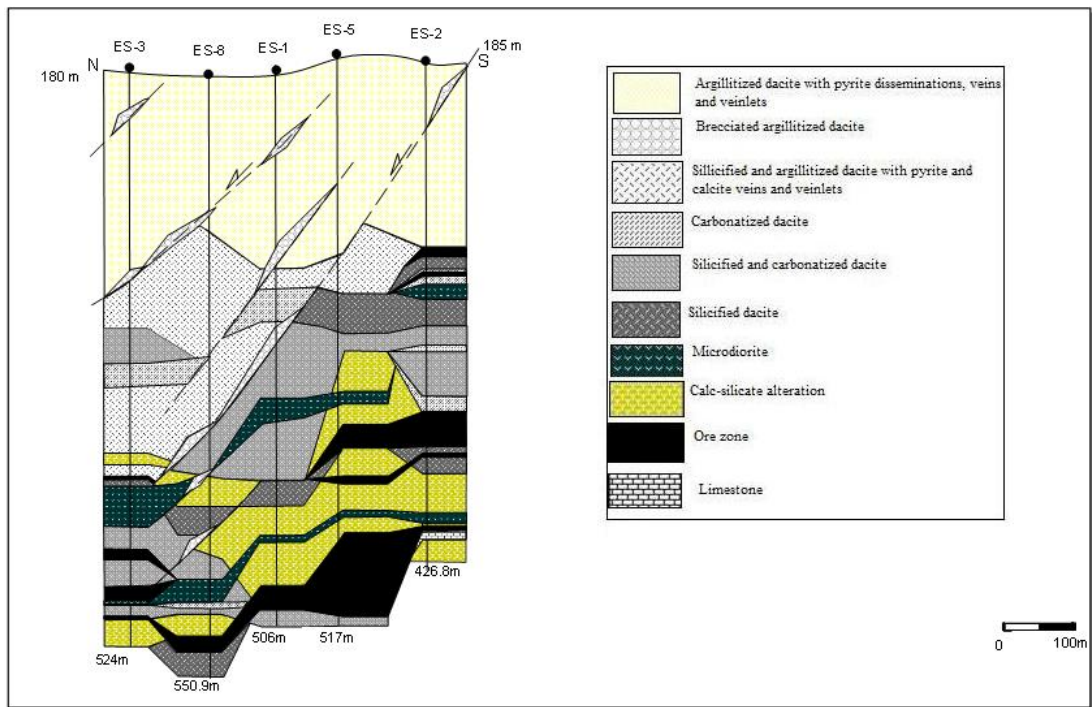


Figure 4.39. N-S section using ES-3, ES-8, ES-1, ES-5 and ES-2

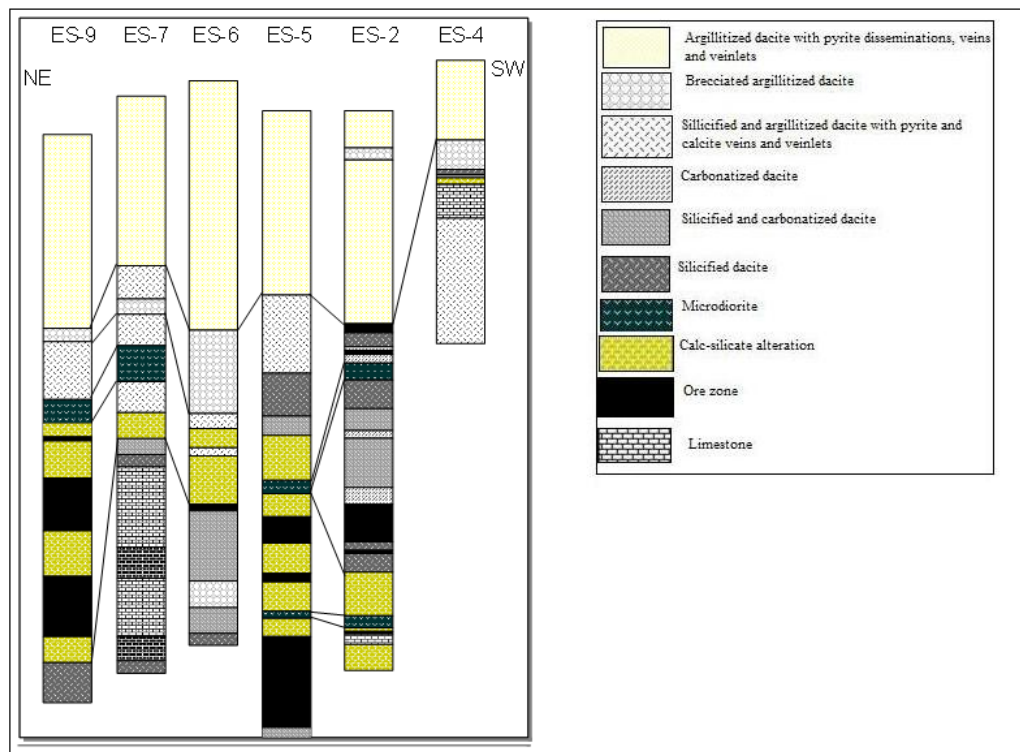


Figure 4.40. Drill logs of ES-3, ES-8, ES-1, ES-5 and ES-2 (North to South)

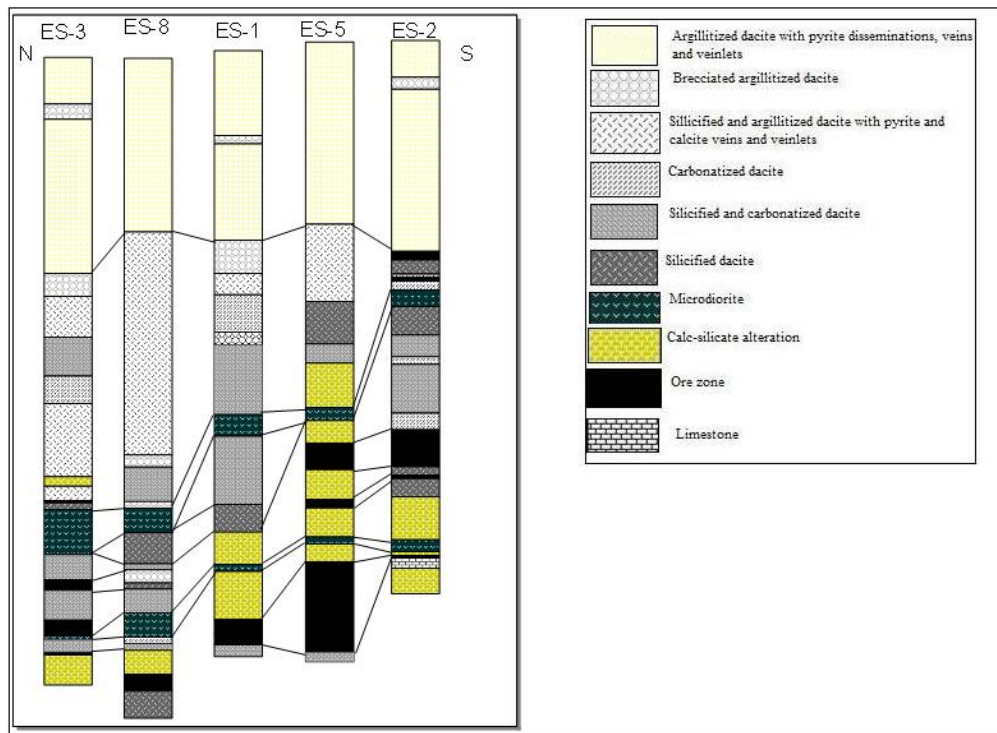


Figure 4.41. Drill logs of ES-9, ES-7, ES-6, ES-5, ES-2 and ES-4 (Northeast to Southwest)

Two major microdiorite porphyry dikes parallel to each appear to cut the dacitic rocks (see N-S cross-section Figure 4.39). The dip and vertical extension of the dikes suggest that they are not channeled through the fault planes, instead they are oblique to major fault zones. The spatial association of the calc-silicate and other alterations with the dikes is supportive of the argument that the dikes are the driving mechanism of the alterations. There are two major ore zones, and these are definitely hosted by the calc-silicate alterations. The general dip and vertical extension of the ore zones along with the calc-silicate alterations are conformable to those of dikes. This also supports that the alterations and ore deposition should be related to emplacement of the dikes into the dacitic rocks. The thickness of the ore zones decreases towards north (as far as the available holes are concerned). The limestone is almost absent or rare in N-S cross-section. Therefore, this could be used as a piece of evidence that a classic skarn type hydrothermal system is not likely at Balya mine. However, there are several limestone lenses within the dacitic rocks in E-W section. The spatial association of the ore zone and calc-silicate alteration is also present in the E-W section. However, the dips are gentler compared to dip amount in N-S section.

## CHAPTER 5

### GEOCHEMISTRY

Geochemical analyses were conducted on a total of 22 samples selected from core samples from 9 drill holes and 3 samples from the least altered volcanic host rock. The samples have been collected from the intervals where the alteration mineralogy is ideal as much as possible for comparison and correlation of different alteration types. These samples were then cleaned, grinded and powdered prior to geochemical analyses in the “Sample Preparation Laboratory” of the Ezcacıbaşı ESAN Madencilik. After the sample preparation, they were shipped to the Activation Laboratories (Canada) for major and trace element geochemistry. Inductively Coupled Plasma (ICP) is the analytical method used for major elements analysis, and the analytical package of WRA (internal lab. coding for majors) has been adopted. On the other hand, Inductively Coupled Plasma Mass Spectrometry (ICP/MS) was used for trace element analysis based on the analytical package of WRA4B2. Fused sample was diluted and analyzed by Perkin Elmer Sciex ELAN 6000, 6100 or 9000 ICP/MS. The results of analyses are presented in Table 5.1 to 5.3.

The geochemical data for the least altered volcanic rocks were used for geochemical characterization of the volcanic rocks hosting the mineralization. The data obtained from the altered samples were used for the understanding of the geochemical tracers, element mobility and geochemical characterization of alterations in conjunction with the alteration assemblage.

#### **5.1. Geochemistry of volcanic rocks**

The volcanic rocks are subalkaline, and have calc-alkaline nature (Figure 5.1a and 5.1b). They are classified as High-K, and calcic-alkali to calcic type (Fig. 5.1c and 5.1d).

Based on their alumina saturation index, the rocks are metaluminous to peraluminous in character. For the composition of the volcanic rocks classical nomenclature diagrams have been adopted using Minpet 2.02 software.

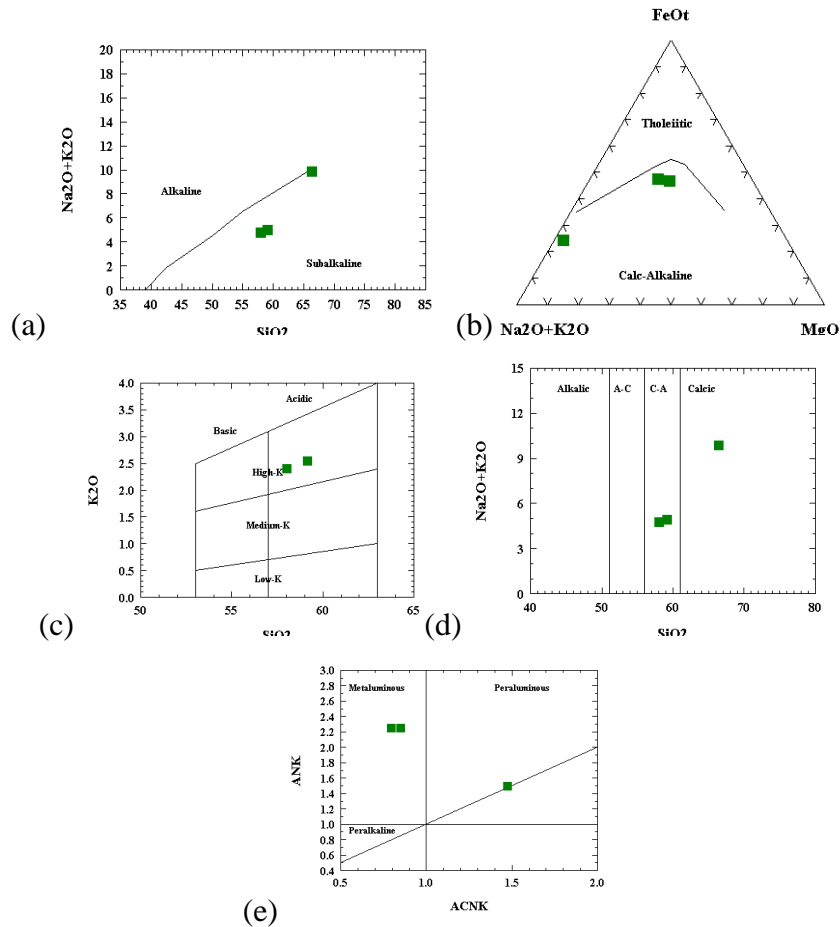


Figure 5.1. Major element characteristics of the volcanic rocks (discrimination lines are from (a) & (b): Irvine and Baragar (1971); (c): Gill (1981); (d) Peacock (1931), (e) Maniar and Piccoli (1989))

According to Cox et al. (1979), the rocks are mostly andesite in composition based on their major element compositions (Figure 5.2a). However, since the major oxides are the most mobile elements during hydrothermally altered settings like Balya deposit site, it is not appropriate to rely on this compositional classification. Instead, the volcanic rocks should be classified using elements which tend to behave immobile during alteration like high field strength elements (HFS, Y, Nb, Zr and Ti). Therefore, the discrimination diagrams based on immobile trace element data were used for the nomenclature and classification (Figure 5.2b, 5.2c and 5.2d; Winchester and Floyd, 1977).

Table 5.1. Major element contents of samples (Slc: Silicified, Crb: Carbonatized)

Sample No	Lab. Sample no.	Lithology	SiO <sub>2</sub> (%)	Al <sub>2</sub> O <sub>3</sub> (%)	Fe <sub>2</sub> O <sub>3</sub> (%)	MnO (%)	MgO (%)	CaO (%)	Na <sub>2</sub> O (%)	K <sub>2</sub> O (%)	TiO <sub>2</sub> (%)	P <sub>2</sub> O <sub>5</sub> (%)	LOI (%)
E3.1	16908	Argillitized Dacite	61,05	15,35	3,88	0,074	1,31	2,83	0,1	6,08	0,502	0,09	7,01
E7.11	16909	Limestone	6,41	2,23	0,79	0,023	0,46	39,29	0,08	0,22	0,085	< 0,01	37,18
E2.23	16910	Early calc-silicate alteration	11,58	2,9	16,9	0,926	1,57	4,04	0,14	2,01	0,126	0,03	16,37
E2.22	16911	Early calc-silicate alteration	41,26	13,49	4,94	0,682	3,38	31,61	0,05	0,66	0,57	0,1	3,14
E5.2	16912	Argillitized Dacite	61,39	16,72	4,45	0,092	0,87	0,68	0,16	8,06	0,559	0,05	5,11
E6.9	16913	Slc. and Crb. Dacite	61,77	6,24	8,33	0,343	2,56	4,59	0,17	4	0,09	0,04	10,55
E2.28	16914	Ore zone	42,38	12,14	0,59	0,645	1,47	3,05	0,22	9,86	0,403	0,09	5,82
E7.4	16915	Slc. and Argillitized Dacite	58,54	18,79	0,69	0,021	1,39	4,08	0,94	6,94	0,836	0,13	6,94
E1.15	16916	Silicified and carbonatized dacite	67,84	16,08	4,68	0,005	1,07	0,33	0,27	3,85	0,525	0,04	4,62
E5.10	16917	Silicified, carbonatized dacite	9,77	5,2	1,14	0,059	0,25	45,99	0,02	0,7	0,221	0,03	35,15
E5.16	16918	Early calc-silicate alteration	32,07	6,08	7,59	1,087	1,66	17,91	0,21	3,55	0,272	0,02	17,12
E4.10	16919	Argillitized, silicified dacite	61,56	14,3	3,73	0,038	0,96	2,38	0,57	8,97	0,369	0,16	4,91
E7.3	16920	Argillitized Dacite	62,09	15,06	5,94	0,009	0,78	0,51	0,17	4,38	0,501	0,19	6,75
E4.13	16921	Argillitized, silicified dacite	60,39	14,03	5,32	0,025	0,99	1,79	0,31	10,08	0,363	< 0,01	5,1
E9.12	16922	Early calc-silicate alteration	46,87	1,6	8,07	0,397	0,59	25,55	< 0,01	0,25	0,023	< 0,01	15,27
E6.11	16923	Slc. and weak crb. Dacite	57,76	16,5	0,77	0,058	0,7	7,07	2,63	7,14	0,677	0,27	5,12
E3.15	16924	Late calc-silicate alteration	39,78	9,97	7,5	0,401	4,14	29,88	0,05	1,22	0,342	0,05	5,15
E5.22	16925	Late calc-silicate alteration	23,57	0,58	18,24	0,523	6,96	11,1	0,03	0,11	0,151	< 0,01	15,62
E3.2	16926	Early calc-silicate alteration	37,66	4,37	9,45	0,527	5,31	26,46	0,07	2,48	0,073	0,03	12,01
E3.16	16927	Late calc-silicate alteration	21,45	6,04	8,83	1,158	3,99	5,52	0,24	2,27	0,096	< 0,01	14,59
E2.30	16928	Late calc-silicate alteration	17,62	5,83	2,89	0,218	2,63	39,59	0,14	0,98	0,207	0,02	24,73
E2.21	16929	Early calc-silicate alteration	32,77	10,2	17,17	0,493	0,71	30,2	0,06	1,02	0,107	< 0,01	6,74

B173		Fresh (least altered) dacite	66,5	16,1	3,2		0,4	0,5	0,0	0,2	9,6	0,1	3,1
B174		Fresh (least altered) dacite	59,2	15,0	5,0	0,1	3,6	6,0	2,4	2,5	0,5	0,2	5,1
B175		Fresh (least altered) dacite	58,0	14,4	5,5	0,1	4,7	6,4	2,3	2,4	0,5	0,2	4,6

Table 5.2. REE (Rare Earth Elements) element contents (ppm) of samples (Slc: Silicified, Crb: Carbonatized)

<b>Samp le No</b>	<b>Lab. Sample no.</b>	<b>Lithology</b>	<b>Y</b>	<b>Ce</b>	<b>Eu</b>	<b>Dy</b>	<b>Er</b>	<b>Tm</b>	<b>Yb</b>	<b>La</b>	<b>Pr</b>	<b>Nd</b>	<b>Sm</b>	<b>Gd</b>	<b>Ho</b>	<b>Lu</b>
E3.1	16908	Argillitized Dacite	18	93,4	1,27	3,4	1,8	0,29	1,9	51,4	9,79	33,7	6,3	4,8	0,6	0,28
E7.11	16909	Limestone	4	10,7	0,15	0,7	0,4	0,06	0,4	5,5	1,19	4,4	0,9	0,8	0,1	0,06
E2.23	16910	Early calc-silicate alteration	24	51,8	0,7	4,6	2,7	0,4	2,1	26,2	5,79	22,2	4,9	4,6	1	0,24
E2.22	16911	Early calc-silicate alteration	22	46,8	1,76	3,8	2,2	0,35	2,3	31,7	4,99	20	4,7	4,2	0,8	0,33
E5.2	16912	Argillitized Dacite	30	99,7	1,21	5	3	0,49	3	52,2	10,3	35,3	6,5	5,6	1	0,44
E6.9	16913	Slc. and Crb. Dacite	20	10,1	0,72	3,2	2,2	0,35	2,4	6,2	1,13	4,7	1,4	2,3	0,7	0,36
E2.28	16914	Ore zone	24	34,2	0,47	4,5	2,8	0,48	3,1	16,5	3,95	15,1	3,6	3,7	1	0,44
E7.4	16915	Slc. and Argillitized Dacite	15	41,4	0,64	2,7	1,8	0,33	2,1	18,4	4,36	15,5	3,2	2,8	0,6	0,34
E1.15	16916	Silicified and carbonatized dacite	426	144	1,23	28,5	20,4	2,48	11,1	76,6	14,9	49,8	9	16,5	7,2	1,57
E5.10	16917	Silicified, carbonatized dacite	10	23,3	0,35	1,7	1	0,17	1,1	12,2	2,64	10,2	2	1,8	0,4	0,16
E5.16	16918	Early calc-silicate alteration	21	24,8	0,64	3,3	2,1	0,34	2,1	13	3,18	14	3,5	3,1	0,7	0,29
E4.10	16919	Argillitized, silicified dacite	16	56,3	0,87	2,7	1,6	0,25	1,7	30,4	5,87	21,3	4	3,2	0,6	0,27
E7.3	16920	Argillitized Dacite	19	77,7	1,04	3,3	1,9	0,31	2,1	41,5	8,13	29,6	5,3	3,9	0,7	0,3
E4.13	16921	Argillitized, silicified dacite	8	32,4	0,37	1,4	0,9	0,17	1,1	17,9	3,38	11,4	2,1	1,7	0,3	0,18
E9.12	16922	Early calc-silicate alteration	5	19,2	0,97	1	0,5	0,08	0,5	4,3	3,18	11,5	1,5	1,3	0,2	0,07
E6.11	16923	Slc. and weak crb. Dacite	20	59,8	1,01	3,7	2	0,34	2,1	30,2	6,71	24,8	5,1	4,5	0,7	0,32
E3.15	16924	Late calc-silicate alteration	20	38,4	1,03	3,2	2	0,31	1,9	20,8	4,63	18,7	4,1	3,4	0,7	0,27
E5.22	16925	Late calc-silicate alteration	6	40,6	0,72	1,1	0,7	0,1	0,7	25,3	3,96	13,2	2,1	1,4	0,2	0,12
E3.2	16926	Early calc-silicate alteration	7	8,2	0,74	1,1	0,7	0,1	0,7	4,1	1,52	9,8	2,4	1,6	0,2	0,1
E3.16	16927	Late calc-silicate alteration	8	14,6	0,3	1,4	0,8	0,12	0,7	6,6	1,75	6,9	1,6	1,4	0,3	0,1
E2.30	16928	Late calc-silicate alteration	13	75,7	1,94	3	1,6	0,28	1,5	44,6	8,63	33,4	6	4,1	0,6	0,22

E2.21	16929	Early calc-silicate alteration	6	4,6	0,89	1,1	0,6	0,08	0,6	2,7	0,57	2,9	1,1	1,2	0,2	0,09
B173		Fresh (least altered) dacite	10,6	34,9	0,6	1,9	1,1	0,2	1,3	19,3	3,8	13,2	2,6	2,4	0,4	0,2
B174		Fresh (least altered) dacite	19,4	72,9	1,3	3,6	2,1	0,3	2,1	39,0	8,2	30,4	5,3	5,2	0,7	0,3
B175		Fresh (least altered) dacite	19,5	74,9	1,4	3,6	2,1	0,3	2,1	39,5	8,3	31,6	5,5	5,1	0,7	0,3

Table 5.3. Trace element contents (ppm) of samples

Sample No	Lab. Sample no.	Lithology	Sc	V	Cr	Co	Ga	Sr	Zr	Cs	Ba
E3.1	16908	Argillitized Dacite	7	70	< 20	16	18	171	159	7,9	6434
E7.11	16909	Limestone	1	32	50	< 1	2	609	9	< 0,5	109
E2.23	16910	Early calc-silicate alteration	3	28	40	18	14	23	86	1,1	232
E2.22	16911	Early calc-silicate alteration	17	103	100	7	16	40	144	1,4	116
E5.2	16912	Argillitized Dacite	9	77	< 20	13	19	125	203	2,2	1677
E6.9	16913	Slc. and Crb. Dacite	3	37	20	31	9	65	96	2,9	490
E2.28	16914	Ore zone	8	28	50	6	17	269	161	2,5	2137
E7.4	16915	Slc. and Argillitized Dacite	17	163	100	14	20	268	199	14,4	926
E1.15	16916	Silicified and carbonatized dacite	8	81	< 20	14	18	27	168	3,1	226
E5.10	16917	Silicified, carbonatized dacite	5	33	40	< 1	5	373	58	1,5	50
E5.16	16918	Early calc-silicate alteration	5	50	90	2	11	65	43	6,9	454
E4.10	16919	Argillitized, silicified dacite	6	53	30	16	15	226	123	6,9	2335
E7.3	16920	Argillitized Dacite	8	82	< 20	15	17	65	159	3,3	986
E4.13	16921	Argillitized, silicified dacite	6	56	< 20	17	15	248	126	4,1	2195
E9.12	16922	Early calc-silicate alteration	< 1	7	< 20	9	4	81	25	18,9	38
E6.11	16923	Slc. and weak crb. Dacite	12	121	< 20	13	16	439	167	7	891
E3.15	16924	Late calc-silicate alteration	8	64	80	8	14	33	77	0,8	145
E5.22	16925	Late calc-silicate alteration	4	40	60	19	8	34	22	0,7	4
E3.2	16926	Early calc-silicate alteration	4	29	60	2	10	92	44	10,6	169
E3.16	16927	Late calc-silicate alteration	3	20	110	9	9	33	34	1	248

E2.30	16928	Late calc-silicate alteration	6	75	100	3	19	137	43	8,2	158
E2.21	16929	Early calc-silicate alteration	3	42	< 20	12	11	36	35	0,5	159
B173		Fresh (least altered) dacite		53,00	10,0	5,8	17,3	283,0	136,0	5,9	1970,0
B174		Fresh (least altered) dacite		92,00	150,0	13,5	16,3	1135,0	155,0	9,7	1405,0
B175		Fresh (least altered) dacite		104,00	230,0	17,2	15,4	780,0	135,0	13,8	1220,0

Table 5.3.cont.

<b>Samp le No</b>	<b>Lab. Sample no.</b>	<b>Lithology</b>	<b>Ta</b>	<b>Tl</b>	<b>Th</b>	<b>U</b>	<b>Ni</b>	<b>Rb</b>	<b>Nb</b>	<b>Hf</b>	<b>Pb</b>
E3.1	16908	Argillitized Dacite	0,9	1,5	16,4	5,5	< 20	300	12	4,2	190
E7.11	16909	Limestone	0,2	0,1	2,3	4,9	20	6	2	0,6	8
E2.23	16910	Early calc-silicate alteration	0,5	3,1	3,8	3,7	80	74	5	2,5	> 10000
E2.22	16911	Early calc-silicate alteration	0,5	< 0.1	5	3,8	20	19	7	3,8	45
E5.2	16912	Argillitized Dacite	1	0,6	18,3	5,6	< 20	219	13	5,3	29
E6.9	16913	Slc. and Crb. Dacite	0,5	0,4	4,7	2	< 20	126	5	2,6	125
E2.28	16914	Ore zone	1,2	4,2	13,9	5,2	< 20	290	11	5	> 10000
E7.4	16915	Slc. and Argillitized Dacite	1,3	2	14,6	3,7	20	303	19	5,2	136
E1.15	16916	Silicified and carbonatized dacite	0,8	0,5	17,9	6,5	< 20	128	12	4,6	18
E5.10	16917	Silicified, carbonatized dacite	0,4	0,1	5	5,3	20	22	5	1,9	28
E5.16	16918	Early calc-silicate alteration	0,6	0,4	3,3	4,4	< 20	150	6	1,8	8510
E4.10	16919	Argillitized, silicified dacite	1,1	16,9	21,8	8,4	< 20	309	11	3,3	322
E7.3	16920	Argillitized Dacite	0,9	0,5	15	4,1	< 20	150	11	4,4	6
E4.13	16921	Argillitized, silicified dacite	0,9	0,9	20,9	4,7	< 20	301	11	3,5	23
E9.12	16922	Early calc-silicate alteration	< 0.1	0,1	2	4,1	< 20	16	< 1	0,8	131
E6.11	16923	Slc. and weak crb. Dacite	1	0,6	13,6	5,3	< 20	196	13	4,4	10
E3.15	16924	Late calc-silicate alteration	0,8	< 0.1	8,3	5,3	20	39	10	2,3	23
E5.22	16925	Late calc-silicate alteration	0,3	< 0.1	3,8	2,7	< 20	8	3	0,9	649
E3.2	16926	Early calc-silicate alteration	0,2	0,2	5,8	2,9	< 20	85	2	1,2	13

E3.16	16927	Late calc-silicate alteration	0,2	2,7	3,9	3,8	< 20	75	3	1,1	> 10000
E2.30	16928	Late calc-silicate alteration	0,6	0,2	10,2	11,3	40	99	6	2,1	158
E2.21	16929	Early calc-silicate alteration	0,2	< 0.1	1,8	4,6	< 20	24	2	0,7	< 5
B173		Fresh (least altered) dacite	1,0	2,2	14,8	6,3		343,0	12,2	4,1	1610,00
B174		Fresh (least altered) dacite	0,9		16,6	6,5		87,0	10,6	4,4	71,00
B175		Fresh (least altered) dacite	0,8		15,8	5,9		72,5	10,0	3,9	173,00

These diagrams indicate that the volcanic rocks in the Balya deposit site range from trachyandesite through dacite to rhyodacite in composition. This is in agreement with the previous works suggesting andesitic and dacitic compositions for the volcanic rocks. However, presence of abundant magmatic quartz with corroded and embayed outlines, and lacking of rhyolitic and or trachytic flow textures as also defined in the petrography section, suggest that the volcanic rocks could be classified as dacite.

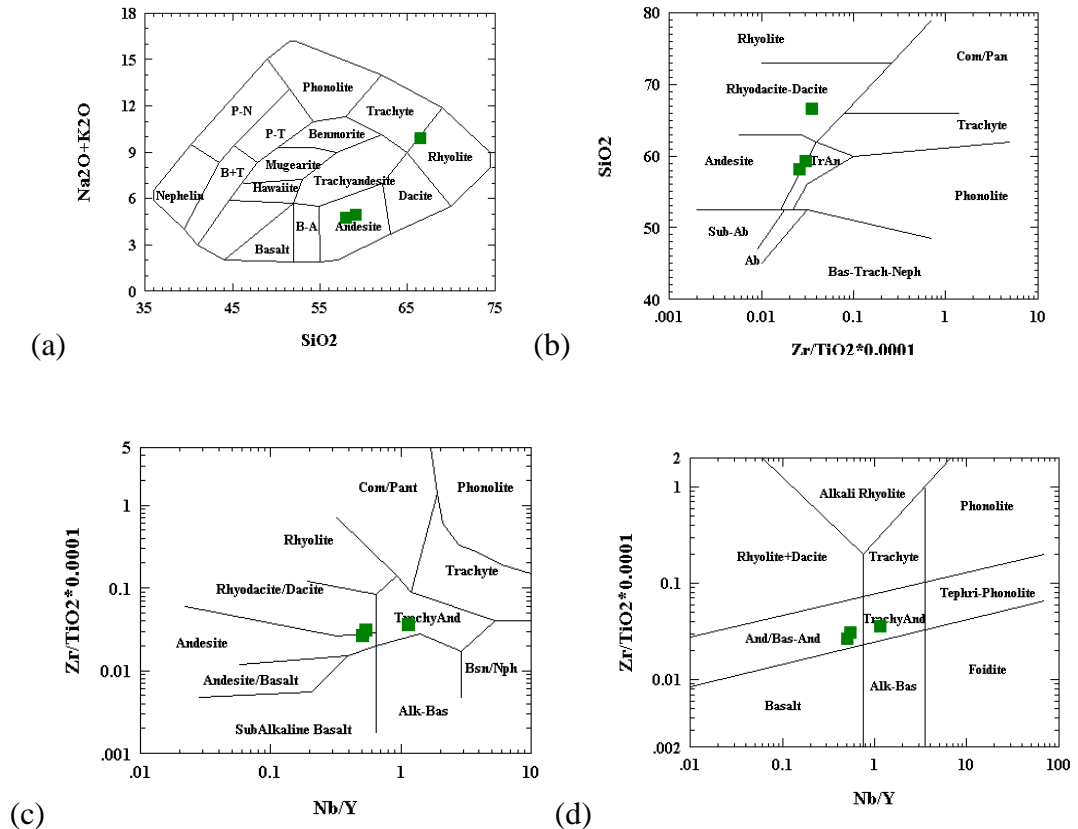


Figure 5.2. Nomenclature of the volcanic rocks using discrimination diagrams (discrimination lines are from (a): Cox et al. (1979); (b), (c), (d): Winchester and Floyd (1977))

The dacitic rocks are enriched in large ion lithophile elements (LILE) with respect to high field strength elements (HFSE) (Figure 5.3a), and display a marked depletion of K, and enrichment of Th suggesting either a crustal contamination or a subduction signature. Also, the light rare earth elements (LREE) are enriched with a steep slope with respect to heavy rare earth elements (HREE) (Figure 5.3b) indicating a subduction components.

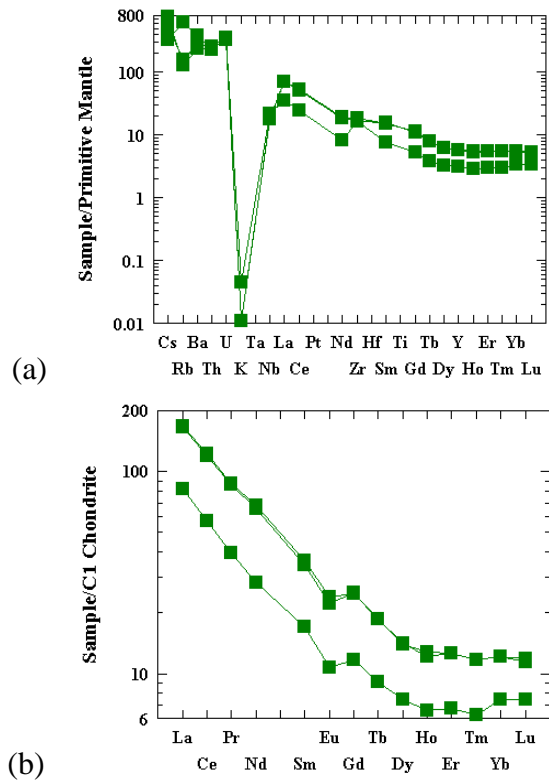


Figure 5.3. (a) multi-element diagram (spidergram), and (b) REE pattern of the volcanic rocks (normalization values (primitive mantle and chondrite) are from Taylor and McLennan (1985))

The dacitic rocks show geochemical characteristics of the syn-collisional to late orogenic settings (Figure 5.4a). They also plot in volcanic arc (VAG) and syn-collisional setting (Figure 5.4b and 5.4c). These collectively would be the indications of a setting where subductional and crustal components are both observed. Therefore, a post-collisional origin could be assigned for the tectonic environment at which the rocks have been formed.

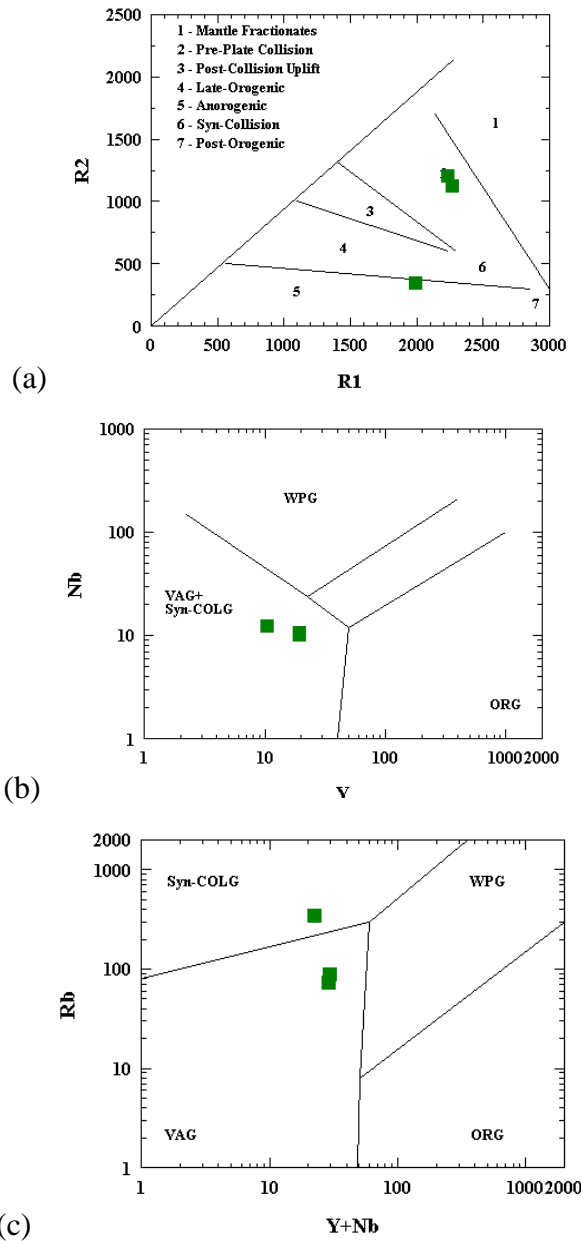


Figure 5.4. Tectonic discrimination of the volcanic rocks in the Balya deposit (discrimination lines are from (a): Batchelor and Bowden (1985); (b) & (c): Pearce et al. (1984))

## 5.2. Alteration Geochemistry

### 5.2.1. Element mobility during calc-silicate alteration

For the mobility and relative depletion-enrichment of patterns, the elements were plotted along traverses from fresh (or least altered) to late calc-silicate alterations. The  $\text{SiO}_2$  appears to be the most depleted component in the calc-silicate alteration

(most probably related to leaching during early calc-silicate alteration) with a prominent depletion at the ore zone (Figure 5.5).  $\text{Al}_2\text{O}_3$  is almost constant from dacite to late calc-silicate alteration. However, it seems to be depleted at the ore due to a probable replacement of garnets formed at the early calc-silicate alteration during ore formation. The  $\text{Fe}_2\text{O}_3$  is likely to be enriched in the early calc-silicate alteration due to garnet (andradite) formation, slightly depleted in ore zone due to replacement by ore minerals, and relatively enriched in late calc-silicate alteration due to generation of epidote and tremolite. Since no diopside and other Mg-bearing calc-silicates were formed, the Mg appears to have remained constant throughout the calc-silicate alteration. CaO tends to show enrichment from fresh dacite to late calc-silicate alteration, and this is related to formation of Ca-bearing minerals like garnet and actinolite at the early calc-silicate alteration, and late carbonatization during late calc-silicate alteration.  $\text{Na}_2\text{O}$  exhibits no changes during early, late-calc silicate alteration, and ore zone since no Na-bearing minerals have formed during the calc-silicate alteration and mineralization, or Na was leached out from the host rock.  $\text{K}_2\text{O}$  show an abrupt depletion at the early calc-silicate alteration, followed by enrichment at the ore zone and again depletion at the late calc-silicate alteration. This could be related to the overprinting effects of argillic alteration. As expected,  $\text{TiO}_2$  does not show enrichment and depletion throughout the calc-silicate alteration and ore formation.

### **5.2.2. Element mobility during early and late silicification**

Hydrothermal fluids causing early and late silicification must have resulted in enrichment in  $\text{SiO}_2$ , however since this alteration and the whole rock sequence have been subjected to argillic alteration, what appears from Figure 5.6 is just the reverse (depletion at silicified dacite, not enrichment), and hence the original element mobility patterns should have been masked or superimposed by argillic alteration. In Figure 5.6.  $\text{Fe}_2\text{O}_3$  and  $\text{Na}_2\text{O}$  seem to be slightly enriched, while  $\text{K}_2\text{O}$  seems to be depleted in silicified zone.

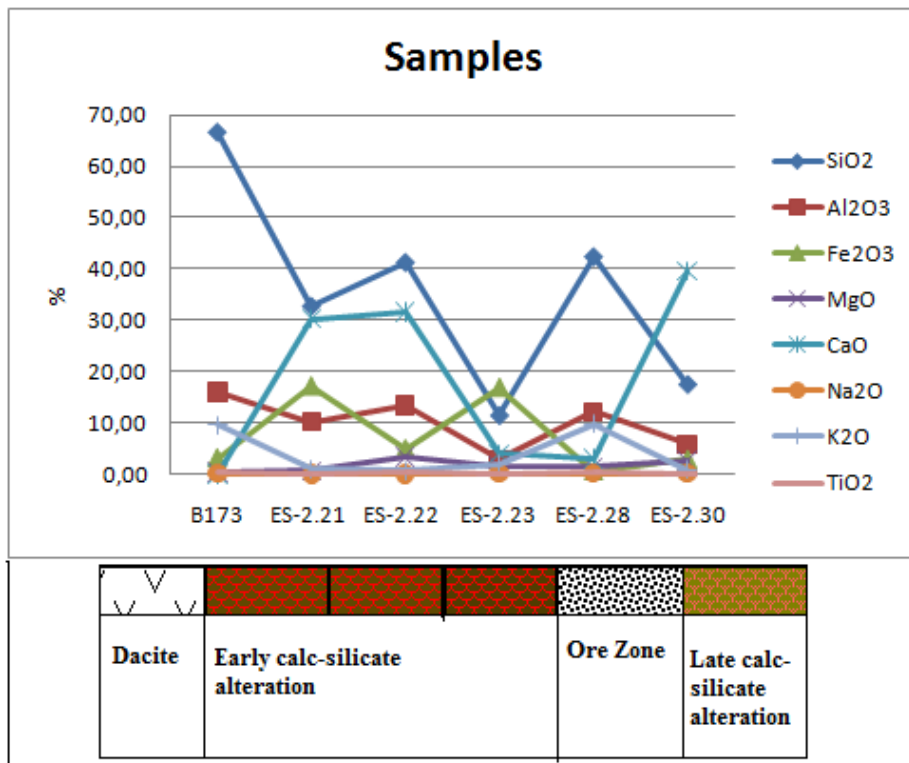


Figure 5.5. Major element distribution of ES-2 samples

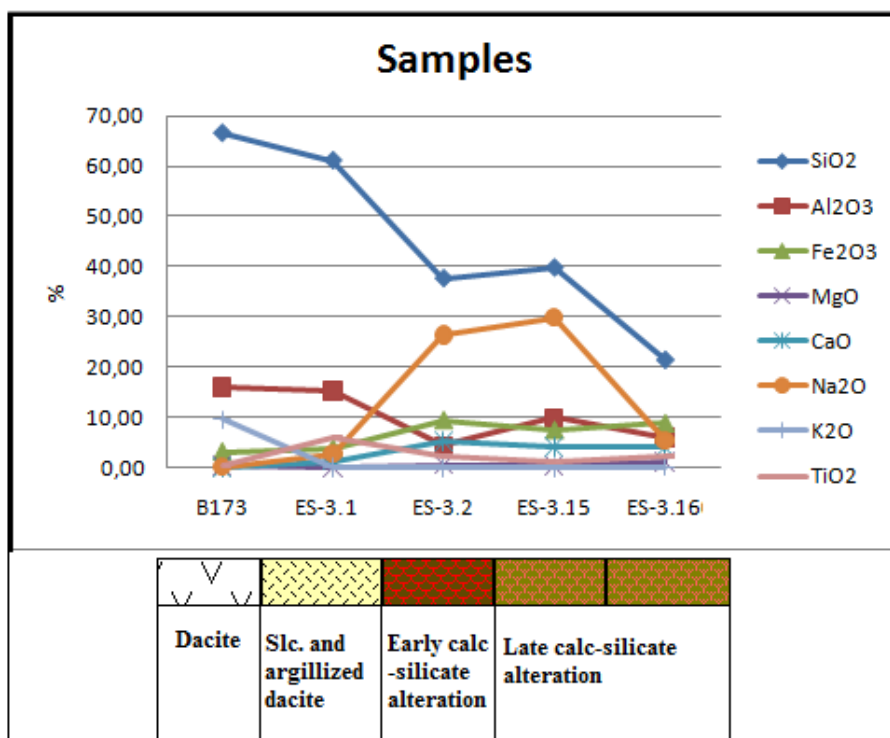


Figure 5.6. Major element distribution of ES-3 samples (Slc: silicified)

Regarding a comparison between silicification and calc-silicate zone,  $\text{SiO}_2$  and  $\text{Al}_2\text{O}_3$  seem to have similar pattern in that silicified and argillized dacite has higher  $\text{SiO}_2$  and  $\text{Al}_2\text{O}_3$  compared with early and late calc-silicate alteration zone (Figure 5.6).  $\text{CaO}$ ,  $\text{Fe}_2\text{O}_3$  are enriched in late calc-silicate alteration zone with respect to silicification.

### 5.2.3. Element mobility during early-late carbonatization

The carbonatization, as the name implies, is characterized by strong enrichment of  $\text{CaO}$  (Figure 5.7) compared to fresh dacite.  $\text{SiO}_2$ ,  $\text{Al}_2\text{O}_3$  and  $\text{K}_2\text{O}$  present similar depletion pattern from the fresh dacite to late calc-silicate alteration, and they all exhibit a depletion at the carbonatization zone. In this sense, Al, Si, K are said to be inversely proportional Ca. Early calc-silicate alteration has relatively higher Si and Al than early carbonatized dacite (Figure 5.7).

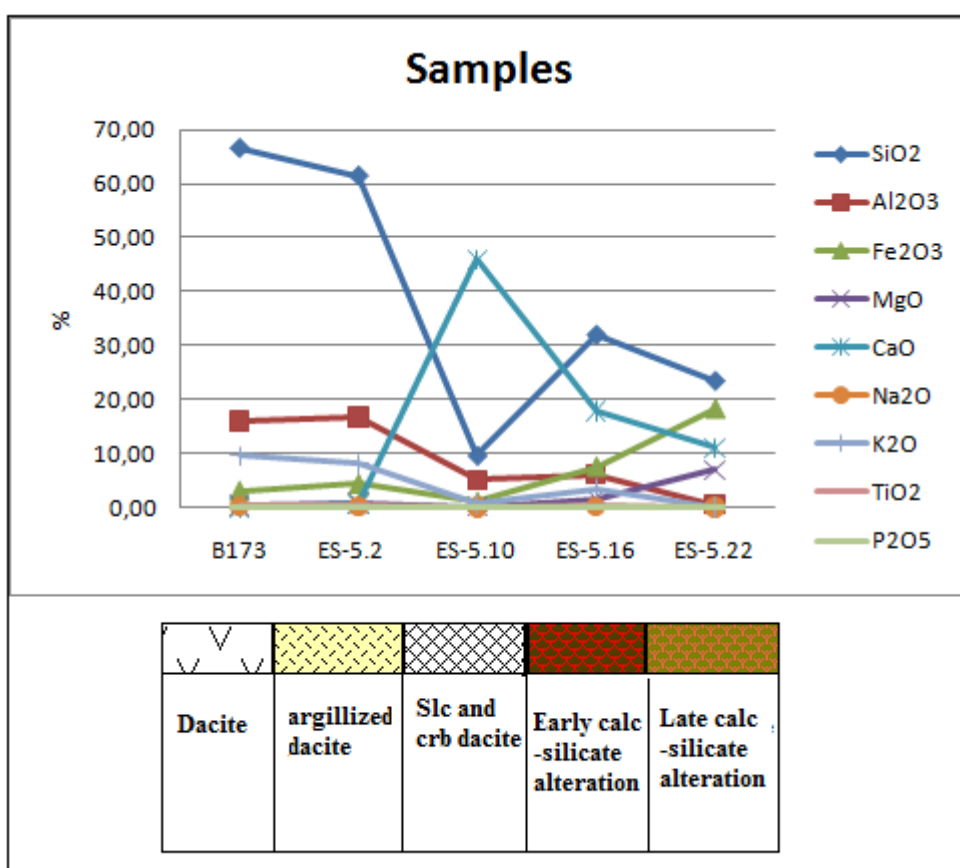


Figure 5.7. Major element distribution of ES-5 samples (Slc: silicification, crb: carbonatization)

### 5.3. Mass Balance Calculations - Mobility of Elements During Alteration

To investigate the relative mobility (gain or loss) of individual elements during alterations, the isocon method (Grant, 1986) was used. The relative gain and loss for some of the alterations was calculated from the slope of a line that pass from the origin through the data point of interest. Diagrams and mass balance calculations are presented in Figures 5.8, 5.9, 5.10 and 5.11.

Isocon method suggests that the concentrations of the elements (either weight percent or moles of elements) in the altered rock can be compared directly with those within the parent or least-altered equivalent. This method was proposed by Gresens (1967) and a graphical solution, termed an isocon diagram, was devised by Grant (1986). Isocon method is used to determine volume change based on the concept that if immobile elements can be identified they can be used to determine if any volume change has taken place (Gresens, 1967). In isocon diagrams,  $\text{SiO}_2$ ,  $\text{Al}_2\text{O}_3$ , and Zr are used for calculating the slope of the isocon because these are the elements/compounds which are considered to be immobile or least mobile. On a graph, element concentrations that have undergone no change from the parent to altered rock will fall on a line intersecting the origin. This line is termed an ‘**isocon**’ (straight line through the origin) and can be related to the equation.

$$C_a = (M_o/M_a)C_o$$

- $C_a$  and  $C_o$  are the final and original concentrations
- $M_a$  and  $M_o$  are the final and original masses of the rock.

The slope of the isocon defines the mass change in the alteration, and the deviation of a data point from the isocon defines the concentration change for the corresponding component. In cases where the (fresh) rock has not been subjected to any alteration (and has undergone no mass change) the isocon would be represented by a line with a slope equal to unity. Since silicification is one of the major alteration types observed in the study area, the isocons in Figures 5.8 to 5.11 were drawn taking  $\text{Al}_2\text{O}_3$  and/or Zr as immobile constituent(s). In these figures, dashed line represents constant  $\text{Al}_2\text{O}_3$  or Zr, i.e. isocon; upper part of dashed line shows element gain, whereas lower side indicates element loss.

Figure 5.8 illustrate the relative gain and loss of elements during silicification overprinted by argillic alteration. For this purpose a sample from the silicified and carbonatized dacite (sample no. 16923) was compared with a relatively fresh host rock (dacite, sample B173). According to isocon diagram, the altered rocks appear to be enriched in CaO, Na<sub>2</sub>O, Sr, La and Sm while depleted in Ba and Rb relative to the sample from fresh dacite.

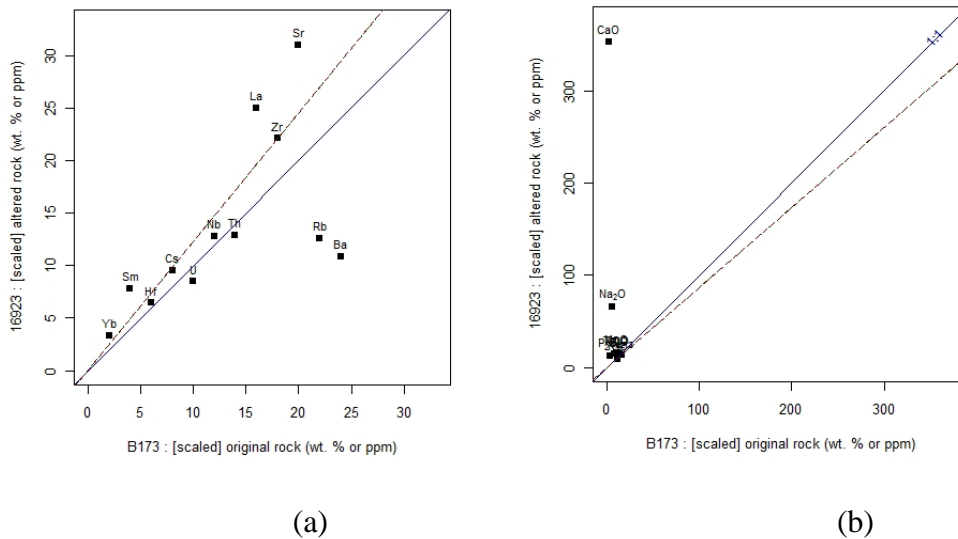


Figure 5.8. Isocon diagrams for samples no. B173 and 16923 (a: trace elements, b: major elements)

For the early silicification and carbonatization, a sample from silicified and carbonatized dacite (sample no. 16923) was compared to argillitized dacite (sample no. 16920) in Figure 5.9. According to the isocon diagram, “silicified and carbonatized” dacite is significantly enriched in CaO and associated element Sr relative to “silicified” dacite, while depleted in Fe<sub>2</sub>O<sub>3</sub>. The altered rock also shows gain in some other elements like K<sub>2</sub>O and MnO (Figure 5.9) as would be expected during carbonatization.

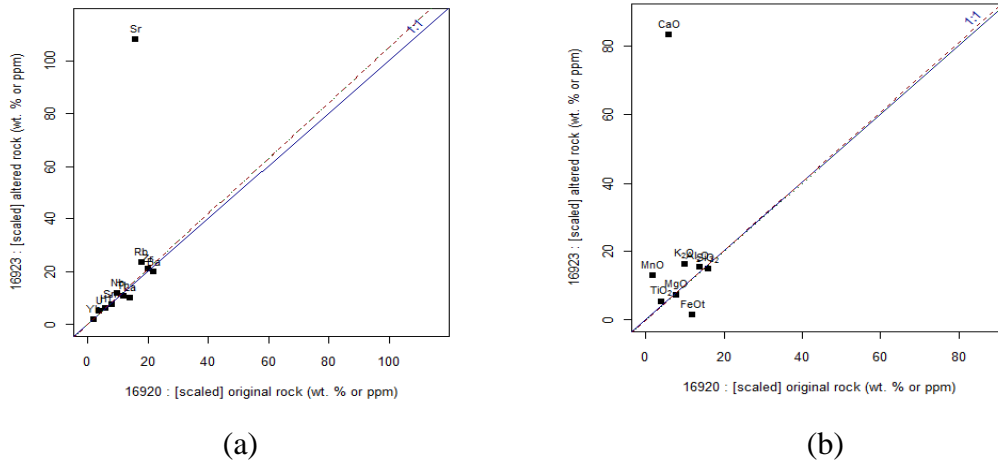


Figure 5.9. Isocon diagrams for samples no. 16920 and 16923 (a: trace elements, b: major elements)

The elemental gain and loss during early silicification was calculated using the sample pair of relatively fresh dacite (least altered) and a silicified and carbonatized dacite (sample 16916). The isocon diagrams (Figures 5.10 and 5.11) prepared for this pair shows that Rb, Sr ve Ba were depleted, and Ca is enriched during early silicification. This means that Sr (although has ionic properties similar to those of Ca) was not enriched as Ca in the alterations. This is because partition coefficient of Sr is controlled by crystal structure of minerals and physico-chemical factors such as as temperature and pressure; therefore, direct proportion between Ca and Sr should not always be expected (Espacially in hydrothermally active zones).

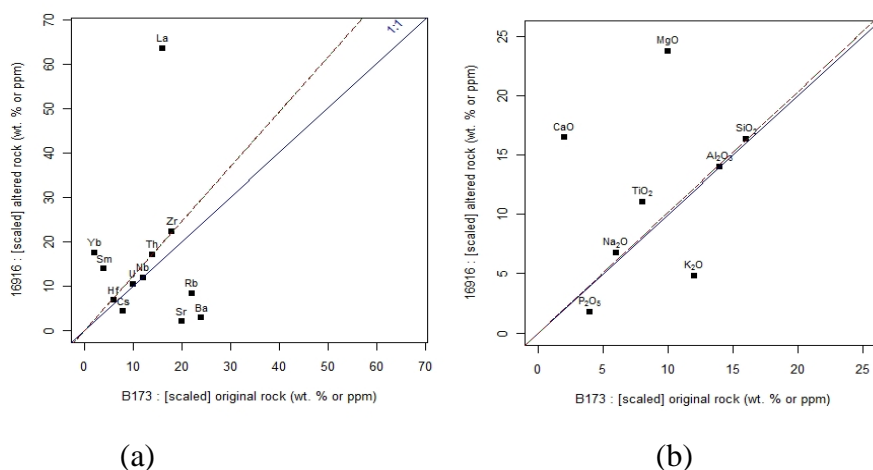


Figure 5.10. Isocon diagrams for samples no. B173 and 16916 (a: trace elements, b: major elements)

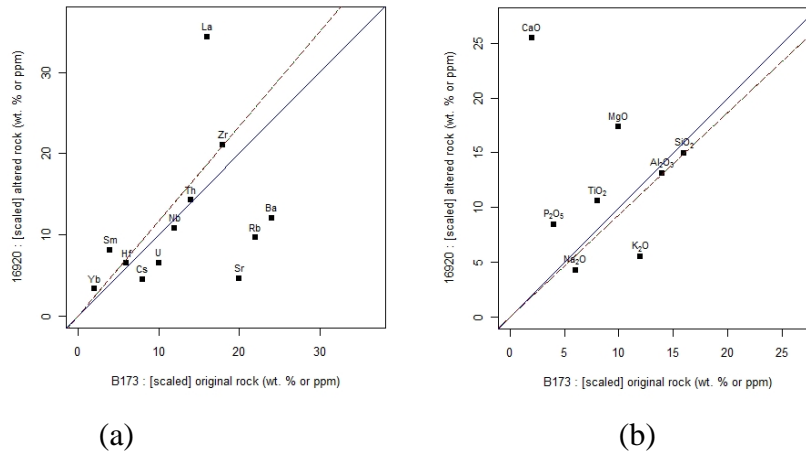


Figure 5.11. Isocon diagrams for samples no. B173 and 16920 (a: trace elements, b: major elements).

## CHAPTER 6

### CONCLUSIONS

The main conclusions drawn from the study are summarized as follows:

1. Wall rocks hosting mineralizations are dacite and dacite porphyry. Subvolcanic mafic intrusion (microdiorite), spatially associated with silicified-carbonatized dacite and in contact with calc-silicate alteration, is observed in most of the drill holes as is revealed by the examination of the drill cores.
2. The major alteration types associated with the Pb-Zn mineralization are silicification, carbonatization and calc-silicate alteration. These alterations are further subdivided into early and late stages as early silicification and late silicification, early carbonatization and late carbonatization, and early calc-silicate and late calc-silicate alteration. All these alterations are overprinted by argillization of a probable supergene origin.
3. According to mineralogical and petrographical studies, the paragenetical succession of alteration zones, from the oldest to the youngest, is given as early silicification, early carbonatization, early calc-silicate alteration, late calc-silicate alteration, late silicification, late carbonatization, and argillization.
4. Hydrothermal quartz is the major constituent of silicification. The early silicification is characterized by coarse grained quartz crystals mainly along the breccia veins and/or massive replacements within the dacitic rocks. The late silicification is characterized by fine grained quartz crystals filling fractures of calc-silicatic rock and replacing characteristic mineral assemblage of calc-silicate alteration

5. The early calc-silicate alteration consists of garnet (andradite) and pyroxene with occasional to rare actinolite, whereas the late calc-silicate alteration contains epidote, tremolite and calcite-quartz assemblage.

6. The early carbonatization is comprised by single or isolated calcite crystals, and characterized mainly by calcite vein and veinlets along fractures of silicified-brecciated dacite and replacements of minerals of early silicification and hydrothermally brecciated rock. The late carbonatization occurs mainly as veins or massive replacements throughout the late calc-silicate alteration, and is characterized by calcite crystals replacing the garnet and pyroxene of early calc-silicate alteration as primary calcite veins and veinlets.

7. Argillic alteration comprises the latest alteration phase, overprinting all the other alterations. Being associated with manganese oxide-hydroxide-bearing, clay-altered dacitic rocks with abundant oxidized pyrite, the argillic alteration seems to have resulted from the leaching of the pyrite-rich dacitic rocks by circulating meteoric water.

8. The major ore minerals are sphalerite and galena with minor chalcopyrite and pyrite. Depending on the cross-cutting and replacement textures, the relative time of formation of sulfide minerals, from the earliest to the latest, are as follows: pyrite, galena, chalcopyrite, sphalerite. Pyrite, as disseminations, veins and veinlets are commonly observed in clay-altered and silicified dacitic rocks and these crystals are replaced by galena and sphalerite commonly along the fracture zones. Galena occurs as massive ore bodies associated with late calcite replacing the late calc-silicate assemblage, and disseminations away from the calc-silicate alteration typically within the argillic alterations. The chalcopyrite occurs both as exsolutions in sphalerite minerals and as massive crystals rimming the sphalerite along with galena. Sphalerite occurs either as massive or disseminated types in calc-silicate alteration assemblage and it is also associated with carbonatized dacite. Mineralogic-petrographic studies, along with geochemical data, suggest the Pb-Zn mineralization is synchronous with late carbonatization and silicification.

9. Lateral-vertical correlation of drill logs suggests that thickness of the ore zone tends to increase towards south (as far as the available holes are concerned). Lack of

limestone in N-S cross-section is an evidence against the presence of a classic skarn type hydrothermal system in Balya area.

10. Unaltered volcanic rocks have calc-alkaline nature and are metaluminous to peraluminous in character. These dacitic volcanic rocks display high LILE/HFSE ratios, a marked depletion of K and enrichment of Th, pointing out to either a crustal contamination or a subduction signature. Geochemical characteristics similar to those from syn-collisional to late orogenic, and volcanic arc (VAG) to syn-collisional settings, collectively suggest the presence of both subductional and crustal components in the genesis of the volcanics. Therefore, a post-collisional origin could be assigned for the tectonic environment at which the rocks were formed.

11. Alteration geochemistry reveals that  $\text{Fe}_2\text{O}_3$  and CaO are enriched during calc-silicate alteration, whereas  $\text{SiO}_2$  is depleted.  $\text{Al}_2\text{O}_3$  and  $\text{TiO}_2$  are almost constant from dacite to late calc-silicate alteration. Silicified zones were enriched in  $\text{Fe}_2\text{O}_3$  and  $\text{Na}_2\text{O}$ , and depleted in  $\text{K}_2\text{O}$ . Strong enrichment of CaO and depletion of  $\text{SiO}_2$ ,  $\text{Al}_2\text{O}_3$  and  $\text{K}_2\text{O}$  were observed during carbonatization.

## REFERENCES

- Ağdemir, N., Kırıkoğlu, S., Lehmann, B., Tietze, J., 1994, Petrology and alteration geochemistry of the epithermal Balya Pb–Zn–Ag deposits, NW Turkey, *Mineral Deposita*, v:29, 366–371.
- Akyol, Z., 1977, Balya madeni civarının jeolojisi. *Jeoloji Müh.*, 3, 19-27.
- Akyol, Z., 1979, Balya kurşun—çinko maden yatağı: *Jeoloji Mühendisliği.*, no:7, s 47-59.
- Akyol, Z., 1982, Balıkesir Balya cevherli sahalarının jeolojisi, mineralojisi ve maden potansiyelinin değerlendirilmesi, *İstanbul Yerbilimleri*, 3, 163-189.
- Altıner, D., Özkan-Altıner, S. and Koçyiğit, A. 2000. Late Permian foraminiferal biofacies belts in Turkey: palaeogeographic and tectonic implications. In: Bozkurt, E., Winchester, J.A. and Piper, J.A.D. (eds), *Tectonics and Magmatism in Turkey and Surrounding Area*. Geological Society, London, Special Publications 173, 83-96.
- Aygen, T., 1956, Balya bölgesi jeolojisinin incelenmesi, MTA Publ., D11, 95 pp.
- Batchelor, B., and Bowden, P., 1985, Petrogenetic interpretation of granitoid rock series using multicationic parameters, *Chemical Geology*, 48, 43-55.
- Berg, G., 1901, Beitrage zur Kenntnis der Kontakt metamorphen Lagerstätte von Balla Maden, *Zeitsehr, f, prakt Geol Hall*
- Bingöl, E., Akyürek, B., and Korkmazer, B., 1975, Geology of the Biga peninsula and some characteristics of the Karakaya blocky series, *Cong. Earth Sc. for the 50th Ann. Republic Turkey*, MTA Enstitute , 70-77.

- Bozkurt, E., and Mittwede, S. K., 2001, Introduction to the Geology of Turkey-A synthesis, *International Geology Review*, v. 43, p. 578-594.
- Budakođlu, M., Pratt, L. M., 2005, Sulfur-isotope distribution and contamination related to the Balya Pb-Zn Mine in Turkey, *Environmental Geology*, v:47, 773-781.
- Cox, K. G., Bell, J. D. and Pankhurst, R. J., 1979, *The Interpretation of Igneous Rocks*, George Allen and Unwin, London.
- Enderle, J., 1900, Über eine anthrakolithische Fauna von Balia Maden in Kleinasien. *Beitr. Pal. Öst.-Ung.*, 13, 49-109., Wien.
- Ercan, T., Satır, M., Steinitz, G., Dora, A., Sarıfakiođlu, E., Adis, C., Walter, H.J. and Yıldırım, T., 1995, Biga Yarımadası ile Gökçeada Bozcaada ve Tavşalı adalarındaki (KB Anadolu) Tersiyer Volkanizmasının özellikleri: *MTA Derg.*, 117, 55-86.
- Ercan, T., Türkecan, A., Guillou, H., Satır, M., Sevin, D., Sarođlu, F., 1998, Features of the Tertiary volcanism around Sea of Marmara, *Mineral Res. Expl. Bull.*, 120, 97-118
- Genç, Ş.C., and Yılmaz, Y., 1995, Evolution of the Triassic continental margin, northwest Anatolia. *Tectonophysics*, 243, 193-207.
- Gill, J.B, 1981, *Orogenic andesites and plate tectonics*, SpringerVerlag, Berlin, 390pp.
- Gjelsvik, T., 1962, Investigations of Lead-Zinc Deposits in Northwest Anatolia, Turkey, *M.T.A Bull.*, v: 59.

- Göncüoğlu, M. C., Toprak, V., Kuşçu, I., Erler, A., and Olgun, E., 1991, Orta Anadolu Masifi'nin batı bölümünün jeolojisi, Bölüm 1: Güney Kesim: Turkish Petroleum Corporation Report no 2909, 140 p (in Turkish).
- Göncüoğlu, M. C., Turhan, N., Sentürk, K., Özcan, A., Uysal, S., and Yaliniz, M. K., 2000, A geotraverse across northwestern Turkey: Tectonic Units of the Central Sakarya region and their tectonic evolution, in Bozkurt, E., Winchester J. A., and Piper, J. D. A., eds., Tectonic and magmatism in Turkey and the surrounding area: Geological Society of London, Special Publication, no. 173, p. 139-161.
- Grant, 1986 J.A. Grant, The Isocon diagram; a simple solution to Gresens' equation for metasomatic alteration, *Economic Geology* v. 81; no. 8; p. 1976-1982.
- Gresens, R.L., 1967, Composition volume relationships of metasomatism, *Chemical Geology*, v. 2, p. 47-55.
- Irvine, T.N. and Baragar, W.R.A., 1971, A guide to the chemical classification of the common volcanic rocks, *Canadian Journal of Earth Sciences*, 8: 523-548.
- Kaaden, G, 1957, Çanakkale, Biga, Edremit yarımadası bölgesindeki jeolojik saha çalışmaları ve maden yatakları hakkında rapor, MTA report, No: 133, Ankara.
- Koçyiğit, A., 1987, Hasanoğlan (Ankara) yöresinin tektonostratigrafisi: Karakaya orojenik kuşağının evrimi, *Yerbilimleri*, 14, 269-293.
- Kovenko, V., 1940, Balya kurşun madenleri M.T.A, Mecn. s. 4/2, Ankara.
- Leven, E.J.A. and Okay, A.I., 1996, Foraminifera from the exotic Permian-Carboniferous limestone blocks in the Karakaya Complex, northwest Turkey, *Rivista Italiana Paleontologia e Stratigrafia* 102, 139-174.

- Maniar, P.D. and Piccoli, P.M., 1989, Tectonic discrimination of granitoids, Geological Society of America Bulletin, 101: 635-643.
- Mohr Meer, H., 1959, Balya mıntıkasındaki kurşun zuhurlarının prospeksiyonu hakkında toplu rapor MTA Report, No: 2703
- Okay, A.I., Siyako, M. & Bürkan, K.A., 1991, Geology and tectonic evolution of the Biga Peninsula, northwest Turkey. Bulletin of the Technical University of İstanbul 44, 191-256.
- Okay, A. I., and Mostler, H., 1994, Carboniferous and Permian radiolarite blocks in the Karakaya Complex in northwest Turkey, Turkish Journal of Earth Sciences 3, 23-28.
- Okay, A. I., and Tüysüz, O., 1999, Tethyan sutures of northern Turkey, in Durand, B., Jolivet, L., Horvath, D., and Serranne, M., eds., The Mediterranean basins: Tertiary extension within the Alpine orogen: geological Society of London, Special Publication, no. 156, p. 475-515.
- Okay, A.I., 2000, Was the Late Triassic orogeny in Turkey caused by the collision of an oceanic plateau? In "Tectonics and Magmatism in Turkey and Surrounding Area" (eds. E. Bozkurt, J.A. Winchester and J.A.D. Piper), Geological Society, London, Special Publication, 173, 25-41.
- Okay, A.I. and Göncüoğlu, M.C., 2004, Karakaya Complex: a review of data and concepts. Turkish Journal of Earth Sciences, 13, 77-95.
- Okay, A.I. and Altıner, D. 2004. Uppermost Triassic limestone in the Karakaya Complex - stratigraphic and tectonic significance, Turkish Journal of Earth Sciences 13, 187-199.
- Peacock, M.A., 1931, Classification of igneous rock series, Journal of Geology, 39, 1-54.

- Pearce, J.A., Harris, N.B.W. and Tindle, A.G., 1984, Trace element discrimination diagrams for the tectonic interpretation of granitic rocks, *Journal of Petrology*, 25: 956-983.
- Philippon, A., 1915, *Reisen und Forschungen im westlichen Kleinasien I*, Reft. Univ, İstanbul
- Pickett, E.A., and Robertson, A.H.F., 1996, Formation of the Late Paleozoic-Early Mesozoic Karakaya Complex and related ophiolites in NW Turkey by Paleotethyan subduction-accretion. *J. Geol. Soc. London*, 153, 995-1009.
- Pickett, E.A., and Robertson, A.H.F., 2004, Significance of the Triassic volcanogenic Nilfer Unit for Paleotethys and the Karakaya suture zone in NW Turkey, *Turkish Journal of Earth Sciences* 13, 97-143.
- Seymen, I., 1981, Stratigraphy and metamorphism of the Kirsehir massif around Kaman (Kirsehir-Turkey): *Geological Society of Turkey Bulletin*, v. 24, p. 101-108 (in Turkish with English abstract).
- Şengör, A. M. C., and Yılmaz, Y., 1981, Tethyan evolution of Turkey: A plate tectonic approach: *Tectonophysics*, v 75, p. 181-241.
- Şengör, A. M. C., Yılmaz, Y. and Sungurlu, O., 1984, Tectonic of the Mediterranean Cimmerides: nature and evolution of the western termination of Paleo-Tethys. In J.E. Dixon and A.H.F. Robertson (eds.), *The geological evolution of the Eastern Mediterranean*, Geological Society of London Special Publication 17, 77-112.
- Taylor, S. R., and McLennan, S. M., 1985, *The continental crust: It's composition and evolution*, Blackwell Scientific, Oxford, 312p.
- Tekeli, O., 1981, Aladağ ofiyolitli melanjının özellikleri: *Türkiye Jeol. Kur. Bült.*, v. 24/1.

Weiss, K, E. (1901): Kurze Mitteilungen über Lagerstätten im Westlichen Anatolien  
Zeitschrift für prakt. Geol, Vol IX, Berlin

Winchester, J.A. and Floyd, P.A., 1977, Geochemical discrimination of different  
magma series and their differentiation products using immobile elements,  
Chemical Geology, 20: 325-343.